R-08-112

Porewater in the rock matrix

Site descriptive modelling SDM-Site Laxemar

H N Waber, T Gimmi, A deHaller
Rock-Water Interaction, Institute of Geological Sciences
University of Bern

J A T Smellie
Conterra AB

May 2009

Svensk Kärnbränslehantering AB
Swedish Nuclear Fuel
and Waste Management Co

Box 250, SE-101 24 Stockholm
Phone +46 8 459 84 00

ISSN 1402-3091
SKB Rapport R-08-112

Porewater in the rock matrix

Site descriptive modelling
SDM-Site Laxemar

H N Waber, T Gimmi, A deHaller
Rock-Water Interaction, Institute of Geological Sciences
University of Bern

J A T Smellie
Conterra AB

May 2009

Preface

This report describes the porewater investigation carried out on drillcore material from deep boreholes within the Laxemar Site Investigation programme. Porewater residing in the low-permeability matrix of a rock body cannot be sampled by conventional groundwater sampling techniques, but has to be characterised by indirect methods based on drillcore material. Such determination might be subjected to various types of induced perturbations, which need to be understood for the interpretation of the data at *in situ* conditions. Once the produced data can be judged to reliably represent *in situ* conditions, they might be used for the characterisation of the exchange between porewater and fracture groundwater and, based on quantitative models, help to establish the conceptual model of the palaeohydogeological evolution of the site during Holocene and Pleistocene times.

At the Laxemar and Forsmark sites, porewater investigations based on various diffusion experiments utilising fresh drillcore material have been conducted for the first time in crystalline rocks. This required a rigorous control of the acquired data and supporting experiments in order to understand possible perturbation effects such as stress releases, the drilling process, and by sample de-saturation. The present report presents applied methods and their uncertainties, the chemical and isotopic porewater data generated from the raw data, model attempts for the *in situ* porewater composition, transport properties of the rock, and implications of the porewater geochemistry on the palaeohydrogeological evolution of the Laxemar site. To interpret the porewater data, special emphasis is given to the integration of geological, hydrogeochemical, hydrological and palaeoclimate data from the overall Laxemar site descriptive model and, when appropriate, vice versa.

The original works by the ChemNet modellers are presented in four level III reports containing complementary information for the bedrock hydrogeochemistry Laxemar Site Descriptive Model (SDM-Site Laxemar, R-08-93) level II report.

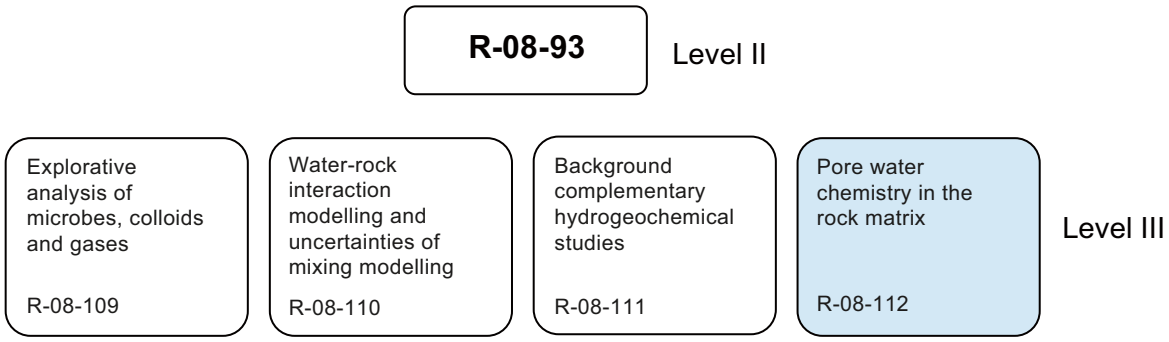

There is also a fifth level III report: Fracture mineralogy of the Laxemar area by Sandström et al. R-08-99.

Summary

Porewater investigations in the Laxemar subarea were aimed at elaborating the hydrogeochemical evolution of the site based on the potential of porewater acting as an archive to events that have happened over recent geological time (i.e. several hundreds to a few millions of years), and to define the potential of matrix diffusion to contribute to solute transport in the geosphere.

A once established chemical and isotopic signature might be preserved in the porewater over long geological time periods. The degree of preservation depends on: a) the distance of the porewater sample to the nearest water-conducting fracture in three dimensions (i.e. the fracture network), b) the solute transport properties of the rock (i.e. diffusion coefficient, porosity), and c) the period of constant boundary conditions (i.e. constant fracture groundwater composition). Complex situations occur in the case of overlap or superimposition of changes induced by variable boundary conditions in Holocene and Pleistocene times when frequent climatic and hydrogeological changes occurred. As a consequence, no simple correlation between two independent natural tracers (e.g. Cl^- and $\delta^{18}O$) can be expected. The porewater data have to be interpreted by taking all these influencing factors into account.

Porewater residing in the rock matrix cannot be sampled by conventional groundwater sampling techniques and therefore needs to be characterised by indirect methods based on drillcore material. Together with the above-mentioned dependencies, it becomes obvious that porewater data obtained for a single sample from a borehole can only be interpreted to a limited degree. More information can be extracted if profiles are sampled along a borehole, and/or small-scale profiles sampled from a water-conducting fracture into the host rock, and by comparing such data to present day fracture groundwater compositions in the nearest water-conducting fracture(s). Within the SKB site investigation programmes at Oskarshamn and Forsmark, porewater investigations have been developed and tested for the first time in crystalline rocks /Waber and Smellie 2008a/.

The chemical and isotopic composition of porewater extracted from drillcore material sampled from boreholes KLX03, KLX08 and KLX17A in the Laxemar subarea, depends on the location of the three boreholes and the porewater samples with respect to the hydraulic domains and the occurrence of deformation zones. The porewater data show a distinction between bedrock characterised by high transmissivity and a high frequency of water-conducting fractures at shallow to intermediate depth, and bedrock characterised by low transmissivity and a low frequency of water-conducting fractures at greater depth. In the more transmissive, shallow to intermediate depth interval, porewater is of a general Na-HCO_3 chemical type with a Cl^- concentration of less than 1,000 mg/kgH_2O. Combined with the oxygen and hydrogen isotope composition, the distance between porewater sample and nearest water-conducting fracture in the borehole, and the quantitative modelling of a natural tracer profile sampled at high resolution in borehole KLX17A, the porewater signatures may be explained in terms of exchange with Holocene meteoric fracture groundwater of present-day type, of Holocene thermal maximum type (at about 7,000–4,000 years BP) and of glacial or glacio-lacustrine type. Furthermore, Na-HCO_3 type porewater signatures with low Cl^- concentrations and observed farther away from water-conducting fractures indicate an evolution from Pleistocene meteoric fracture groundwater of warm climate origin (possibly Eemian Interglacial) and cold climate periods (early Weicheselian or older). Cold climate influence from the last glaciation with $\delta^{18}O$ values around –14‰ VSMOW occurs between about 135–350 m depth in boreholes KLX03 and KLX17A, and down to about 500 m depth in borehole KLX08. Porewater of the Na-HCO_3 type, with low Cl^- concentrations and of present-day and/or warm climate influence occur at about the same depth intervals in boreholes KLX03 and KLX17A, and down to about 600 m depth in borehole KLX08.

Below the dilute to brackish Na-HCO_3 type porewater at shallow to intermediate depth a change to higher mineralised porewater of a general Na-Ca-SO_4 and Ca-Na- SO_4 chemical type occurs in boreholes KLX03, KLX17A, and KLX08, respectively. At present, this porewater type occurs over a restricted vertical depth interval (about 120 m) roughly coinciding with the proposed repository depth at about 430 m depth in boreholes KLX03 and KLX17A and at about 620 m depth in borehole KLX08. The change coincides with a marked decrease in transmissivity, in the frequency of water-conducting features and, in boreholes KLX03 and KLX08, the transition zone from Ävrö

granite to quartz monzodiorite. In boreholes KLX03 and KLX17A, Cl^- concentrations range from 5,000 to 7,600 mg/kgH_2O and are associated with strongly variable water isotope compositions ($\delta^{18}O$ about –5‰ to –13‰ VSMOW). In borehole KLX08, Cl^- concentrations range from 2,500 to 6,000 mg/kgH_2O with associated $\delta^{18}O$ values from –2‰ to –10‰ VSMOW. High concentrations of Ca^{2+} and SO_4^{2-} up to gypsum saturation have to be expected for these types of porewater based on geochemical modelling. Chemical and isotopic composition of these porewater types cannot be explained by interaction with a known type of fracture groundwater and more advanced interaction with the Ävrö granite, but must originate from different processes. Based on ion-ion ratios, isotope composition and geochemical model calculations, the evolution of this type of porewater is most probably related to fracture groundwater that was subjected to permafrost related processes. The large distance to the nearest water-conducting fracture of all but one porewater samples of the general Na-Ca-SO_4 and Ca-Na-SO_4 type porewaters suggests that these signatures have been established a long time ago, certainly before the Last Glacial Maximum, and most probably at shallower depth.

More dilute porewater of Na-HCO_3 type (borehole KLX03) and Na-Ca-Cl-(HCO_3) type (borehole KLX08) occur again below the depth interval of the Na-Ca-SO_4 type porewater. Here, Cl^- contents vary between about 500 to 3,000 mg/kgH_2O and associated $\delta^{18}O$ values of between about –8‰ to –11‰ VSMOW. Towards the bottom of boreholes KLX03 and KLX08 at depths of about 930 m and 820 m, respectively, the Cl^- concentrations increase again to more than 5,000 mg/kgH_2O in KLX03 and more than 8,000 mg/kgH_2O in KLX08. The oxygen isotope composition of these deep Na-Ca-Cl-(HCO_3) type to Na-Ca-Cl type porewaters is generally enriched in ^{18}O compared to the more shallow porewaters. It appears that at these low-transmissive depths, the porewaters display complex, superimposed signatures that cannot be resolved based on the low sample frequency and the absence of high quality fracture groundwater data.

Solute transport in the rock matrix is dominated by diffusion and matrix diffusion was identified to occur at least over several decametres into the rock matrix as shown by the quantitative description of profiles described by Cl^- $\delta^{18}O$ and δ^2H in the porewater and sampled at high resolution from a water-conducting zone into the intact rock matrix in borehole KLX17A. The conducted transport modelling and parameter sensitivity analysis further revealed that the observed porewater signatures at shallow to intermediate depth may be explained in terms of exchange with Holocene meteoric water of present-day type, Holocene thermal maximum type, glacial or glacio-lacustrine type, and Pleistocene meteoric water of warm climate (possibly Eemian interglacial) and cold-climate periods (early Weichselian or older). Only weakly developed and and of restricted occurences are porewater signatures influenced by fracture groundwater related to Baltic Sea water and almost absent seem signatures influenced by fracture groundwater related to Littorina Sea water.

Contents

1 Introduction

Crystalline rocks are generally characterised by two hydraulic regimes, namely the water-conducting zones related to regional and/or local fracture networks and the bedrock mass of low permeability between the water-conducting zones. In the first regime, the hydraulic transmissivity is generally above 10^{-9} m^2s^{-1} and solute transport takes place by advection. In the second regime, the rock matrix, the hydraulic transmissivity is low to very low ($T << 10^{-10}$ m^2s^{-1}) and solute transport is increasingly dominated by diffusion. The mass of porewater present in the rock matrix of a crystalline rock, however, is significant and its influence on fracture groundwater and future deep repositories needs to be understood.

Porewater in the rock matrix and groundwater in the fracture network always tend to reach chemical and isotopic equilibrium. This interaction depends on the existence of an interconnected pore system in the rock matrix that contains a solvent, i.e. porewater, where solute transport can take place, and on the residence time of groundwater in the water-conducting zones. During such interaction, the porewater (and rock matrix) acts either as a sink or a source for solutes depending on the concentration gradient established between porewater and fracture groundwater. Thus, the porewater does not only act as an archive of past fracture groundwater compositions and therefore of the palaeohydrogeological history of a site, but also as a possible sink for radionuclides (e.g. /Neretnieks 1980/).

In contrast to groundwater flowing in a fracture network, porewater that resides in the low permeable rock matrix cannot be sampled by conventional groundwater sampling techniques. The chemical and isotopic composition of porewater has, therefore, to be derived by indirect extraction techniques based on originally saturated drillcore material. This requires thoroughly tested core preservation techniques and a concerted logistical effort extending from the drilling process to sampling to the laboratory investigations. In addition, the obtained data need to be carefully evaluated for potential perturbations induced, for example, by drilling activities, stress release, sample treatment in the laboratory, and to what degree they are representative of *in situ* conditions.

The matrix of crystalline rocks contains different types of pore spaces where different types of pore fluid reside (cf. /Pearson 1999, Waber and Smellie 2008a/ for discussion). This total pore space, the *physical porosity*, is described by the ratio of void volume to the total volume of the rock. It includes the volume not occupied by mineral grains such as pore spaces between mineral grains, dead-end pores, microfractures, porous minerals (often secondary minerals) and mineral fluid inclusions /Norton and Knapp 1977/. The *connected porosity* of a rock describes the volume of connected pore space between mineral grains and is smaller than the total porosity. Exchange between (quasi) stagnant porewater and flowing groundwater can only occur in the porosity accessible for solute transport. Transport of a substance can take place either by advection or by diffusion and only through pores of which the minimum pore throat size is larger than the maximum size of the substance transported and where no charge exclusion effects occur.

In the case of advective flow and transport, the Darcy flux and the linear velocity of a tracer are related by the *advective transport porosity*. This advective transport porosity does not include isolated pores or dead-end pores and is smaller than the connected porosity. In the low permeable rock matrix, solute transport by diffusion becomes important. The porosity accessible to diffusion, the *diffusion porosity*, is determined by various diffusion experiments (in-, out-, and through-diffusion). As for other porosity measurements, the porosity derived from diffusion experiments might have different numerical values depending: a) on the rock texture (e.g. anisotropy due to foliation and bedding, grain size variations), and b) on the solute used in the experiments (e.g. ions with large hydration spheres versus ions with small hydration spheres). For the diffusion of the water molecules themselves, the diffusion porosity becomes close to the water-loss porosity. For the diffusion of solutes the diffusion porosity is less than the water-loss porosity, but higher than the advective transport porosity (cf. /Pearson 1999/ for discussion).

The bulk of the fluid contained in the physical porosity of the rock matrix, the *'matrix pore fluid'*, cannot be sampled by conventional groundwater sampling techniques. Because of the above-mentioned different accessibility of the total pore space, the matrix pore fluid is composed

of different fluid types. These include: a) the water in microfractures where minor advective flow might occur, b) the water in the pore space of a rock that is only accessible by diffusion, c) the water residing in isolated pores, and d) the fluid enclosed in mineral fluid inclusions.

The term *'porewater'* as used here refers to the water in the connected pore space of the rock matrix that is accessible for diffusion-dominated interaction with groundwater circulating in nearby (micro-) fractures.

A chemical and isotopic signature established in the porewater at a certain time in the hydrogeological evolution of a site might be preserved over long, geologic time periods. The degree of the preservation of chemical and isotopic signatures depends on: a) the distance of the porewater sample from the nearest water-conducting fracture in three dimensions (i.e. the fracture network), b) the solute transport properties of the rock (i.e. diffusion coefficient, porosity), and c) the period of constant boundary conditions (i.e. constant fracture-groundwater composition). Constant boundary conditions over the time period considered greatly facilitate the interpretation of an observed porewater signature. In reality, however, overlaps of changes induced by variable boundary conditions seem more common. This is certainly the case for the first few metres of the rock matrix adjacent to the nearest water-conducting fracture and over the time periods of concern here, i.e. the Holocene and Pleistocene, during which frequent climatic and hydrogeologic changes occurred. In addition, the significance of the signature (with respect to the measurement error) depends on the chemical gradient between porewater and fracture groundwater.

During the porewater/fracture groundwater interaction, the porewater composition is subjected to modification by the diffusive exchange (transient vs. steady state, species-specific diffusion coefficients) and water-rock interactions (larger reactive mineral surface area, longer residence time) in addition to the evolutionary processes identified for the fracture groundwaters. Furthermore, several of the fracture groundwater end-members have similar water isotopic, but different chloride compositions and vice versa. Therefore it is not surprising that a different relationship between these natural tracers is established in the porewaters compared to the fracture groundwaters where these components have been used successfully to trace the input of post-glacial meltwater, Littorina/Baltic Sea and recent meteoric end member types into the bedrock groundwater system /Laaksoharju et al. 2009, Gimeno et al. 2009/. The different distances of porewater samples to the nearest water-conducting fracture and the species-specific diffusion coefficients mean that the superposition of two sequential events will result in different signatures. The behaviour of porewater signatures therefore differs from that of two mixing components mainly because it depends on the time of interaction with a specific fracture groundwater composition. In turn, the porewater might still have retained signatures of fracture groundwaters (e.g. glacial, warmer climate) that have been long since flushed from the fracture system by more recent fracture groundwaters.

Within the SKB Site Investigation programmes at Oskarshamn and Forsmark, porewater investigations have been developed and tested for the first time in the crystalline rocks. The investigations aimed a) to elaborate the hydrogeological evolution of a site due to the potential of porewater acting as an archive of what has happened over recent geological time (i.e. several hundreds to a few millions of years), b) to define the potential of matrix diffusion to contribute to the retardation of radionuclide transport in the geosphere, and c) to provide the basis for a better constrained treatment of the interaction between porewater and repository barrier materials (e.g. bentonite, canister), potentially leading to a deterioration in their physical properties. For safety assessment considerations, it is therefore important to know the composition of the porewater and its evolution over recent geological time, certainly during the last thousands to hundreds of thousands of years in accordance with the expected lifespan of a repository.

From the Laxemar subarea samples for porewater investigations have been collected from three different boreholes (KLX03, KLX08 and KLX17A). These deep boreholes have been drilled at different inclinations up to 1,000 m borehole length and they were selected because they are situated in different fracture and hydraulic domains and also penetrate different deformation zones (cf. /Wahlgren et al. 2008, Rhén et al. 2009/). In contrast, the mineralogy of all encountered rocks is similar being mainly of granitic to quartz-monzodioritic compositions with some minor intercalations of more mafic, dioritic rock types. In all three boreholes hydraulic logging has been performed and some groundwater samples could be collected from water-conducting fractures.

Where available, the chemical and isotope composition of the porewater is compared to that of fracture groundwater sampled from nearby water-conducting fractures. Preferably such groundwater is sampled from fractures isolated by inflatable packers in the same borehole, or in neighbouring boreholes at similar depth.

This report summarises the results obtained from the porewater investigations carried out on rock material from boreholes KLX03, KLX08, and KLX17A from the Laxemar subarea. The data are compared to the hydraulic data and fracture groundwater data obtained from the same boreholes and collectively interpreted in a palaeo-hydrogeological evolution sense. A detailed description of the applied concepts and methods is given in /Waber and Smellie 2008a/.

2 Hydrogeological setting of porewater samples

From the Laxemar subarea rock matrix porewater has been analysed from three boreholes (KLX03, KLX08 and KLX17A) that were drilled at different locations at an elevation above sea level of about 15.8 m, 24.3 m and 27.6 m, respectively (Figure 2-1). The boreholes were drilled at different inclinations up to 1,000 m borehole length into different rock types and different hydraulic and structural domains. The major rock types encountered by the boreholes are Ävrö granite and quartz monzodiorite with some minor intercalations of more mafic, dioritic rock types. Hydraulic logging has been performed on all three boreholes, but unfortunately only a few reliable CCC (Complete Chemical Characterisation) groundwater analyses exist from water-conducting fracture zones /Laaksoharju et al. 2009/. No drillcore samples exist from any of the upper 100 m (along borehole) percussion drilled part of the boreholes.

Borehole KLX03 was drilled at an inclination of 75° in hydraulic domain HRD-C, which is comprised mostly of Ävrö granite to around 620 m borehole length and thereon of quartz monzodiorite down to the bottom of the borehole at 1,000.4 m borehole length. The major deformation zone ZSMEW946A was intersected between about 722–842 m borehole length /Wahlgren et al. 2008/.

Borehole KLX08 is situated northeast of KLX03 and comprises predominantly of Ävrö granite until a transition to quartz-monzodiorite at 930 m borehole length. It was drilled at an inclination of 60° initially in hydraulic domain HRD-N down to about 221 m borehole length, then through hydraulic domain HRD-EW007 from 211 to 702 m borehole length and finally through hydraulic domain HRD-C to the end of the borehole at 991 m borehole length, similar to KLX03. In the Ävrö granite dominated interval from about 600 m to 702 m borehole lengths significant horizons of diorite/gabbro, up to 30 m in thickness, occur. Borehole KLX08 intersects two major deformation zones (ZSMEW007A at about 210 m to 300 m and ZSME946A at about 480 m borehole length) and smaller possible deformation zones between about 600 m and 660 m borehole length.

The westernmost borehole KLX17A was drilled at an inclination of about 61° down to 701 m borehole length through mainly Ävrö granite which continues to the bottom of the hole. It represents hydraulic domain HRD-W and intersects two major deformation zones at shallow levels, ZSMEW900A (100–130 m borehole length) and ZSMEW900B (220–250 m borehole length). A continuous profile of porewater samples was collected for some 20 m from a water-conducting fracture in the ZSMEW900A deformation zone down into the adjacent rock matrix, to investigate the most recent (i.e. Holocene to Pleistocene) interaction between porewater and fracture groundwater.

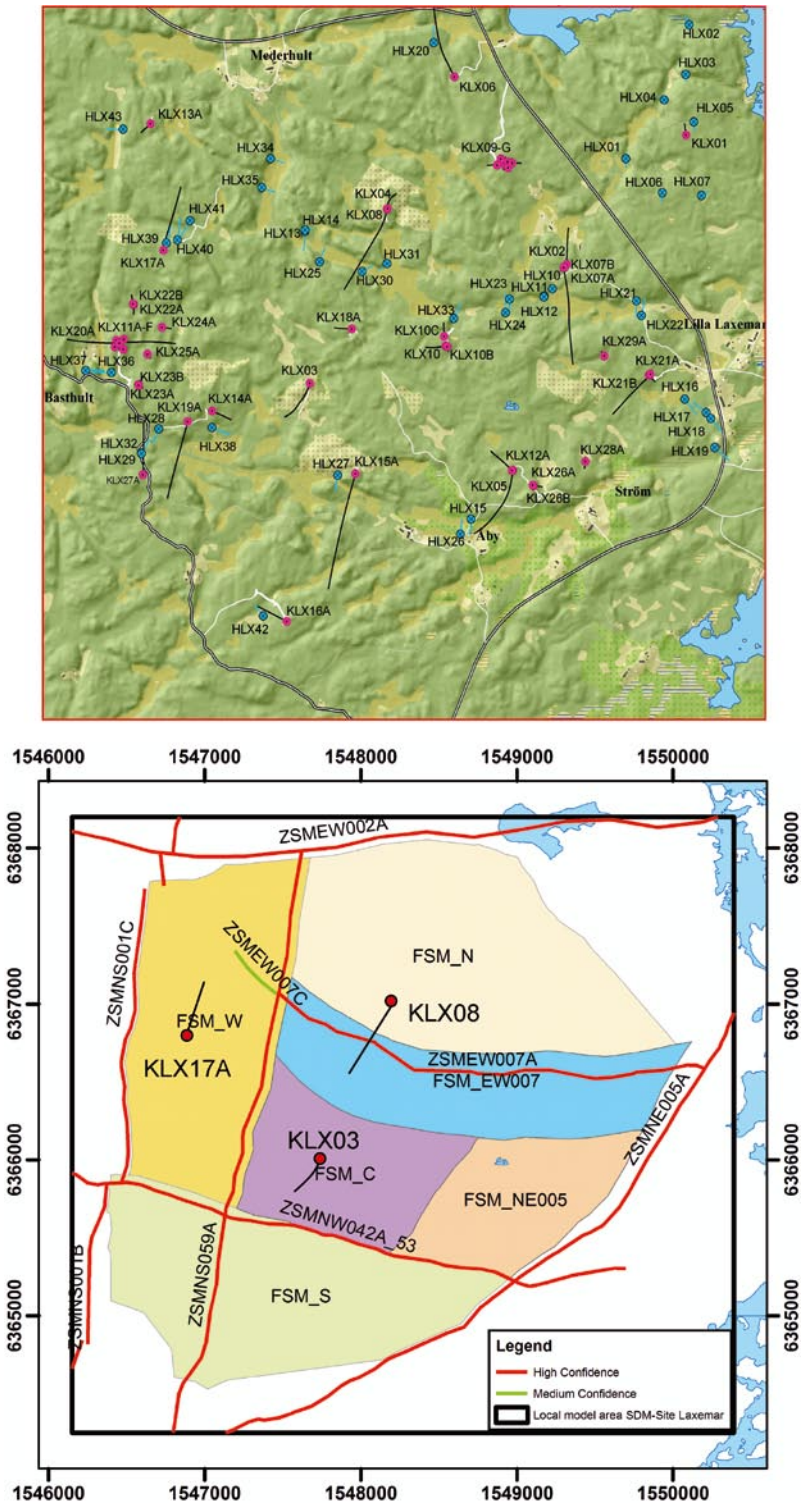

Figure 2-1. *Map (upper) showing the localisation of boreholes KLX03, KLX08, and KLX17A used for porewater investigations in the Laxemar subarea and a simplified map (lower) showing the relationship of the boreholes to the majordeformation zones and the fracture domains (as indicated as coloured sectors) after /Rhén et al. 2008, Wahlgren et al. 2008/.*

3 Sampling strategy, methods and data uncertainty

As mentioned above, porewater residing in the rock matrix cannot be sampled by conventional groundwater sampling techniques and needs to be characterised by indirect extraction techniques applied to drillcore material. Such indirect techniques present several challenges concerning on-site drilling and sampling and the experimental and analytical procedures conducted in the laboratory on the selected drillcore material. A detailed description of the applied procedures and evaluation of potential perturbing effects (e.g. different sources for solutes in experiment solutions, desaturation and stress release of rock samples etc.) can be found in /Waber and Smellie 2006b and 2008a/.

The success of porewater investigations relies on obtaining the original freshly drilled saturated rock core material from boreholes and immediate on-site conditioning of such material within minutes after drillcore recovery. This requires a concerted effort between the teams on the drill site and in the laboratory, including immediate sample preservation on site, rapid transport of the sample to the laboratory and sample preparation for the individual experiments. In addition, rather large sized core samples are required due to the low porewater content and to minimise possible artefacts induced from the time of drilling to the time of analysis. Finally, there is also the great difficulty attached to predicting the location and orientation of a water-conducting fracture in a future borehole. Therefore, the porewater investigations initially aimed to characterise the composition of porewater that resides in as large as possible non-fractured and homogeneous rock portions. In these cases, core samples have been collected at regular intervals of about 50 metres along complete core lengths at least 5 metres from the nearest open fracture visible in the drillcore. Only at a later stage in the programme has sampling also focussed on a fracture profile where samples were collected continuously along a profile extending (preferably perpendicularly) from a water-conducting zone into the undisturbed host rock matrix.

For legibility reasons, the samples in this report are labelled with increasing numbers with increasing depth (i.e. borehole length) using the borehole name as prefix (Table A-1); similar labelling was used for the laboratory studies /Waber and Smellie 2006a, b, c, 2008b/. The conversion of this sample description to the SKB sample number is given in Table A-1.

In order to differentiate generally between an approximate borehole length or borehole elevation, and more specifically when designating accurately a depth interval or sample location, the following terminology is used:

- A specific depth interval is labelled as –404 to –420 m, i.e. elevation between –404 to –420 m.a.s.l (metres above sea level).
- An approximate depth or depth interval is labelled ‘about or approximately 500 m depth’ or ‘about or approximately 500 to 700 m of depth’.
- Any location related to borehole length is signified specifically as ‘432 m borehole length’, or generally as ‘about or approximately 500 m borehole length’ or ‘about or approximately 500 to 700 m borehole length’.
- Repository depth refers to –400 to –700 m elevation.

(Note: The data presented and discussed in this report are based on primary borehole length measurements taken in the field and the elevation data calculated in Sicada. Adjusted elevation data based on single-hole interpretation measurements would only minimally modify the results, and therefore in this context are regarded to be unimportant for plotting purposes).

3.1 Sampling for porewater investigations

From the three boreholes drillcore sections of about 25–45 cm in length were taken at regular depth intervals of approximately 50 m from homogeneous, non-fractured bedrock volumes at least 5 metres away from any water-conducting fractures. In addition, sections were collected continuously along a profile extending from a water-conducting zone in deformation zone ZSMEW900A

encountered by borehole KLX17A starting at an elevation of about –70 m. The depth along the borehole and the elevation, the latter corresponding to the sample reference depth corrected for borehole inclination and altitude, of the samples are given in Table A-1. This table contains additional information about the lithology of the samples and their relation to water-conducting fractures.

To preserve the original water saturated state of the rock material and to minimise potential perturbing effects induced by exposure of the rock sample to air, the drillcore samples were immediately gently cleaned using a dry towel following drilling and selection, then wrapped into two heavy-duty PVC bags and finally in plastic coated aluminium foil. All three layers were repeatedly flushed with nitrogen, evacuated and heat-sealed. The time for the sample selection and packing was minimised to less than 10–15 minutes after core recovery. The packed samples were then air freighted to the laboratory in Bern where they were immediately stored at 4°C in a cool room and prepared for the various measurements and experiments within about 24 hours after arrival.

3.2 Porewater data

Information about the chemical and isotopic composition of porewater in the low permeability rock matrix was obtained by combining the data of different porewater extraction experiments, different porosity measurements and geochemical modelling.

Following arrival at the laboratory, the core sections were unpacked, wrapped in parafilm™ to minimise evaporation, and cut by dry sawing for sub-samples to be used for out-diffusion experiments, diffusive equilibration technique for water isotopes (diffusive isotope exchange), determination of the water content, grain density, and mineralogical investigations where applicable.

3.2.1 Water content and porosity

The water content of the rock samples was determined by two largely independent methods. It should be noted that reliable results for the water content and the water-loss porosity are only obtained if the measurements are conducted on originally saturated core material, i.e. no evaporation of porewater and/or re-saturation of the rock sample has occurred.

The first method is the commonly used gravimetric measurement of the water loss from the saturated to the desaturated state of a rock sample. Here the water content by drying, WC_{Drying}, has been derived by heating the samples at 105°C until the onset of stable weight conditions (± 0.002 g). If possible, three sub-samples consisting of an intact piece of core and broken core material each with a mass between about 100 g and 500 g were dried to stable weight conditions to account for effects of textural heterogeneity of the rocks and artefacts, which may have been induced by drilling and/or possible stress release. Depending on the sample mass, the drying process lasted up to 20 weeks for the low permeable rock samples from the Laxemar subarea. For about half of the samples, the core section used in the out-diffusion experiment with a mass of about 1,000 g was also dried to stable weight conditions, something which could take up to 9 months.

In the second method, the water content, $WC_{IsoExch}$, was derived by the diffusive equilibration technique for water isotopes (see below). As for the isotopic composition, the relative error of $WC_{IsoExch}$ could be reduced from about 5–10% in the early stages to less than 3% in the final stages of the Laxemar site investigation programme.

The water-loss porosity or connected porosity, Φ_{WL}, was calculated from the water content derived by either of the above methods and known grain density, ρ_{grain}, according to:

$$\Phi_{WL} = \frac{WC_{wet} \cdot \rho_{grain}}{WC_{wet} \cdot \rho_{grain} + (1 - WC_{wet}) \cdot \rho_{water}} \quad (1)$$

where WC_{wet} is the water content based on the wet weight of the sample, ρ_{grain} is the grain density and ρ_{water} is the density of the porewater.

Alternatively, the bulk wet density, $\rho_{bulk,\,wet}$, was determined from the volume and mass of large-scale samples used for the out-diffusion experiments /Waber and Smellie 2006a, c, 2008b/. For these samples Φ_{WL} is approximated according to:

$$\Phi_{WL} = WC_{wet} \cdot \frac{\rho_{bulk,\,wet}}{\rho_{water}} \qquad (2)$$

3.2.2 Out-diffusion experiments

Experimental Set-up

Out-diffusion experiments were performed on complete core samples of about 120 mm to 190 mm in length and about 50 mm in diameter by immersion in ultra-pure water (typically between 80–110 mL). To accelerate the out-diffusion, the vapour tight PVC containers containing the core samples were placed in a constant temperature (45°C) water bath that was gently rotated throughout the experiment to avoid chemical stratification of the experiment solution. Blank experiments were run with each batch of prepared drillcore samples. The weight of the core sample (between about 580–1,040 g, see Appendix), the experiment container, and the artificial test water used was measured before and after the experiment to ensure that no loss of test water occurred during the entire experiment. Weighing of the core before and after the experiment gives additional valuable information about the saturation state of the core at the beginning of the experiment.

After equilibrium with respect to chloride was achieved (see below), the core was removed from the container and the experiment solution was immediately analysed for pH and alkalinity (by titration). The remaining solution was split into different aliquots for chemical and isotopic analyses. Major cations and anions were analysed by ion-chromatography with a relative error of ± 5% (2σ) based on multiple measurements of standard solutions. Dissolved silicon was analysed by photometry with a relative error of ± 5% (2σ). In all experiments batches, cation and anion concentrations of the final solution of the blank experiments were below or at detection limit, which is 0.1 mg/L for Cl^-. On aliquots of some selected samples, chlorine ($\delta^{37}Cl$) and strontium isotope ($^{87}Sr/^{86}Sr$) analyses were performed by mass spectrometry at the University of Waterloo and University of Bern, respectively.

The complete data sets for the individual boreholes are given in /Waber and Smellie 2006a, b, c, 2008b/.

Equilibrium control of the out-diffusion experiment

The out-diffusion experiments were run under closed system conditions. The control of the mass flux of chloride and, towards the end of the experiment, the equilibrium control of the diffusive exchange occurred by taking small samples (0.5 mL) of the experiment solution at regular intervals and analysing their anion content. The experiments were terminated and the supernatant solution removed for chemical and isotope analyses well after the chloride concentrations had reached a plateau as a function of time, i.e. when equilibrium conditions were reached. Modelling of these time series gave indications about the marginal zone in the drillcore sample disturbed by the drilling process (drilling disturbed zone, DDZ) and stress release and possible contamination by drilling fluid induced by such disturbance of the drillcore material. It further allowed an estimation of the chloride pore diffusion coefficient (Chapter 5). The experiments run at 45°C were terminated after about 90–110 days and those run at 20°C after about 190 days. The extracted 0.5 mL time-series samples were analysed using specially designed ion chromatographic equipment. The analytical error of these determinations is about ± 10% (2σ) based on multiple measurements of the standard solutions of equally small volumes.

Conversion of final solution concentrations to porewater concentrations

Porewater concentrations can be converted from the chloride concentration of the final experiment solution by mass balance calculations given that equilibrium conditions in the out-diffusion experiment are achieved. At equilibrium, the chloride concentration in the connected porosity of the rock

sample will be equal to that of the experiment solution. With knowledge of the mass of porewater in the rock sample, the chloride concentration of the porewater can be calculated according to:

$$C_{PW} = \frac{\left(M_{PW} + M_{TEWi} - \sum^{n} M_S\right) \cdot C_{TEW\infty} - (M_{TEWi} \cdot C_{TEWi}) + \sum^{n} M_S \cdot C_S}{M_{PW}} \quad (3)$$

For the analysis of the time series with a model neglecting the removal of solution (cf. Chapter 5), the measured concentrations were approximately corrected according to:

$$C_{equil,corrected} = \frac{C_{TW_\infty} \cdot \left(M_{TEWi} - \sum^{n} M_S\right) + \sum^{n} M_S C_S}{M_{TEW_i}} \quad (4)$$

where C = concentration, M = mass, n = number of samples and the subscripts PW = porewater, TEW = experiment solution, S = small-sized sample taken for chloride time-series, i = at beginning of experiment, and ∞ = at end of experiment.

The last term in equation (3), $\Sigma M_S \cdot C_S$, describes the amount of chloride removed from the initial experiment solution by the chloride time-series samples. The final measured concentration of chloride in the experiment solution, $C_{TEW\infty}$, is corrected for the mass of solution removed by the chloride time-series samples from the initial mass of the experiment solution, M_{TEWi}, in order to obtain the Cl^- concentration in the experiment solution at steady state, $C_{equil.corrected}$ (equation 4). A correction for chloride in the initial experiment solution ($M_{TEWi} \cdot C_{TEWi}$) is necessary if this solution is not entirely free of chloride.

The unit of porewater concentrations is given as mg/kg_{H2O} (and not mg/L) because it is derived on a mass basis rather than a volumetric basis. This is because the density of the porewater is not known beforehand. In reality and within the overall uncertainty band, the difference between mg/kg_{H2O} and mg/L becomes only important at an ionic strength of the calculated porewater above that of sea water (~0.7 M) corresponding to a total mineralisation of ~35 g/L.

3.2.3 Diffusive exchange technique for water isotopes

The stable isotope composition of the porewater was determined by the diffusive isotope exchange technique that was originally developed for argillaceous rocks /Rogge 1997, Rübel 2000/ and later adapted to crystalline rocks /Waber and Smellie 2005, 2006a, 2008a/. This method is based on the premise that the known water isotope composition of test water will equilibrate with the unknown composition of porewater in a rock sample using the gas phase as a diaphragm in a vapour-tight container. For each rock sample, two equilibration experiments with test water of different isotopic composition are conducted in a vapour-tight glass container. After complete equilibration (commonly about 20–30 days, depending on the size and hydraulic properties of the rock samples), the two test water are analysed by conventional ion-ratio mass spectrometry with the results being reported relative to the VSMOW standard with a precision of ± 0.15‰ for $\delta^{18}O$ and ± 1.5‰ for $\delta^{2}H$.

The water content of a rock sample and the stable isotope composition of its porewater are calculated from mass balance relationship of the experiments according to:

$$M_{PW} \cdot C_{PW}\big|_{t=0} + M_{TW} \cdot C_{TW}\big|_{t=0} = \left(M_{PW} + M_{TW}\right) \cdot C_{TW}\big|_{t=\infty} \quad (5)$$

where M = mass, C = isotope ratio, PW = porewater, TW = test water, and the concentrations on the left side of the equation are prior to equilibration (t = 0), while the concentration on the right side is after equilibration is achieved (t = ∞) in the experiment.

Each equilibration experiment reveals two independent equations of the type (5) for $\delta^{18}O$ and $\delta^{2}H$. Conducting two experiments with different test water and thus obtaining four equations allows the calculation of the three unknowns, which are the porewater mass and the $\delta^{18}O$ and $\delta^{2}H$ of the porewater.

By applying Gauss' law of error propagation, it can be shown that the error of the isotope determination depends mainly on the mass ratio of test water to porewater and on the difference in isotopic composition between the two water types. While the latter is easy to achieve, the optimisation of the mass ratio of test water to porewater is more difficult in crystalline rocks with water contents of generally below 0.2 wt.%. During the course of the Laxemar site investigation programme, the propagated error of the isotope diffusive-exchange technique could be reduced from about ± 2‰ VSMOW for $\delta^{18}O$ and ± 17‰ VSMOW for $\delta^{2}H$ in the early stages (boreholes KLX03 and KLX08) to about ± 0.8‰ VSMOW for $\delta^{18}O$ and ± 7‰ VSMOW for $\delta^{2}H$ in the final stages (borehole KLX17A) by optimising experimental and analytical procedures.

3.3 Data uncertainty

From equation (3) it can be seen that the calculation of the concentration of Cl^- (or any other chemically conservative element) in the porewater from out-diffusion concentrations is inversely proportional to water content. The uncertainty of the indirectly derived porewater concentrations thus strongly depends on the accuracy of the water content determination and the degree to which the measured values represent *in situ* conditions. This becomes especially important in rocks with low water content such as the crystalline rocks of Laxemar.

Effects that could deviate the measured water content from *in situ* conditions are related to desaturation and/or resaturation of new pore space created by stress release and the drilling disturbed zone. By applying adequate handling techniques (e.g. immediate vapour tight packing on-site after recovery of the core), desaturation can be minimised if not excluded (Chapter 4) and the effects related to stress release and the drilling disturbed zone are limited to the time the core is in contact with the drilling fluid. Drilling fluid would potentially penetrate the newly created pore space and the measured water content would overestimate that present *in situ*. Note that this effect inevitably will occur during resaturation of a drillcore sample, so that water content measurements by resaturation become less reliable (cf. /Eichinger 2009/ for discussion). As a consequence, the calculated porewater Cl^- concentration would be either too low (in the case where the drilling fluid is lower in Cl^- than the porewater) or too high (in the case of a high chloride drilling fluid) when compared to the *in situ* porewater.

The effects of contamination by drilling fluid induced by stress release and by the drilling process (drilling disturbed zone) have been investigated by /Waber et al. 2009/ on drillcore material from boreholes drilled with traced drilling fluid at Forsmark (borehole KFM02B) and at the Äspö HRL (borehole KA3386A06). As mentioned above, the drilling process and stress release could potentially create new pore space, which might get filled with drilling fluid. Besides the modification of the original water content, this would also result in a modification of the chemical and isotope composition of the porewater. This modification could be in both directions, i.e. towards dilution or enrichment of the original porewater, depending on the drilling fluid composition. In the drilling-fluid contamination study performed on drillcore material from boreholes drilled at Forsmark and at the Äspö HRL, the effect of drilling fluid contamination by stress release could be quantified as being less than 10% and that of the drilling disturbed zone as being less than 1% on the porewater content and composition. The degree of contamination strongly depends on the ratio between the surface area and the total mass of the drillcore sample used and the lower it becomes the smaller this ratio is. This is because the effects of stress release and the drilling process are most pronounced in the rim zone of a core containing the outermost mineral grain layer as e.g. previously illustrated by impregnation techniques /Lin Li 2001, Ota et al. 2003/. For the large kilogramme size samples used for out-diffusion experiments it could be concluded that for the granitic rocks of Forsmark the combined perturbation effects of the measurement of the *in situ* water content and the measurement of conservative porewater compounds can be minimised to less than 10% by adequate sample handling and conditioning in these low-permeability and low-porosity rock types /Waber et al. 2009/. The same uncertainty seems also adequate for the rocks from the Laxemar subarea in spite of their mineralogical and, at least in some cases, textural differences.

The uncertainty of indirectly derived porewater concentrations of conservative compounds is thus mainly related to natural textural heterogeneity of the rock sample and how well the sample mass used for the water content determination takes account of such heterogeneity. Effects of textural

heterogeneity (and possible influences by stress release) will result in a deviation of the measured water content that is inversely proportional to the mass of sample aliquots used. This results in a larger standard deviation for groups of samples with lower masses. The uncertainty band of a porewater concentration of a chemically conservative compound such as Cl or Br is thus best described by the standard deviation of water contents derived from multiple samples and/or to the cumulated analytical error of the water content determination and chemical analyses in the case of a large kilogramme size sample as used in the present out-diffusion experiments.

The uncertainty of the porewater isotope composition using the isotope diffusive-exchange technique is appropriately described by the error propagated according to Gauss. As shown by /Waber and Smellie 2008a/, contamination by drilling fluid would affect the calculated isotope composition only in the case where such contamination would exceed about 10%. Such a high contamination can be excluded based on the results of the drilling fluid contamination study mentioned above.

For the Laxemar subarea, it can thus be concluded that the water contents and water content porosity, the chemical and isotopic composition of porewater, and the pore diffusion coefficients derived by the applied indirect methods, appear indeed to represent *in situ* conditions within the given cumulative analytical uncertainties.

4 Water content and water-loss porosity

Water content, bulk density, and water-loss porosity were determined on originally saturated drill-core material of Ävrö granite (46 core samples), quartz monzodiorite (9 core samples), and diorite (4 core samples) from the Laxemar subarea. Of the Ävro granite samples, 18 out of the 46 are related to the continuously sampled fracture profile in borehole KLX17A. These samples suffered additional and different tectonic alteration compared to most other rock matrix samples, which were collected specifically from undisturbed and intact rock matrix portions. Therefore, the KLX17A fracture profile samples are excluded from statistical considerations.

More than three quarters of the remaining 28 Ävro granite samples considered in the following discussion are located in the upper approximately 500 m of bedrock, while only 6 samples come from the next 500–760 m depth interval. This contrasts with the occurrence of the quartz monzodiorite samples (between about 600–950 m depth) and the diorite samples (between about 490–580 m depth, with one exception). The different depth distribution of the various rock types needs to be kept in mind for the evaluation if the measured petrophysical parameters represent indeed *in situ* conditions. Furthermore, it should be kept in mind that a borehole provides a limited representation of the physical variability of the rock matrix and nearby fractures that are not intersected by the borehole, but that might well have an influence on the porewater extracted from a sample.

4.1 Water content

4.1.1 Water content by gravimetry

All investigated rock samples from the Laxemar subarea have a gravimetrically determined water content of below 0.4 wt.% and for about 50% of the samples it is below 0.2 wt.% (Table A-1). Such small water contents are sensitive to even small influences of contamination by drilling fluid and/or evaporation during sample handling.

Effects of drilling fluid contamination are less than 10% based on *in situ* experiments performed with traced drilling fluid (cf. Section 3.3 and /Waber et al. 2009/). The effect of partial evaporation is also negligible for most samples as indicated by the comparison of the two largely independent methods, i.e. determination of the water content by drying to stable weight conditions (gravimetry, WC_{Drying}) and by the diffusive isotope exchange technique, $WC_{IsoExch}$ (cf. /Waber and Smellie 2008a/ for discussion). As can be seen from Figure 4-1, larger deviations in water contents obtained by the two methods are only observed for samples located in the near vicinity of water-conducting fractures, i.e. in tectonically altered zones, and, with one exception, for shallow Ävro granite samples (mainly from the fracture profile sampled in KLX17A). It appears that the larger deviation between the two methods is related to the textural heterogeneity and alteration state of such samples as reflected by the large standard deviation of the gravimetric water content determined on multiple aliquots of the drillcore samples. Thus, the majority of the water contents obtained from originally saturated samples represent the water content present in the rock under *in situ* conditions.

The gravimetric water content of rock samples from boreholes KLX03, KLX08 and KLX17A (deeper levels only) is larger in the Ävrö granite (0.26 ± 0.08 wt.%, n = 28) compared to the diorite (0.16 ± 0.05 wt.%, n = 4) and the quartz monzodiorite (0.14 ± 0.07 Vol.%, n = 9). None of the rock types show a correlation between water content and sample depth. However, a general trend towards decreasing water contents with increasing depth is observed due to the depth distribution of the different rock types (see above). Similarly, and as mentioned above, there exists a correlation between water content and the distance of the porewater sample to the nearest water-conducting fracture (Figure 4-1 right, cf. also Section 4.3).

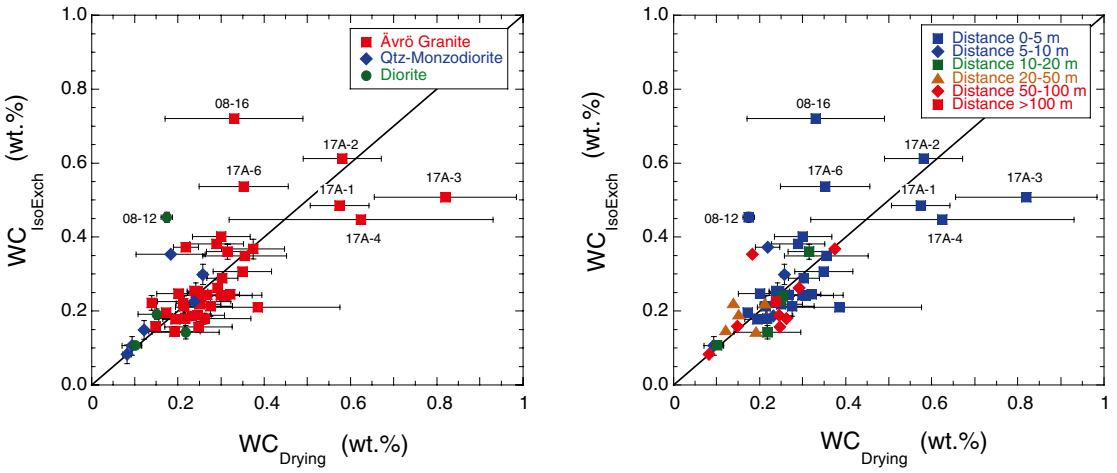

Figure 4-1. *Comparison of the gravimetric water content derived by drying to stable weight conditions and the water content derived by the diffusive isotope exchange technique. Left: water contents as a function of rock type, right: water contents as a function of the distance between the porewater sample and the nearest water-conducting fracture. Larger deviations between the two methods are only observed for samples located close to a water-conducting fracture (sample coding: 08-xx = samples from borehole KLX08, 17A-xx = samples from borehole KLX17A).*

4.1.2 Water content by the diffusive isotope exchange technique

The water content derived via isotope exchange between porewater and test water using the vapour phase as a diaphragm is similar or identical to the gravimetric water content (Figure 4-1, Table A-1) for most samples. Exceptions are related to a few samples collected in or near the tectonically altered fracture zones in boreholes KLX08 and KLX17A (Figure 4-1, right). In the course of the Laxemar site investigations the error attached to this water content could be reduced by method improvement.

The water contents derived by the diffusive isotope exchange technique describe the same general trends as those derived by gravimetric methods. The good agreement between the differently, largely independently derived water contents gives confidence that the measured value represents the water content as present under *in situ* conditions.

4.2 Bulk density

Bulk density measurements were derived from the wet mass and volume of the large-sized drillcore sample used in the out-diffusion experiments (Table A-2). The average bulk wet density is lowest for the Ävrö granite (2.70 ± 0.04 g/cm^3, n = 28), followed by the quartz-monzodiorite (2.79 ± 0.03 g/cm^3, n = 9) and the diorite (2.91 ± 0.09 g/cm^3, n = 4). This density distribution is consistent with the mineralogical composition of the different rocks, i.e. with the proportion of higher density mafic minerals (biotite, amphibole, epidote, titanite, opaque minerals) to lower density leucocratic minerals (quartz, feldspars, mica; cf. /Waber and Smellie 2006b, Drake et al. 2006, Drake and Tullborg 2009a/).

4.3 Water-loss porosity

The Ävrö granite has the largest average water-loss porosity (0.69 ± 0.21 Vol.%, n = 28), followed by the diorite (0.45 ± 0.16 wt.%, n = 4) and the quartz monzodiorite (0.38 ± 0.20 Vol.%, n = 9).

The water-loss or connected porosity of the porewater samples displays a general trend towards decreasing values with increasing depth, independent of rock type (Figure 4-2, Table A-2). However, this trend appears to mimic more the dependency on the distance between the porewater sample and the nearest water-conducting fracture (Figure 4-2, right) as the open fracture frequency also generally decreases with increasing depth /Ehrenborg and Dahlin 2005, Dahlin and Ehrenborg 2006, Mattsson and Dahlin 2007/.

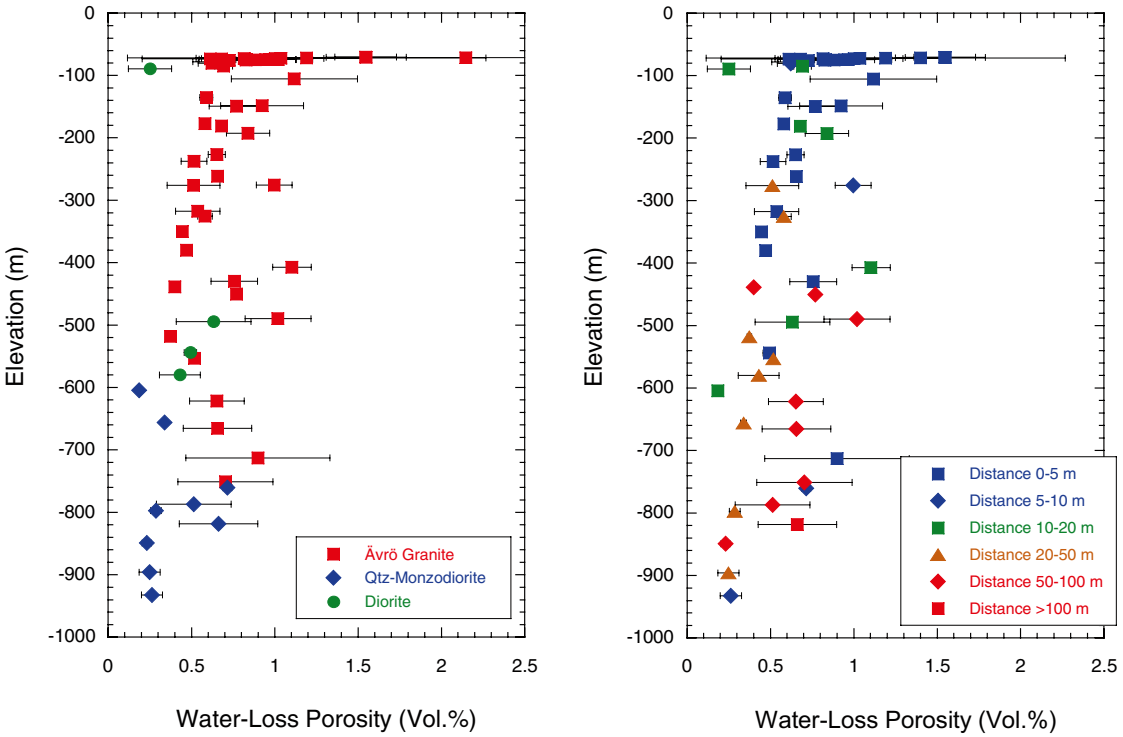

Figure 4-2. *Water-loss (connected) porosity as a function of rock type (left) and distance of the porewater sample to the nearest water-conducting fracture (right) versus elevation of porewater samples.*

Exceptions to this general trend can be seen between about –400 to –500 m and again between –640 to –820 m of elevation (Figure 4-2). In these intervals, the water-loss porosity is almost twice as high as the background value independent of lithology, of distance to the nearest water-conducting fracture, and of the borehole from which the samples were taken (Table A-2). In any case, the variability with depth of the water-loss (connected) porosity outside the uncertainty band is related to the degree of rock alteration, which is a product of past and present chemical and physical processes (for details cf. /Wahlgren et al. 2008 /).

5 Transport properties of rock matrix

In order to interpret the porewater data in a hydrogeological sense, the solute transport properties of the rock matrix need to be known. For the scale of the obtained rock samples, such information has been derived from measurements and modelling of Cl^- concentration time series obtained from the out-diffusion experiments as explained in Sections 5.1 and 5.2. In Section 5.3, the possible spatio-temporal evolution of porewater is discussed in response to the concentrations in the water-conducting fractures, using the obtained transport properties of the matrix.

5.1 Theoretical background

The out-diffusion experiments were performed on rock cores of about 200 mm in length and 50 mm in diameter, which were emplaced in vapour-tight containers containing water initially devoid of chloride (Section 3.2.2). The cores were completely immersed in this experiment solution such that all surfaces were exposed to the fluid. Note that the diffusion parameters have been derived from originally saturated core material with a total mass of about 1 kg (Table A-2), compared to conventional through-diffusion experiments performed on much smaller sized (about 50–100 g) and often re-saturated samples (e.g. /Skagius and Neretnieks 1986, Ohlsson 2000/).

In view of the dimensions of the core with its large cylindrical outer surface compared to the top and bottom surfaces, transport through the latter was neglected for the modelling and diffusion across the mantle surface only was considered. This allowed using a one-dimensional radial transport equation to describe diffusion within the rock:

$$\theta \frac{\partial C}{\partial t} = \frac{1}{r}\frac{\partial}{\partial r}\left(rD_e \frac{\partial C}{\partial r} \right) \quad , \qquad (0 < r < a) \tag{6}$$

where θ : volumetric water content accessible for Cl (equal to the water-loss or connected porosity if no anion exclusion occurs), C : porewater concentration, $D_e = \theta D_p$: effective diffusion coefficient with D_p : pore diffusion coefficient, a : radius of the core, r : space coordinate, and t : time.

The containers were gently rotated throughout the experiment to ensure complete mixing of the experiment solution. Thus, mixing of the fluid surrounding the core is much faster than the (expected) diffusion within the pores of the rock. It is then justified to assume that the solutes diffusing out of the core spread quickly within the surrounding experiment solution such that their concentration is uniform. In this case, the boundary condition at $r = a$ (i.e. at the interface of the core and experiment solution) becomes:

$$V_w \frac{\partial C_w}{\partial t} = -AD_e \left. \frac{\partial C}{\partial r} \right|_{r=a} \tag{7}$$

where V_w : volume of the experiment solution surrounding the core, $C_w = C(r = a,t)$: concentration in the experimental solution, $A = 2\pi aL$: cylindrical outer surface of the core, and L : length of the core. At $r = 0$, a zero gradient boundary condition applies. Initially, the concentration in the surrounding experiment solution is zero, whereas for the porewater a homogeneous value is assumed of $C(r < a, t = 0) = C_i$. This last assumption is reasonable considering the generally good match between data and the simulation results of the out-diffusion experiments.

An analytical solution for the above equations describing diffusion out of a cylinder into a well-mixed reservoir is /Crank 1975/:

$$C(r,t) = C_{eq} - (C_i - C_{eq}) \sum_{n=1}^{\infty} \frac{4(\alpha+1)\exp\left(-D_p q_n^2 t / a^2\right)}{\left(4 + 4\alpha + \alpha^2 q_n^2\right)} \frac{J_0(q_n r/a)}{J_0(q_n)} \tag{8}$$

Here, $\alpha = V_w/(\pi a^2 L\theta)$: ratio of the reservoir volume to the volume of porewater within the cylinder, $C_{eq} = C_i/(\alpha + 1)$: final equilibrium concentration, and the $q_n s$ are the positive, non-zero roots of

$$\alpha q_n J_0(q_n) + 2J_i(q_n) = 0 \quad (9)$$

which were obtained for each value of α numerically with a Newton-Raphson algorithm. The $J_0(x)$ and $J_i(x)$ are Bessel functions of the first kind of order zero and one, respectively. In applying the above solution, the small effect of the removal of the 0.5 mL aliquots from the reservoir solution on the transient phase is neglected. However, this effect was accounted for when calculating the initial concentration C_i from the final equilibrium concentration C_{eq} and the corresponding mass balance.

5.2 Diffusion coefficient of chloride

The time series data for dissolved Cl^- of all investigated porewater samples could be well described by assuming that the equilibration between the porewater and the surrounding solution occurred by diffusion in the porewater only. Equilibrium conditions with respect to Cl^- concentrations in the experiment solution and the remaining porewater were commonly reached after about 50 to 80 days of out-diffusion (Figure 5-1).

The obtained pore diffusion coefficients are tabulated in Table A-2 and the model fits graphically reproduced in Figure A-1. The pore diffusion coefficients for Cl^- largely independent from rock type although small differences related to the degree of foliation occur. The average pore diffusion coefficient for Cl^- in the Ävro granite is 5.8×10^{-11} m²/s ± 2.7×10^{-11} m²/s (n = 11), of the quartz monzodiorite 8.4×10^{-11} m²/s ± 5.5×10^{-11} m²/s (n = 3), and of the diorite 3.8×10^{-11} m²/s ± 4.1×10^{-12} m²/s (n = 2) at a temperature of 25°C. No clear correlation is established between the chloride pore diffusion coefficient and the sample depth and the same range of diffusion coefficients is covered at shallow and at great depth (Figure 5-2). Because also the water-loss porosity of the modelled samples shows no correlation with depth, but are rather homogeneously distributed between about 0.5 and 0.8 wt.% (Figure 5-2), there is also no trend between the effective diffusion coefficient for Cl^- and the sample depth. The values the of effective diffusion coefficient for Cl^- at 25°C vary between 1.2×10^{-13} and 1.2×10^{-12} m²/s for all samples.

The lack of any depth dependence of these parameters for the Ävrö granite and quartz monzodiorite is additional supporting evidence that the samples did not suffer from significant perturbations induced by stress release because a positive correlation with depth would be expected in such a case.

Figure 5-3 shows the relationship between the effective diffusion coefficient $D_e = \theta D_p$ of Cl^- at 25°C and the water-loss porosity of the corresponding rock samples. Two groups and a trend towards increasing D_e with increasing water-loss porosity appear to be present. The grouping is neither a function of rock type (Figure 5-3, left) nor a function of depth of the samples (Figure 5-2). Some indications exist, however, that the grouping might be related to the proximity of a porewater sample to the nearest water-conducting fracture (Figure 5-3, right). Interestingly, the samples, which are collected closer to such fractures have lower water-loss porosity and consequently a lower D_e of chloride. From the limited data set available it cannot be concluded if this reflects a minimisation of the connected pore space due to mineral alteration and secondary mineral formation during hydrothermal alteration and/or weathering of the rocks.

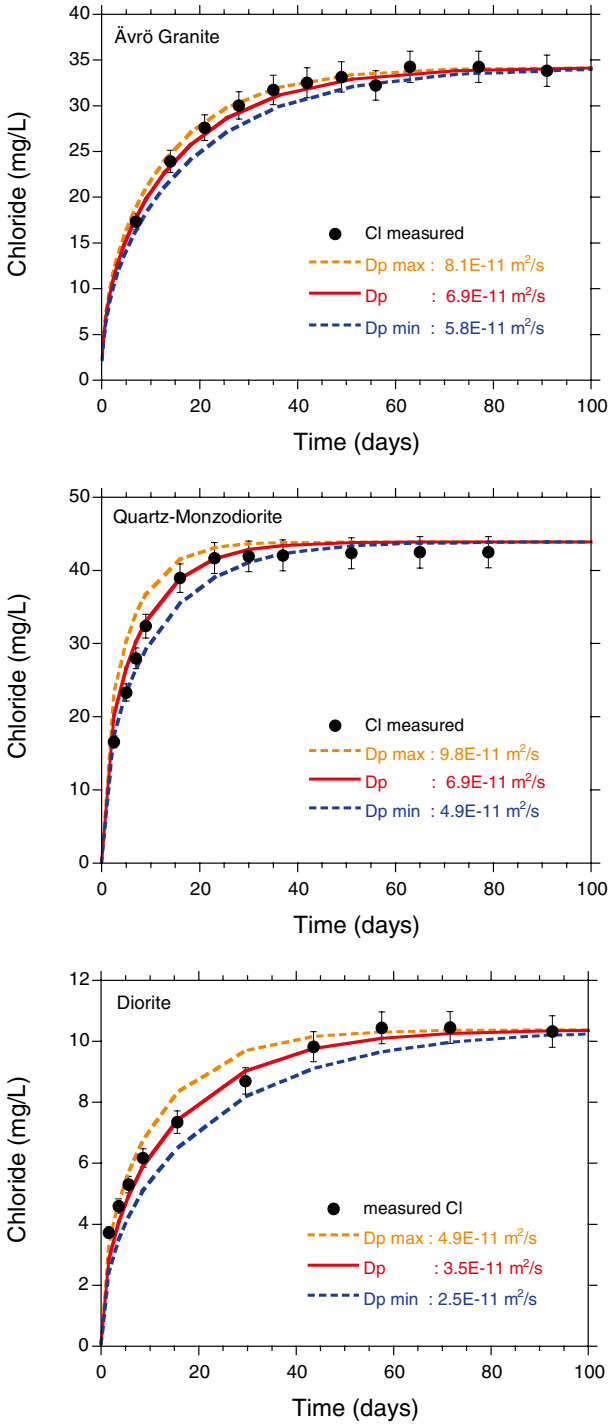

Figure 5-1. *Model fits to the measured chloride time-series data of the out-diffusion experiments. The examples show the best fit curves (red) delivering the pore diffusion coefficient, D_p, for chloride at 25°C in Ävro granite (sample KLX03-7), quartz monzodiorite (sample KLX03-16), and diorite (sample KLX08-13). The uncertainty range (D_p min and D_p max) is given by a factor of 2 around the best-fit value.*

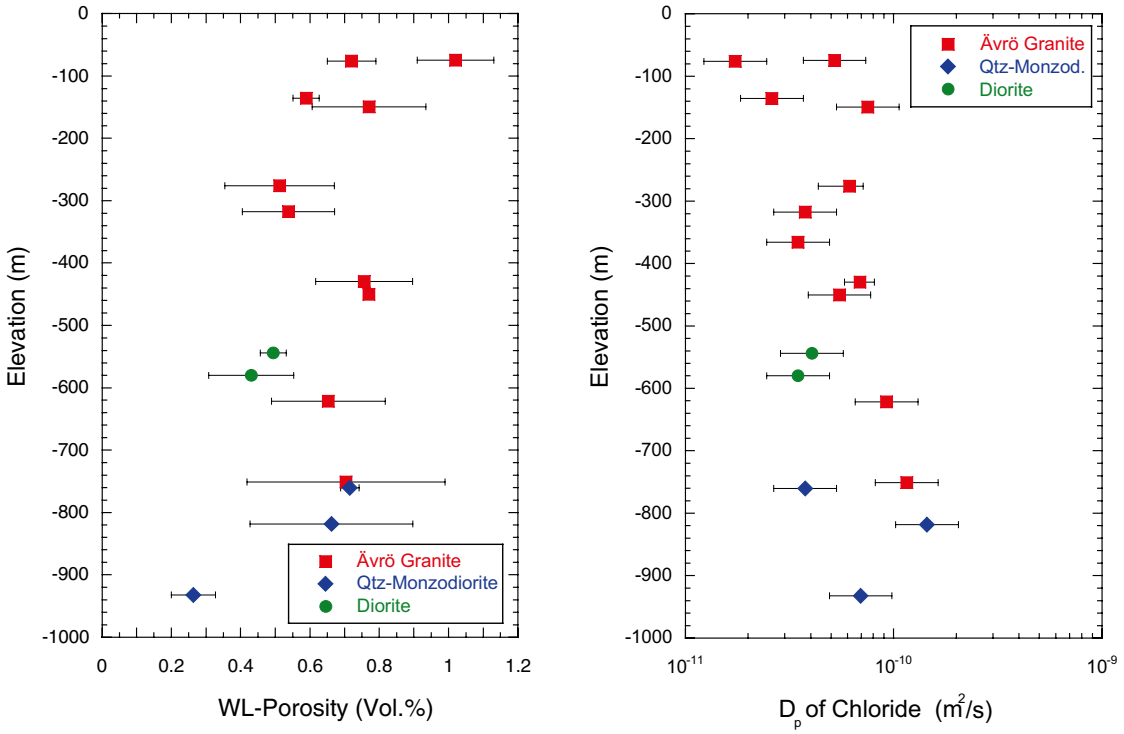

Figure 5-2. *Pore diffusion coefficients of chloride at 25°C (right) and water-loss porosity of corresponding samples (left) as a function of rock type and elevation of porewater samples. Error bars indicate the standard deviation of multiple determinations of the water-loss porosity and the uncertainty range for the pore-diffusion coefficients given by a factor of 2 around the modelled best fit to the measured data (see text).*

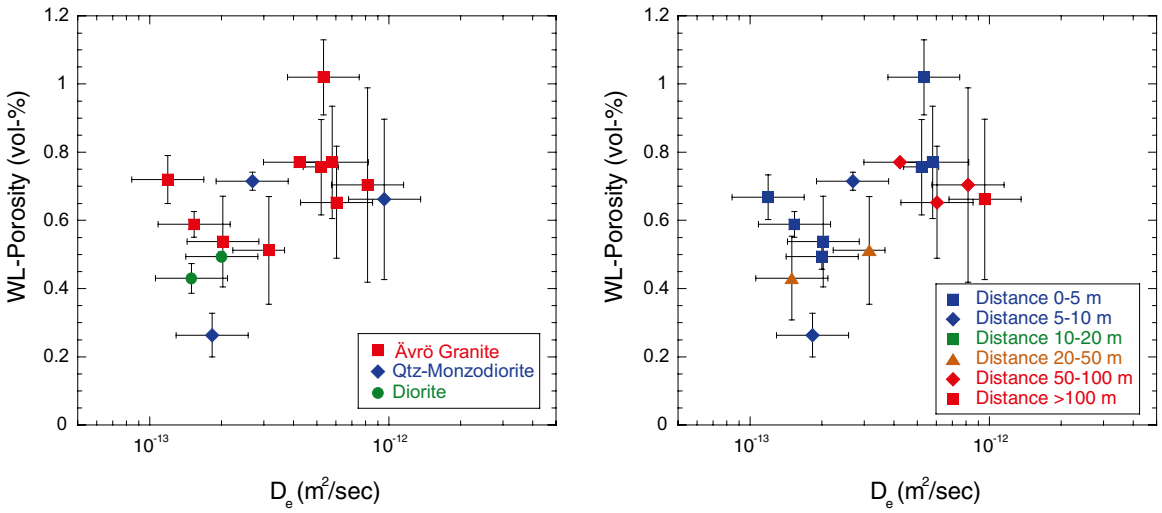

Figure 5-3. *Effective diffusion coefficient of chloride at 25°C versus the water-loss porosity of corresponding samples and as a function of rock type (left) and distance of the porewater sample to the nearest water-conducting fracture (right). Error bars indicate the uncertainty range of D_e given by the difference of a factor of 2 around the best fit for D_e (cf. Figure 5-1) and the standard deviation of multiple water-loss porosity determinations.*

5.3 Scenarios of diffusive exchange

With diffusion being identified as the dominant solute transport process in the rock matrix, the chemical and isotopic concentration of the porewater sample can be brought into an evolutionary context as a function of time (or space) using the fracture groundwater as boundary conditions for the diffusion domain. Figure 5-4 illustrates schematically the concentration change induced in a porewater sample as a function of distance to the nearest water-conducting fracture and for time periods of 6,000 years and 12,000 years. In such a hypothetical system this could, for example, approximately correspond to the time of ingress of Littorina water and the last deglaciation melt-water, respectively. A pore diffusion coefficient for chloride, Dp_{Cl}, at 25°C of 5.8×10^{-11} m²/s corresponding to the average of the measured values for the Ävrö granite was used for the calculations. Note that at *in situ* temperatures of 10°C the Dp_{Cl} would be reduced by about a factor of 1.5 and the distances shown in Figure 5-4 and given below would be reduced by about a factor of 1.2 ($\sqrt{1.5}$).

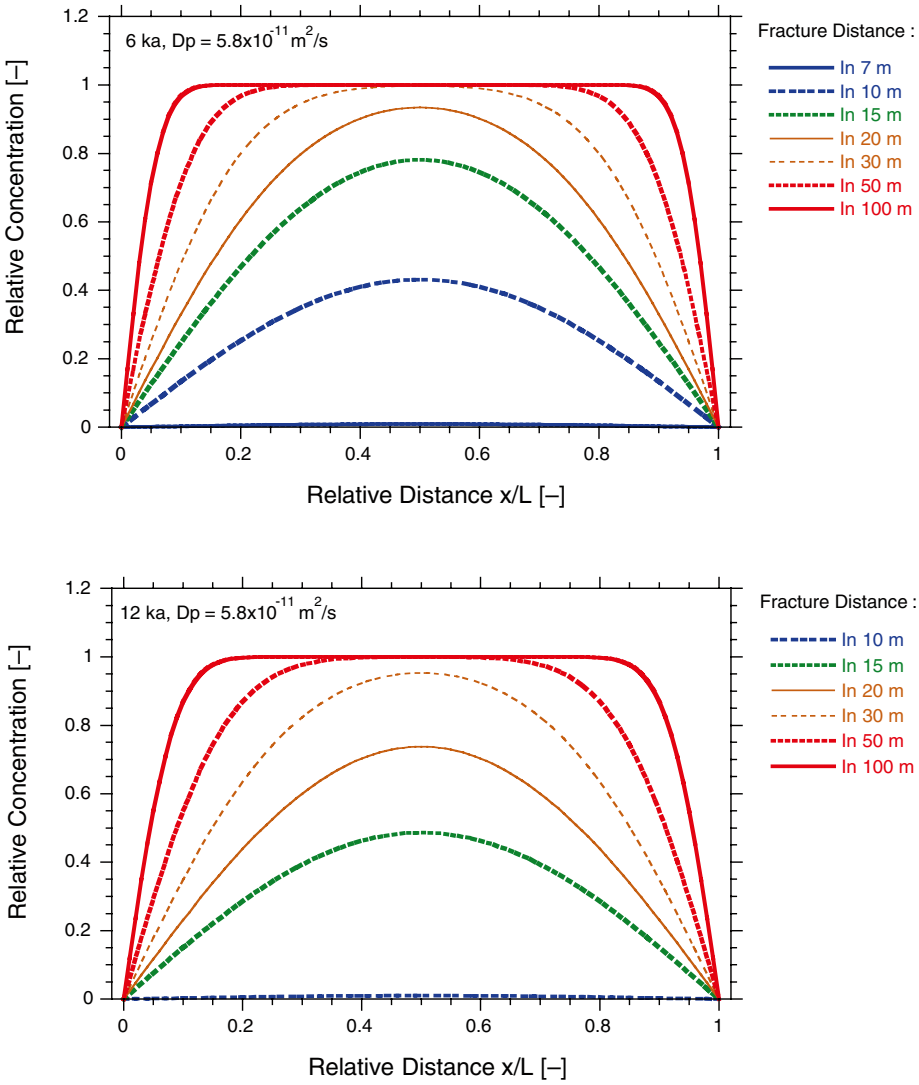

Figure 5-4. *Relative concentration changes induced on the porewater composition of a sample located at different distances between two water-conducting fractures for a time period of 6,000 years (top) and 12,000 years (bottom). The average measured pore diffusion coefficients of chloride for the Ävrö granite, Dp_{Cl}, = 5.8×10^{-11} m²/s, was used in the calculations.*

From Figure 5-4 it can be seen, for example, that a signature of a once established chloride content of Littorina water (e.g. 6,500 mg/L) would be completely diluted in a porewater sample located 3.5 metres or less from a fracture above and below (i.e. distance between fractures = 7 m or less) or reduced by about 60% (i.e. to 3,900 mg/L) in a porewater sample located 5 metres from a fracture above and below, if fresh water would have circulated in both these fractures over the last 6,000 years (Figure 5-4, top). Similarly, a once established glacial isotope signature in a porewater sample (e.g. modern glacial with a $\delta^{18}O$ of –17‰ VSMOW) would be completely erased over a distance of 5 metres or less from a fracture, changed to about 25% of the fracture-groundwater value (e.g. to about –15.5‰ VSMOW with a fracture groundwater of –11‰ VSMOW) over a distance of 10 metres, or still be preserved at a distance of more than about 15 metres between the two fractures, assuming constant isotope composition in the fracture groundwater over 12,000 years of interaction (Figure 5-4, bottom).

All further interpretations of porewater data and their comparison with present-day and past fracture groundwaters should be consistent with such basic type scenarios, but one has to keep in mind the possible limitations of a one-dimensional interpretation of the borehole data. Steeply dipping fractures close to a collected porewater sample might not be detected by the borehole, but could still affect the porewater sample data.

6 Porewater composition

Concentrations of chemically conservative elements dissolved in the matrix porewater were derived by non-destructive out-diffusion experiments and mass balance calculations using water-content data of the investigated rock samples (cf. Section 2.2.2). For chemically reactive elements, additional geochemical modelling is required to account for mineral reactions during the experiment. Such derivation of the complete *in situ* porewater composition was, however, outside the scope of the present study.

The non-destructive character of the experiments is important. This is because other fluid reservoirs exist in the rock besides the matrix porewater in the connected pore space, namely fluid trapped in mineral fluid inclusions. Different generations of such fluid inclusions with variably high salinity (up to 20 eq-wt.% NaCl) are known to occur mainly in quartz and feldspar of the rocks of the Laxemar-Simpervarp area including Äspö (e.g. /Smellie et al. 2003, Waber and Smellie 2006b/). During destructive extraction techniques, the salts of such inclusions will be released and inhibit the derivation of the matrix porewater concentrations even for conservative elements. The out-diffusion experiments used here to derive the matrix porewater concentrations were carefully tested for such possible perturbations and found to be free of any measurable influence by fluid inclusion leakage /Waber and Smellie 2006b/.

Out-diffusion experiments were conducted using originally saturated drillcore material of Ävrö granite (55 core samples), quartz monzodiorite (7 core samples), and diorite (4 core samples) from boreholes KLX03, KLX08, and KLX17A in the Laxemar subarea. The continuously sampled fracture profile in borehole KLX17A, which consists of 29 Ävro granite samples (including sub-samples), is discussed in Chapter 7. The complete datasets of the out-diffusion experiments are given in /Waber and Smellie 2006a, b, c, and 2008b/.

6.1 Chloride in matrix porewater

Chloride concentrations in matrix porewater of the rocks at the Laxemar subarea cover a large range of less than 100 mg/kg_{H2O} to more than 8,000 mg/kg_{H2O} (Table A-3). In spite of the different occurrences of the three sampled boreholes with respect to the major tectonic and deformation zones (Figure 2-1), there are some striking similarities between the Cl^- concentration, the general chemical type of porewater and the spatial distribution and relation to structural features in these boreholes. These are:

- In all three boreholes, changes in the porewater Cl^- concentrations are related to the frequency and transmissivity of water-conducting fractures as observed by difference flow logging as seen from Figures 6-1 and 6-2.
- In all three boreholes low porewater Cl^- concentrations occur in the shallow levels down to about 430 m depth and reaching even down to intermediate levels (about 620 m depth) in borehole KLX08.
- In all three boreholes the first increase in the porewater Cl^- concentration to values higher than 4,000 mg/kg_{H2O} is associated with a distinct change in the chemical type of the porewater (cf. Section 6.2.1).
- The largest increase in the porewater Cl^- concentration occurs at greatest depth in the quartz monzodiorite in boreholes KLX03 and KLX08. For borehole KLX17A no data are available from these depths.

The relation between porewater Cl^- concentrations, or other natural tracers such as the porewater oxygen and hydrogen isotope composition (Section 6.3) and the frequency and transmissivity of water-conducting fractures, is not a simple one and cannot be described by a simple correlation. This is because the exchange between porewater and fracture groundwater occurs by diffusion. Unlike mixing, where the different concentrations of two (or more) fracture groundwaters are immediately

equilibrated, the slow exchange by diffusion between porewater and fracture groundwater might not have attained equilibrium at the time of sample collection and a transient state is still established. The relation between porewater Cl^- concentrations and frequency and transmissivity of water-conducting fractures is thus not a simple correlation between only two independent variables. Much more the relationship depends on a) the initial condition in the matrix, b) the time period of constant boundary conditions (i.e. fracture-groundwater concentration), c) the diffusion properties of the rock matrix, and d) the distance from the porewater sample to a water-conducting fracture. Depending on the length of the time periods with constant fracture-groundwater concentrations, and the distance of the porewater sample to the conducting fracture, the time lag induced by the exchange by diffusion might also result in the superposition of successive different concentrations in the fracture groundwater (e.g. dilute meteoric followed by brackish-marine).

A simple correlation between porewater Cl^- concentrations and frequency and transmissivity of water-conducting fractures can, therefore, not be expected and the data have to be interpreted by taking all these dependences into account. In addition, it has to be kept in mind that the borehole information is limited with respect to the occurrences of water-conducting fractures and their detection. Nevertheless, the interpretation of porewater data can provide valuable information about the palaeohydrogeological evolution of a site over the last few thousand to hundreds of thousands of years, that might not any longer be derived from the dynamic fracture groundwater system.

6.1.1 Spatial distribution of Cl^- concentrations in porewater

In the shallow to intermediate depth levels down to about 520 m borehole length (about 430 m depth) in boreholes KLX03 and KLX17A and down to about 750 m borehole length (620 m depth) in borehole KLX08, the Cl concentration in the porewater of the rock matrix is below 1,500 mg/kg_{H2O}. In all three boreholes, these depth intervals are characterised by a high frequency of fractures with a high transmissivity (Figures 6-1 to 6-3).

At greater depths, between about 520 and 640 m borehole length (about 430–550 m depth) in boreholes KLX03 and KLX17A, strongly increased Cl^- concentrations of 5,000–7,600 mg/kg_{H2O} are observed (Figure 6-1 and Figure 6-3). The high Cl^- concentrations are associated with a distinct chemical type of the porewater (brackish Na-Ca-SO_4 type; cf. Section 6.2). In both boreholes, this depth interval is almost free of water-conducting fractures. In borehole KLX03 this increase also occurs but, in addition, increases towards the change in lithology from Ävrö granite to quartz monzodiorite (Figure 6-1).

Borehole KLX08 shows a different depth distribution of porewater Cl^- concentrations (Figure 6-2). Here, pronounced increase Cl^- concentration does not occur until about 800 m borehole length where the fracture frequency decreases. Between 800–910 m borehole length (about 650–770 m depth) the concentrations increase towards the quartz monzodiorite to about 6,000 mg/kg_{H2O}. As in the other boreholes, the high Cl^- concentrations are associated with the same distinct chemical type (here mainly a Ca-Na-SO_4 type) and also a different isotopic composition (cf. Section 6.3). Although they occur at different depth intervals in the various boreholes, it appears that these porewaters have a common evolution and carry hydrogeochemical records that differ from the porewater at shallower and greater depths.

Below these zones, the Cl^- concentrations in the porewater drop again at the top of the quartz monzodiorite in boreholes KLX03 and KLX08. In borehole KLX03 this drop is associated with the occurrence of fractures of high hydraulic transmissivity, while such features seem absent in borehole KLX08 at these depths (Figure 6-1 and Figure 6-2).

Towards the deepest parts of the boreholes, the Cl^- concentrations then increase with increasing depth to values around 5,000 mg/kg_{H2O} in borehole KLX03 and above 8,000 mg/kg_{H2O} in borehole KLX08. In both boreholes these high Cl^- concentrations in the porewater coincide again with changes in chemical type of the porewater and a decrease in the frequency of water-conducting fractures (Figure 6-1 and Figure 6-2). For borehole KLX17A no data are available from these depths (Figure 6-3).

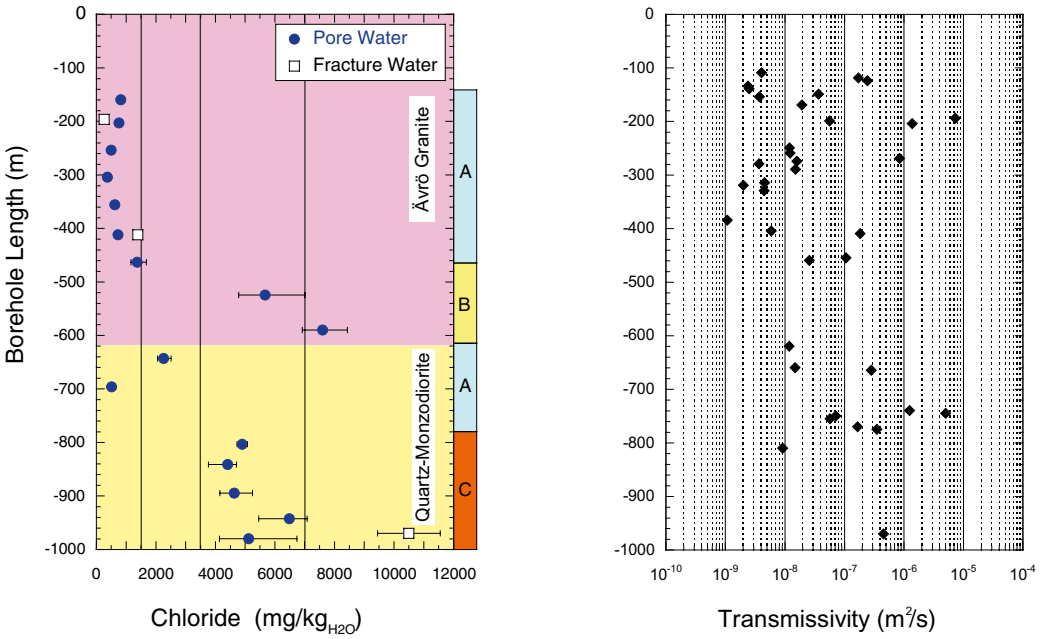

Figure 6-1. *Borehole KLX03: Chloride concentration in porewater (closed symbols) and fracture groundwater (open symbols) as a function of sampling depth (left) and compared to the measured hydraulic transmissivity of water-conducting fractures (right, data from /Rouhiainen et al. 2005/). General chemical types of porewater are: A = dilute Na-HCO_3 type, B = brackish Ca-Na-SO_4 type, C = brackish Na-Ca-Cl-(HCO_3) type, and D =saline Na-Ca-Cl type; vertical lines indicate concentration ranges used in the site visualisation model /Laaksoharju et al. 2009/.*

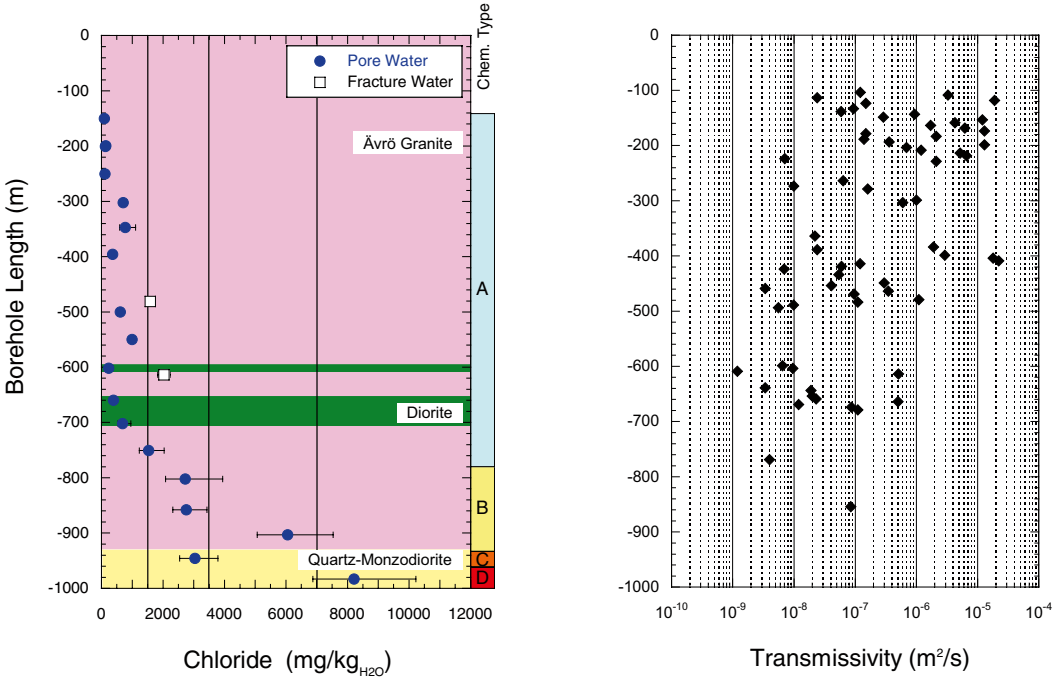

Figure 6-2. *Borehole KLX08: Chloride concentration in porewater (closed symbols) and fracture groundwater (open symbols) as a function of sampling depth (left) and compared to the measured hydraulic transmissivity of water-conducting fractures (data from /Sokolnicki and Pöllänen 2005/).*

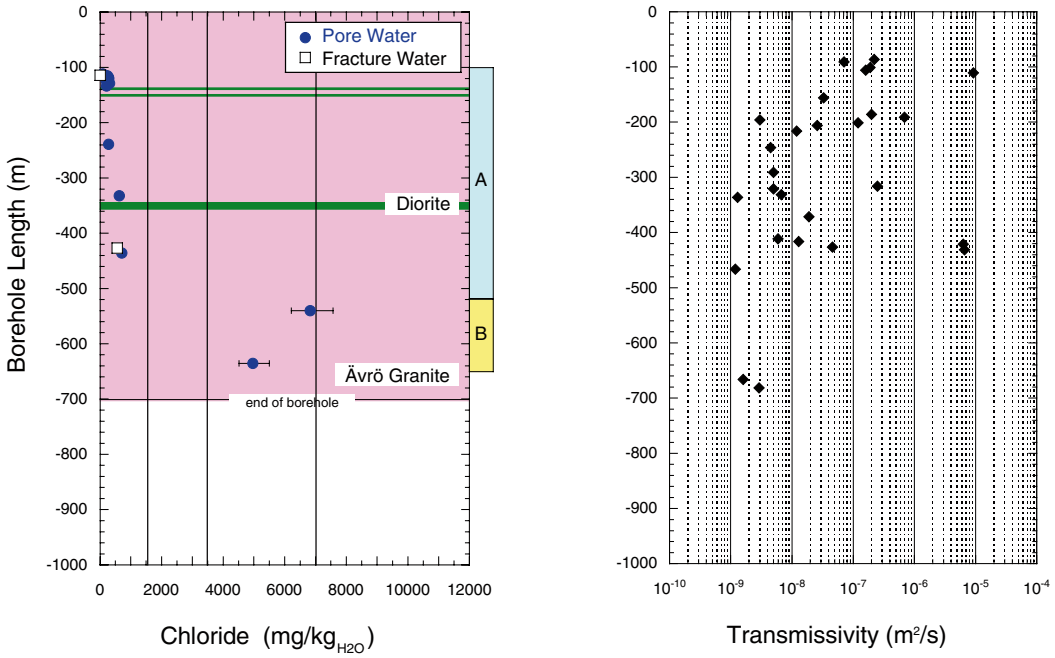

Figure 6-3. *Borehole KLX17A: Chloride concentration in porewater (closed symbols) and fracture groundwater (open symbols) as a function of sampling depth (left) and compared to the measured hydraulic transmissivity of water-conducting fractures (data from /Pöllänen and Kristiansson 2007/). General chemical types of porewater as in Figure 6-1.*

6.1.2 Relation between porewater and structural features

Chloride concentrations in the porewater of the rocks collected from boreholes KLX03 and KLX17A, which are situated in the centre of different fracture domains, show an almost identical distribution with depth (Figure 6-1 and Figure 6-3). A similar concentration profile, but shifted to greater depth, is observed for borehole KLX08, which intersects several major and minor deformation zones (including ZSMEW007A and ZSMEW946A) between about 200 m and 550 m depth (Figure 6-2). Some indications how these distribution patterns have developed can be obtained by comparing the Cl concentrations in addition to the distance of the porewater sample to the nearest water-conducting fracture (Figure 6-4).

Porewater samples with Cl^- concentrations of below 1,500 mg/kgH_2O, as they are present in the upper 430 m of the bedrock (KLX03, KLX17A) and deeper at 620 m (KLX08), were all collected within a distance between about 1 to 20 m, except for two samples at –275.9 m and –325.5 m elevation in boreholes KLX08 and KLX03, respectively (Figure 6-4). Indeed, most of the samples were collected within less than 5 m from the nearest water-conducting fracture. In a borehole the observation of steeply inclined fractures is limited and thus the real distance to the nearest water-conducting fractures might even be shorter. If solute transport in the rock matrix is assumed to take place by diffusion, then the time can be estimated that is required to equalise a previously established porewater signature with that in the fracture groundwater. As shown in Chapter 5, given a constant fracture-groundwater composition over the entire time interval, it would last about 6,000 years to impose the Cl^- concentration of the fracture groundwater on the porewater in the Äspö granite matrix located 3.5 m or less away from water-conducting fractures above and below. Similarly, in a distance of 5 m to the nearest water-conducting fractures, the porewater signature would become similar within about 5% to that of the fracture groundwater after about 12,000 years and remain unchanged over a distance of about 15 m. This suggests that, in these shallow zones with a high frequency of water-conducting fractures, the porewater will, in geological terms, quickly attain the concentration signatures of the fracture groundwater and no signatures older than these maximum times would be preserved.

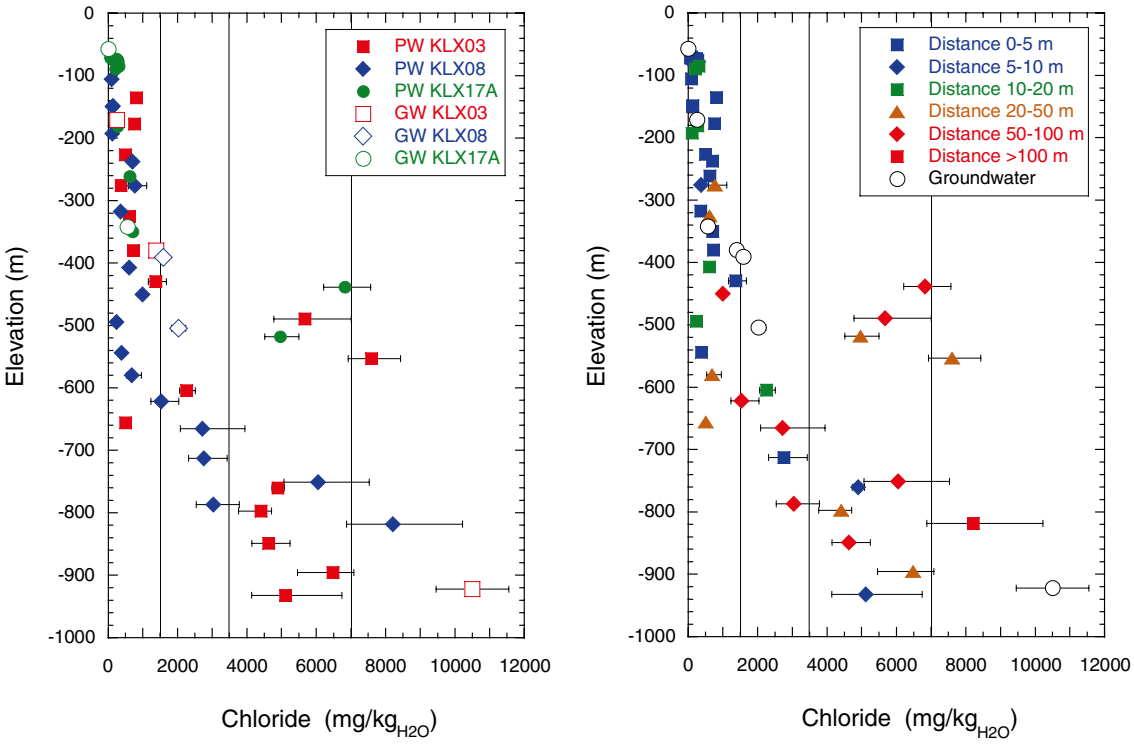

Figure 6-4. *Chloride concentration in porewater (PW, closed symbols) and related Category 1–3 groundwaters of boreholes KLX03, KLX08 and KLX17A from the Laxemar subarea on the left, compared with the distance of the porewater sample at one dimension from the nearest water-conducting fracture on the right (groundwater data from (cf. Sicada dataset, Extended data freeze Laxemar 2.3).*

At greater depth, Cl^- concentrations between 5,000–7,600 mg/kg$_{H2O}$ associated with a change in the chemical type of the porewater are observed. In boreholes KLX03 and KLX17A this occurs in an interval from about 430–550 m depth, while in borehole KLX08 a similar increase is observed between about 650 m and 770 m depth. Porewater samples with such high Cl^- concentrations have in common is that they are located more than 20–50 m away from the nearest water-conducting fracture in the three boreholes (Figure 6-4). Under the above outlined assumptions it would take considerably longer (about 80,000 years at a distance of 20 m in all directions) to equilibrate such signatures with a dilute fracture-groundwater signature. It thus appears that these observed signatures represent at least a partially preserved signature(s) of an event(s) several tens of thousands of years old.

The lower Cl^- concentrations further down in the uppermost levels of the quartz monzodiorite (between about 640–700 m and around 945 m borehole length in KLX03 and KLX08, respectively) appear again to be related to a higher frequency of water-conducting fractures between 600–800 m borehole length in borehole KLX03 (Figure 6-1), where also the deformation zone ZSMEW946A occurs (about 722–746 m borehole length).

In borehole KLX08 no transmissive fractures were detected by the differential flow logging in this section, but geological investigations revealed a local deformation zone (KLX08-DZ10) between about 925–940 m borehole length. The distance between the few porewater samples to the nearest water-conducting fracture is about 10–50 m in borehole KLX03 and between about 50–100 m for the single sample in borehole KLX08. Although based on a limited data set, the distances between the porewater sample and water-conducting fractures combined with the large differences in Cl^- concentrations between porewater samples above and below these zones, suggest that relatively dilute groundwater has been circulating in these fractures for quite a long time period. The Cl^- concentrations in the fracture groundwater have not been exceeded and must have been even lower than the lowest Cl^- concentrations observed in the porewater of these zones (about 500 mg/kg$_{H2O}$ in KLX03) for at least several thousands of years. Unfortunately, no CCC (Complete Chemical Characterisation) groundwater analyses exist from water-conducting fracture zones from these depths to compare with the porewater data.

Towards the bottom of the boreholes at greater depth in the quartz monzodiorite, the Cl^- concentrations in the porewater are rather constant about 5,000 mg/kgH_2O in borehole KLX03 and more than 8,000 mg/kgH_2O in the deepest sample of borehole KLX08. At these depths, the frequency of water-conductive fractures is low in both boreholes, the distance to the few fractures varies rather largely (Figure 6-4) and the relationship between porewater Cl concentration and distance to the nearest water-conducting fracture is only poorly defined. Interestingly, the Cl^- concentration (about 10,500 mg/L, cf. Sicada dataset, Extended data freeze Laxemar 2.3) of the fracture groundwater sampled from these depths in borehole KLX03 is higher than that of the porewater. This suggests that dilute fracture groundwater has circulated also at the deepest levels in the boreholes for a considerable time. Only more recently the circulation of higher mineralised water could have commenced as suggested by the transient state and the short distance between the deepest porewater sample and fracture groundwater in borehole KLX03 (Figure 6-1 and Figure 6-4).

6.1.3 Relation between porewater and fracture groundwater

Chloride concentrations of porewater and groundwater are similar down to about 360 m depth independent of their location, i.e. the borehole the samples were collected from (Figure 6-4). Down to this depth, the exchange of chloride between porewater and groundwater circulating in the fractures appears to be at or close to steady state.

In boreholes KLX03 and KLX08 at –379.8 m and –390.7 m elevation fracture groundwater has Cl^- concentrations of 1,390 mg/L and 1,590 mg/L, respectively. This is twice as high as the Cl^- concentration in the associated porewater samples less than 5 m distant form the nearest water-conducting fracture at these depths (Figure 6-4). The preservation of a transient state between porewater and fracture groundwater over such short distance indicates that the circulation of higher mineralised water in the fractures has existed for only a relatively short time. This can have lasted at maximum of about 5,000 years assuming that the Cl^- concentration in the porewater at this time would have been very dilute (i.e. essentially zero) and that water-conducting fractures are present at a distance of 5 metres from both sides of the porewater sample. Obviously, such a low Cl^- concentration in the porewater seems rather unlikely and the circulation of the current type of fracture groundwater has most probably lasted for a shorter time. The overall time range of a few thousand years is, however, supported by the ^{14}C activity of the fracture groundwater sampled in KLX03 at –379.8 m elevation suggesting a residence time in the underground of certainly less than 4,000 years /Laaksoharju et al. 2009/.

In borehole KLX08, this transient state continues down to at least 500 m, more probably to 650 m depth, with the fracture groundwater becoming increasingly more mineralised resulting in a larger gradient between porewater and fracture groundwater (Figure 6-4).

The low fracture frequency and low transmissivity inhibited sampling of fracture groundwater in the depth interval from about 450–600 m depth in boreholes KLX03 and KLX17A where the high Cl^- concentrations in the porewater combined with the anomalous Na-Ca-SO_4 chemical type porewater. Thus, it can hardly be deduced at what time the high Cl^- concentrations in the porewater have been established. Based on the rather large sampling frequency (50 m intervals), it is unknown if the presently observed Cl^- concentration of about 7,600 mg/kg_{H2O} represents the highest concentrations in this depth interval. Furthermore, it is also unknown if they represent the highest concentrations ever reached in the porewater of this interval (i.e. the initial concentrations) or if they represent concentrations already lowered by long-term exchange with dilute fracture groundwater. In the first case, and under present-day fracture groundwater conditions, such a porewater signature in the Ävrö granite could survive for a maximum of about 80,000 to 500,000 years within a distance of 20 m or 50 m from the nearest water-conducting fracture before these samples were collected. In the second case, the time period would become even greater. This time period could become, however, significantly shorter if water-conducting fractures occur at a shorter distance to the porewater sample.

At greater depth, there is only one fracture groundwater sample from borehole KLX03 to compare with the porewater Cl^- concentrations, indicating a transient state with respect to the fracture groundwater. As mentioned above, the short distance between porewater samples and water-conducting fractures (5–10 m) implies that the high chloride fracture groundwater has not been present for a long time in this fracture. In contrast, the deepest porewater sample in borehole KLX08 has, within the uncertainty band, a similarly high Cl^- concentration as recorded from borehole KLX03 (Figure 6-4).

6.2 Bromide in matrix porewater

In many hydrogeologcial systems bromide and chloride behave in a similar fashion as chemically conservative ions. Bromide concentrations in the out-diffusion experiment solutions therefore can be converted also to porewater concentrations using the mass-balance equation (3), assuming that during the out-diffusion experiment equilibrium with Br^- was also attained and that the amount of Br^- removed by the time-series samples is negligible. Both these assumptions seem reasonable. In the out-diffusion experiment solution Br^- concentrations were mainly at or below the detection limit of the conventionally applied ion-chromatographic methods. Only recently, a set of experiment solutions were analysed at lower detection limits by ICP-MS at the British Geological Survey, Keyworth, UK.

Concentrations of Br^- in the experiment solution are low and vary between 0.016 mg/L (detection limit) and 1.16 mg/L with most samples having less than 0.2 mg/L (Table A-4). Converting these concentration to porewater concentrations results in Br-contents between <1 mg/kg_{H2O} and 52 mg/kg_{H2O}. Porewater Br^- concentrations correlate with those of Cl^- independent of depth, porewater type (see below) and the geographic location of the borehole from which the core sample was collected. The concentrations plot, however, not on the dilution lines given by mixtures of seawater or Baltic water with fresh water, but become increasingly enriched in Br^- with increasing Cl^- content compared to these dilution lines (Figure 6-5).

The correlation between Br^- and Cl^- also results in a similar distribution with depth (Figure 6-6) with low concentrations at shallow and intermediate depths, which are interrupted by higher Br^- concentrations associated with the Na-Ca-SO_4 type porewater (unfortunately no data for borehole KLX03), before a general increase to the highest concentrations at greatest depth occurs.

Based on the limited data, the correlation with Cl^- and the similar depth distribution further results in the same relationship between Br^- in porewater and Br^- in fracture groundwater (Figure 6-6). In boreholes KLX03 and KLX17A almost equal Br^- concentrations occur in porewater and fracture groundwater and a steady state situation seems established. In borehole KLX08, different concentrations occur between about 400–500 m depth and a transient state is established. In spite of the gradual increase in porewater Br^- concentrations towards greater depth, the fracture groundwaters at the deepest levels seem to have still higher concentrations and a transient state appears to be established also in the zones.

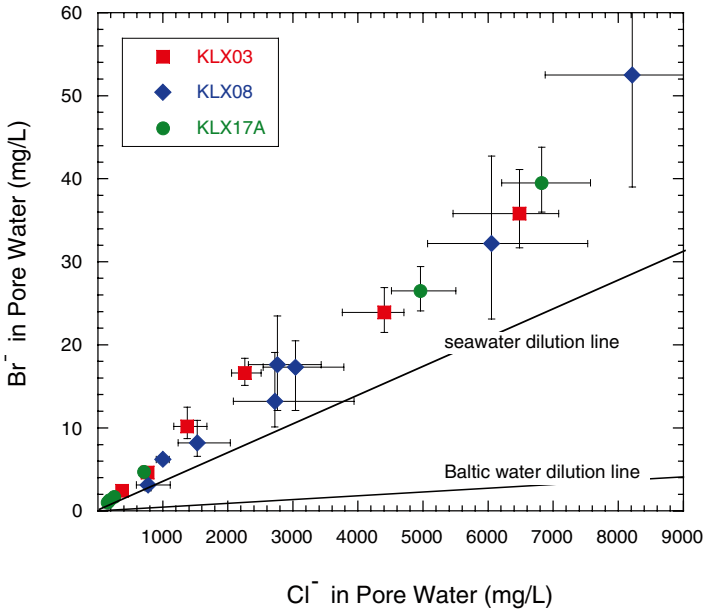

Figure 6-5. *Bromide versus chloride concentration in porewater from drillcore samples collected from different boreholes. The dilution lines for seawater and Baltic water with fresh water are given for comparison.*

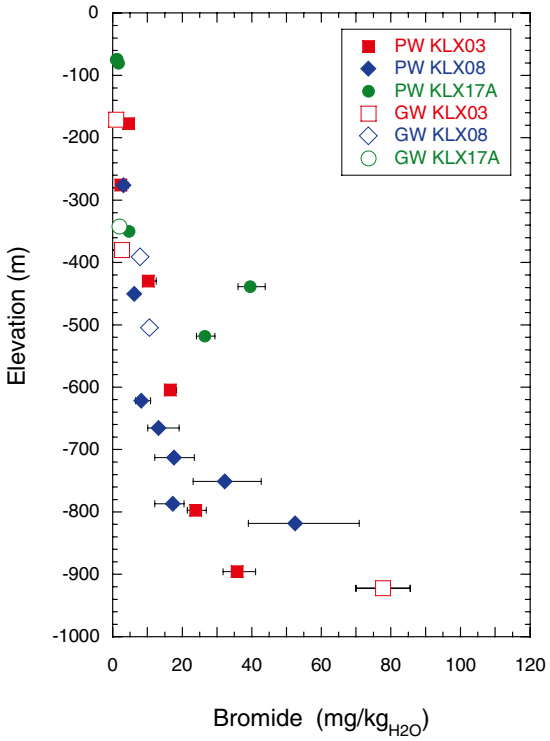

Figure 6-6. *Bromide concentrations in porewater (PW, closed symbols) and related Category 1–3 groundwaters of boreholes KLX03, KLX08 and KLX17A in the Laxemar subarea (groundwater data from /Laaksoharju et al. 2009/).*

6.3 Porewater chemical types

The chemical type of a water composition is defined by the relative proportions of the cation and anion concentrations expressed in meq/L (e.g. /Jäckli 1970/). The chemical type of a pore (or fracture) water reflects to a some extent the geochemical evolution of the water including possibly involved reactions such as mineral dissolution and bacterially mediated redox reactions as well as possible mixing of different water types. For the porewater, the chemical type carries in addition information about the palaeohydrochemical evolution of the site. However, to allow statements about the chemical type of the porewater *in situ*, the concentration inventories from mineral dissolution reactions during the out-diffusion experiments need to be known. In this context it is reasonable to assume that the inventories from such induced dissolution reactions will be similar for porewater drillcore samples made of Ävrö granite and quartz monzodiorite based on their similar mineralogy. Both rock types consist mainly of plagioclase, K-feldspar, quartz, biotite and minor and trace amounts of amphibole, epidote, magnetite, pyrite, and calcite /Waber and Smellie 2006b, Drake et al. 2006/. In the diorite samples, the modal abundances are shifted towards higher contents of mafic minerals (biotite, amphibole, pyroxene) and more anorthitic plagioclase. These minerals are more susceptible to dissolution reactions and consequently different inventories from dissolution during the experiment have to be expected for dioritic rock samples. Indeed, experiment solutions of dioritic porewater samples have, for instance, elevated Mg^{2+} contents /Waber and Smellie 2006c, 2008b/ and $^{87}Sr/^{86}Sr$ ratios (cf. Section 6.3.4), which have to be attributed to enhanced mineral dissolution. Because there are only four porewater samples representing dioritic rock, these samples are not specifically considered for the derivation of porewater chemical types.

6.3.1 Correction for reactions during the experiment

The concentrations of chemically reactive elements in the experiment solution analysed at the conclusion of an out-diffusion experiment are the sum of the concentration of a specific element in the porewater and the contribution to this element by mineral dissolution reactions during the experiment. Estimates of the reactive element inventories from dissolution reactions were obtained

by modelling these geochemical processes during the experiment as a weathering process of a granitic rock with a modal composition and mineral chemistry similar to that of the Ävrö granite. The rock mineralogical and chemical data used in this modelling were those based on porewater samples from borehole KLX03 /Waber and Smellie 2006b/. The calculations were performed using the geochemical code PHREEQC (v. 2-13, 2006, /Parkhurst and Appelo 1999/) and the kinetic rate laws given in the WATEQ4F database of this code. Figure 6-7 shows the evolution of the cation concentration during this type of simulation as a function of time. The concentrations released by mineral dissolution at after 100 days of experimental time are in the order of about 3.3×10^{-6} to 2.3×10^{-5} mol/L for all major cations. These concentrations are less than 1% of the concentrations measured in the experiment solutions. Thus, even when allowing an uncertainty by a factor of ten for these simulations, the obtained concentrations would still be within the analytical uncertainty of the concentrations measured in the experiment solutions.

In the scoping calculation, the highest concentrations are calculated for Si and Al. No secondary minerals were allowed to precipitate in the simulation and the calculated concentrations of Si and Al appear be overestimated. This is indicated by the calculated oversaturation with respect to kaolinite from 100 days onwards of experimental time. Measured concentrations of Si and Al in the final experiment solutions after 90–110 days average 10 mg/L (3.98×10^{-4} mol/L, log mol/L = –3.4) and 0.077 mg/L (3.2×10^{-6} mol/L, log mol/L = –5.5), respectively. The measured Si concentrations correspond about to quartz saturation and compare well with the concentration calculated by the artificial weathering of granite (Figure 6-7). In contrast, the calculated Al concentration is more than one order of magnitude higher than that measured. This is because the formation of secondary minerals such as gibbsite and kaolinite were suppressed in the simulation. As a consequence both these phases are oversaturated in the calculated solution. Gibbsite and kaolinite are known to form during natural weathering of feldspars and it is likely that they are also produced during the out-diffusion experiment. The secondary formation of gibbsite-type layers on the feldspar surface reduces the dissolution kinetics. The present simulation, which did not account for such processes, might therefore overestimate feldspar dissolution and consequently some of the cation concentrations produced by weathering reactions during the out-diffusion experiment. The real contribution of cations from such reactions might thus be even lower than calculated. It follows that the contribution of major cations from mineral dissolution during the out-diffusion experiments is negligible within the analytical uncertainty.

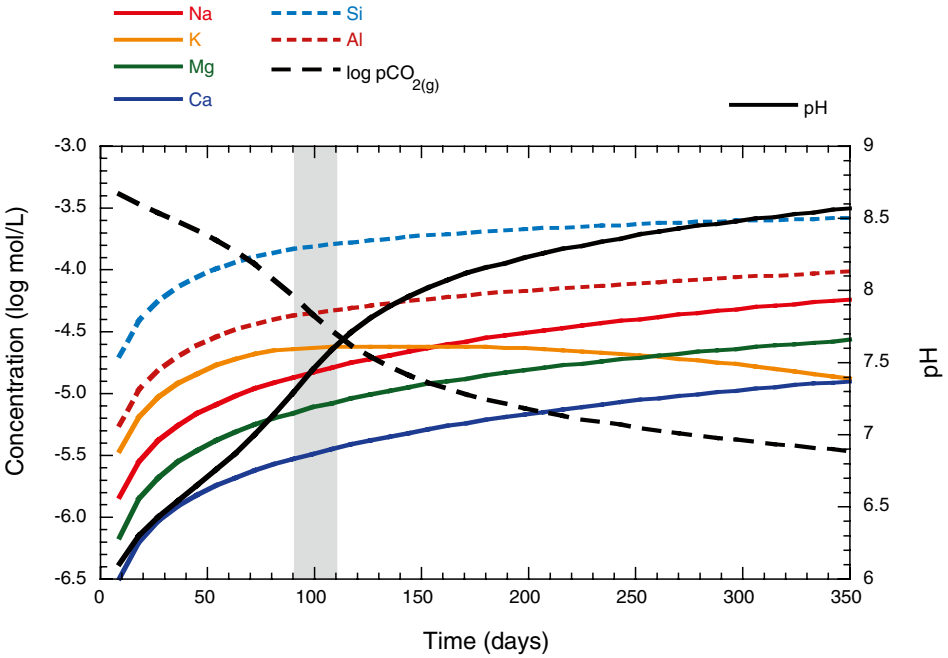

Figure 6-7. *Calculated cation concentrations, $pCO_{2(g)}$, and pH during kinetic weathering of a granite at 45°C. The shaded area gives the experiment time of the out-diffusion experiments conducted with the drill core material from boreholes KLX03, KLX08, and KLX17A.*

Neither the experiments nor the above scoping calculations were intended to determine the dissolved carbon content and the redox potential of the porewater. Nevertheless some semi-quantitative information can be gained from the data about the carbonate and redox systems. Initially, the experiment water is at CO_2 equilibrium with the atmosphere and the partial pressure of the solutions was about $10^{-3.5}$. In a fully closed system, the CO_2 of the experiment solution would become consumed by alumino-silicate weathering reactions. The artificial weathering induced in the out-diffusion experiments therefore results in a decrease of the partial pressure of CO_2 and an increase in pH in the experiment solution as shown in Figure 6-7. This is exactly what happens in nature during the infiltration of groundwater in crystalline rocks (e.g. /Nordstrom et al. 1989/). Given sufficient time, the carbonate system will finally be controlled by calcite, which will precipitate from the groundwater and form the frequently observed low temperature calcite fracture linings in crystalline rocks. In the Laxemar subarea, the occurrence of such low temperature calcite has been confirmed by the presence of ^{14}C in some of the fracture calcites /Drake and Tullborg 2009a/.

For the porewater a similar evolution of the carbonate system can be expected. Thus, in rock samples located close to water-conducting fractures and with dilute to brackish porewater, the sluggish alumino-silicate reactions will not yet have consumed large quantities of CO_2. The pH of such porewater can be expected to be around neutral to slightly alkaline and HCO_3^- will still constitute a major anion in such porewater. In rock samples located at greater distance from the next water-conducting fracture in contrast, the rock-porewater interaction is more advanced and more alkaline pH and low concentrations of CO_2 and HCO_3^- (due to the formation of secondary calcite) have to be expected.

The redox potential is more difficult to assess because it is *a priori* unknown which redox couple governs the redox potential of the porewater. In the out-diffusion experiments SO_4^{2-} is the only redox sensitive parameter analysed. The concentrations of SO_4^{2-} are easily affected by mineral dissolution reaction during the out-diffusion experiments because these were not conducted under redox-controlled conditions. For the rock matrix there exist no records about readily dissolvable sulphate minerals, but there occur traces of pyrite that might become oxidised during the experiment. /Drake et al. 2006/ report pyrite contents between 0–0.2 Vol.% for the Ävrö granite and 0–0.26 Vol.% for the quartz mozodiorite. For an average rock volume of about 370 cm^3 used in the out-diffusion experiments 0.2 Vol.% of pyrite convert to about 5.6 mol of reduced sulphur. One of the limiting factors for pyrite oxidation in the experiments is the amount of oxidant present, i.e. the amount of $O_{2(aq)}$ present in the initial experiment solution. In common with CO_2, the initial experiment solution was also in equilibrium with the atmosphere with respect to oxygen. At 45°C this solution thus contained about 4×10^{-4} mol/L $O_{2(aq)}$. If completely consumed by pyrite oxidation this amount of $O_{2(aq)}$ would result in about 2.1×10^{-4} mol/L of SO_4^{2-} (about 20.2 mg/L). Experiment solutions with high SO_4^{2-} concentrations (i.e. the general Ca-Na-SO_4 chemical type solutions, see below) have average SO_4^{2-} concentrations of about 4.2×10^{-3} mol/L of SO_4^{2-} (about 410 mg/L; see /Waber and Smellie 2006a, 2006c and 2008b/ for complete data). The maximum contamination by pyrite oxidation is therefore less than about 5% in these samples. In contrast, the experiment solutions with low SO_4^{2-} concentrations (i.e. the Na-HCO_3 chemical type solutions, see below) have average SO_4^{2-} concentrations of about 1.1×10^{-4} mol/L of SO_4^{2-} (about 10.7 mg/L). The SO_4^{2-} concentrations of these solutions might thus indeed be modified by some contribution of SO_4^{2-} from pyrite oxidation. However, with respect to the general chemical type of these solutions the induced contamination by pyrite is of no importance because even at the measured concentrations SO_4^{2-} constitutes only a minor anion in these solutions. Thus, sulphide oxidation during the out-diffusion experiment will not strongly affect generic derivation of the porewater chemical type.

In conclusion, the cation inventories derived from mineral dissolution reactions during the experiment are negligible compared to the cation inventories in the porewater. The same accounts for the inventory of SO_4^{2-} derived by induced pyrite oxidation. Thus, the concentrations in the experiment solution measured after equilibration with respect to Cl^- can be used together with those of the anions to derive the general chemical type of the *in situ* porewater. The only unknown concentrations are those of total dissolved carbon and H^+ (i.e. pH) and consequently those of the dissolved carbon species. However, as outlined above and based on experience of natural crystalline groundwater systems, it can be expected that the concentrations of dissolved CO_2 and HCO_3^- will decrease with increasing salinity and residence time /Nordstrom et al. 1989, Michard et al. 1996/ and become minor anions in the saline porewaters located at greater distance from the next water-conducting fracture.

In principle and based on the above conclusions, this would allow modelling the complete *in situ* porewater composition as a function of one of the unknowns mentioned above, i.e. pH or pCO_2. Whereas this seems possible for experiment solutions dominated by Na-HCO_3 or Na-Cl-HCO_3, the system is even less defined for the solutions dominated by Na-Ca-SO_4, which also occur at repository depth. This is because in these solutions SO_4^{2-} represents an additional variable that either needs to be treated purely conservative or fixed by mineral equilibrium. The available data, however, neither support a purely conservative behaviour of SO_4^{2-} during out-diffusion nor are possible mineral controls (other than pyrite) known although indications for other S-bearing minerals exist (see below). As a consequence no porewater composition can be modelled and more detailed mineralogical investigations of the rock matrix are required to constrain the calculation of the *in situ* porewater composition from the general Na-Ca-SO_4 type experiment solutions.

6.3.2 General chemical type

Figure 6-8 shows the different chemical types of out-diffusion experiment solutions presented in a Schoeller diagram. As outlined above, to a large extent these chemical types also represent the chemical type of the *in situ* porewater. Thus, low to moderately mineralised porewater of the Na-HCO_3 chemical type occurs at shallow depths in boreholes KLX03 and KLX17A (down to about 400 m depth) and to intermediate depths in borehole KLX08 (to about 650 m depth). The Cl^- concentration of these porewater samples is generally below 2,000 mg/kg_{H2O} and for most samples even below 1,500 mg/kg_{H2O}. In borehole KLX03, two additional porewater samples of this chemical type occur in the uppermost levels of the quartz monzodiorite between about 650–700 m borehole lengths (Figure 6-1; about 600 to 650 m of depth). Composition and mineralisation of these samples appear to be associated with water-conducting structures related to the deformation zone ZSMEW946A.

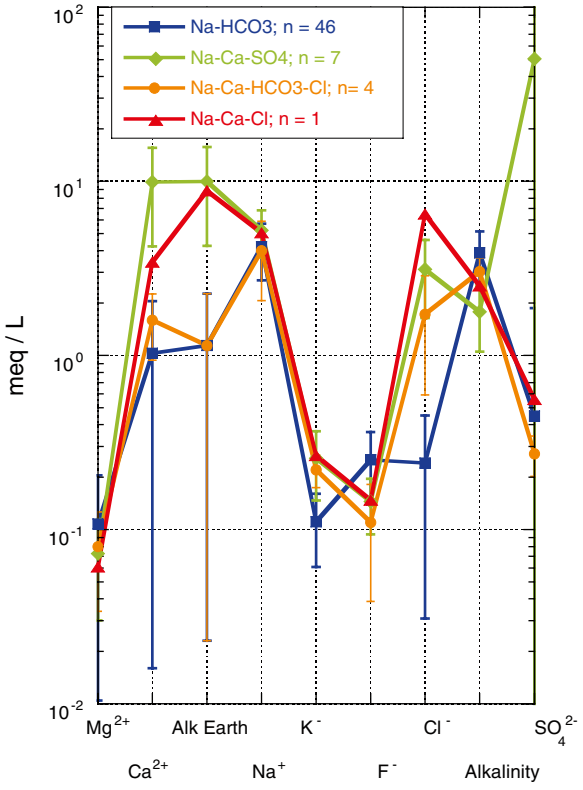

Figure 6-8. *Schoeller diagram showing the average for the different chemical types of experiment solutions from the out-diffusion experiments and the range given by the standard deviations.*

Seven samples from the three boreholes contain porewater of an anomalous chemical type that deserves further discussion (cf. Section 6.1.1). Porewater in these samples is mainly of a general Na-Ca-SO_4 type in boreholes KLX03 and KLX17A and of a general Ca-Na-SO_4 type in borehole KLX08. The corresponding Cl^- concentrations range between about 1,400–7,600 mg/kgH2O in boreholes KLX03 and KLX17A and between about 1,500–6,000 mg/kg_{H2O} in borehole KLX08. The experiment solutions of these samples have SO_4^{2-} concentrations that are more than one order of magnitude higher compared to those of all other experiment solutions (Figure 6-9). Similarly, Ca^{2+} concentrations are higher by more than a factor of three compared to those of experiment solutions from shallower depth and are more similar to those of the deep Na-Ca-HCO_3-Cl chemical type solutions (Figure 6-9).

The mineralogical composition of these seven Ävrö granite samples is identical to samples above and below. Pyrite and calcite as sources for SO_4^{2-} and Ca^{2+} in the experiment solutions occur in similar concentration. Pyrite and traces of other sulphide minerals were detected in all samples, but no additional sulphur-bearing minerals such as sulphates have been observed in the matrix of the Ävrö granite so far. It appears that a sulphate phase such as gypsum, which would be readily dissolvable during the out-diffusion experiments, is absent in the rock matrix. In contrast, traces of sulphate minerals, i.e. gypsum and barite, have been described from some fractures in the Ävrö granite in borehole KLX03 between –516 to –572 m elevation and in KLX08 between –705 to –789 m elevation /Drake and Tullborg 2009a, b/. Based on the S- and O-isotope composition of gypsum its formation was interpreted as have been taken place as anhydrite during Palaeozoic times, which was later hydrated to gypsum. The depth intervals where gypsum was observed overlap with those of the Ca-Na-SO_4 type porewater only in their deepest few decametres, while most of the fracture gypsum was observed at depths associated with Na-Ca-HCO_3-Cl type porewaters. The drillcore samples used for the porewater investigations are free of closed or open fractures, except for sample KLX03-8 (524.63 m borehole length, –489.64 m elevation) where a closed hair fissure is visible. The X-ray diffraction spectra of the filling material of this fissure revealed that it consists solely of calcite and no gypsum is present. Therefore, sulphate mineral phases in fractures cannot be the source of the additional SO_4^{2-} and Ca^{2+} in the experiment solutions. Further support in this direction comes from the different Sr-isotope signatures of the experiment solutions compared to those of gypsum separated from fractures cf. Section 6.3.4).

However, the molar SO_4^{2-} and Ca^{2+} ratios of the Na-Ca-SO_4 type experiment solutions scatter around unity as could be expected if gypsum would be the major source for these solutes (Figure 6-10, left). In addition, the solutions have also distinct Na^+-SO_4^{2-} molar ratios between about 0.1 and 7 that are substantially smaller than all other experiment solutions (Figure 6-10, right). A Na^+-SO_4^{2-} molar ratio of 2 would be typical for solutions that obtain most of their Na^+ and SO_4^{2-} from the dissolution of mirabilite ($Na_2SO_4 \cdot 10H_2O$), a mineral that forms, for example, during freezing of water. Gypsum and mirabilite are highly soluble and dissolve easily when in contact with water. From the perspective of porewater evolution it is rather irrelevant if gypsum and mirabilite are still present in the rock matrix and got dissolved during the time-series experiments or if only some signature of an earlier (natural) dissolution of such minerals is preserved in the solute composition of the porewater. From the perspective of porewater composition, however, it is highly relevant. This is because in the first case (i.e. sulphate minerals present in the rock matrix) this would mean that the porewater would have to be in equilibrium with gypsum and mirabilite because of their high solubility. In the second case (i.e. sulphate minerals absent in the rock matrix), the porewater might well be undersaturated with respect to these phases. Based solely on the solution chemical data this problem cannot be solved and high-resolution mineralogical investigations would have to be applied. In both cases, however, the occurrence of Na-Ca-SO_4 and Ca-Na-SO_4 chemical type porewaters indicate that freezing processes might have played a role in the palaeohydrogeological past of the site. Possible scenarios for freezing processes might be related to time periods when permafrost prevailed in the Laxemar area (cf. Chapter 8).

In boreholes KLX03 and KLX17A, the Na-Ca-SO_4 chemical type occurs between about 460–590 m borehole length and 540–653 m borehole length, respectively (Figure 6-1 and Figure 6-3). In both boreholes this corresponds to about the same depth interval below sea level (about 430–550 m depth). In borehole KLX08, the porewater appears to be slightly more dilute based on Cl^-, but the experiment solutions have the overall highest SO_4^{2-} and Ca^{2+} concentrations (Figure 6-9). In this borehole the Ca-Na-SO_4 chemical type occurs at greater depth between about 750–903 m of bore-

hole length (Figure 6-2) corresponding to a depth below sea level of about 620–750 m. In all three boreholes, the different chemical types occur in depth intervals with a low fracture frequency and almost no water-conducting fractures in the boreholes. In boreholes KLX03 and KLX08 it further occurs towards the bottom of the Ävrö granite where the lithology changes to quartz monzodiorite (Figure 6-1 and and Figure 6-2). In KLX17A the quartz monzodiorite was not encountered. At this juncture in time, and based on limited data, it is unknown to what degree this coincidence influenced (or otherwise) the evolution of this type of porewater.

At the greatest depth in boreholes KLX03 and KLX08, four samples contain porewater of a Na-Ca-HCO_3-Cl chemical type. The real proportion of HCO_3^- to Cl^- in the porewater of these samples cannot be estimated because of reasons outlined above. The experiment solutions of these samples have, however, lower alkalinity values (from which the HCO_3^- concentration is obtained) compared to the Na-HCO_3 type solutions. A saline Na-Ca-Cl type of porewater is only observed in sample KLX08-16 at the end of borehole KLX08, and the corresponding experiment solution of this sample has the highest Cl^- concentration of all samples.

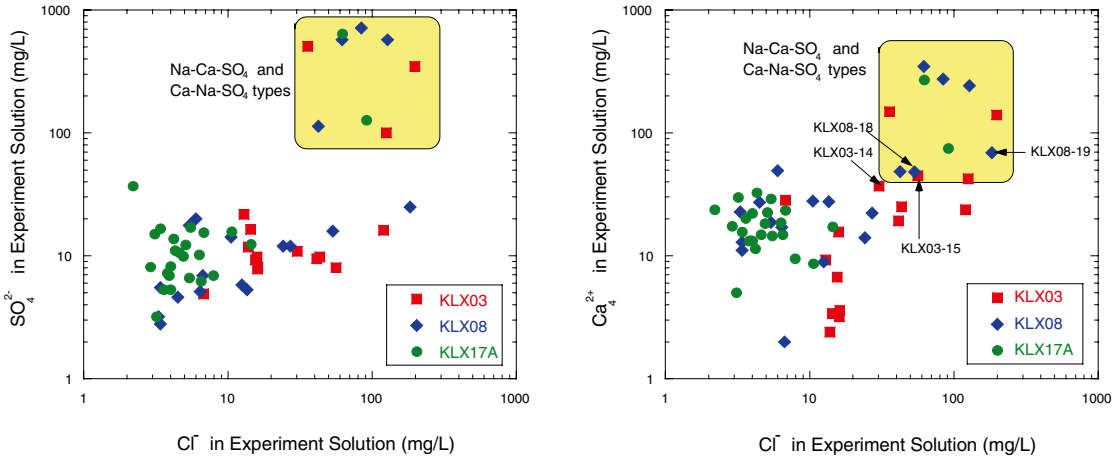

Figure 6-9. *Concentrations of SO_4^{2-} (left) and Ca^{2+} (right) versus Cl^- in experiment solutions displaying the distinct differences in SO_4^{2-} and Ca^{2+} between the Na-Ca-SO_4 and Ca-Na-SO_4 type solutions and the other solutions. Sample numbers in the right-hand plot indicate the deep-seated Na-Ca-Cl-HCO_3 type experiment solutions.*

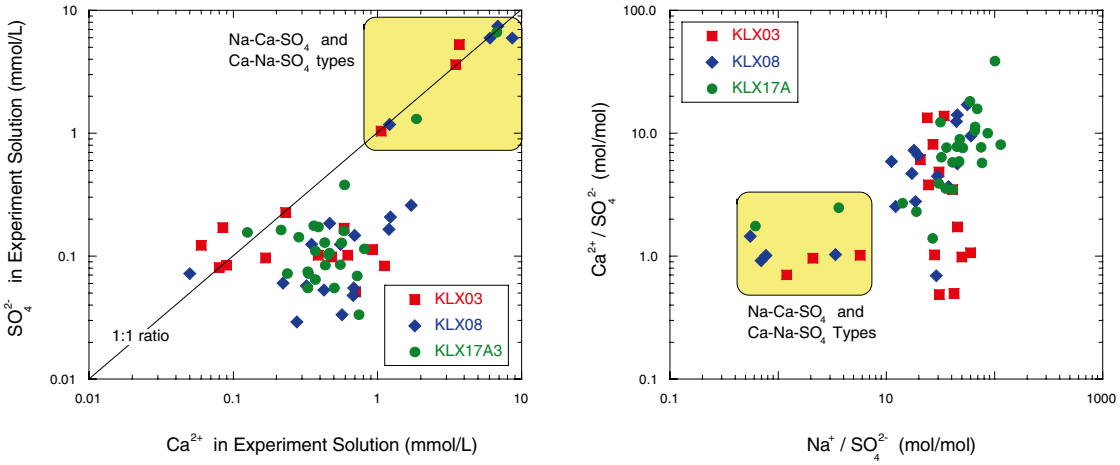

Figure 6-10. *Concentrations of Ca^{2+} versus SO_4^{2-} (left) and the molar ratio of Na^+/SO_4^{2-} versus Ca^{2+}/SO_4^{2-} (right) in experiment solutions displaying the distinct differences between the Na-Ca-SO_4 and Ca-Na-SO_4 type experiment solutions and the other solutions.*

6.3.3 Cl-isotope composition

The stable isotopes of chlorine, ^{35}Cl and ^{37}Cl expressed as $\delta^{37}Cl$, have been measured on the experiment solutions of out-diffusion experiments performed with samples from borehole KLX03 and KLX08 (Table A-4). The $\delta^{37}Cl$ values of these solutions seem to be representative for the *in situ* porewater because in the out-diffusion experiments steady state conditions prevailed for total chloride for more than half of the experimental time allowing also the Cl isotopes to equilibrate. The obtained $\delta^{37}Cl$ values cover a large range from about 0.4 to 3.4‰ SMOC and are all enriched in ^{37}Cl compared to average sea water ($\delta^{37}Cl$ = 0‰ SMOC) and average Baltic Sea water ($\delta^{37}Cl = 0.08 \pm 0.08$‰ SMOC; /Laaksoharju et al. 2009/). They show no unique trend with the total Cl^- concentration in the porewater (Figure 6-11) indicating that the sum of Cl^- in the porewaters stems from different sources with different Cl-isotope signatures and/or fractionation of Cl isotopes occurred during the exchange of porewater with fracture groundwater (see below). Nevertheless, some trends appear to be indicated, for instance: a) the Na-Ca-SO_4 type porewaters suggest a positive correlation between total Cl^- and $\delta^{37}Cl$ (except for one sample), b) deep-seated samples have rather a homogeneous $\delta^{37}Cl$ independent of total Cl^- (also except for one sample), and c) shallow and intermediate depth samples cover a large range of $\delta^{37}Cl$ at rather constant total Cl^- concentrations (Figure 6-11).

As a function of depth, the $\delta^{37}Cl$-values show a large scatter in the uppermost 650 m below surface where they also differ from the $\delta^{37}Cl$ values reported for fracture groundwaters (Figure 6-12). Towards greater depth, where the fracture frequency decreases and the distance to the nearest water-conducting fracture increases, the porewater $\delta^{37}Cl$ values become more homogeneous and are similar to those of the single fracture groundwater sample measured.

At present, these relationships are difficult to explain. In advection dominated systems chlorine isotopes do not fractionate and a correlation with total chloride will be immediately established. Chloride isotope fractionation, however, takes place during diffusion of chloride /Desaulniers et al. 1986, Eggenkamp et al. 1994/. Therefore, in a diffusion-dominated system a correlation between chlorine isotopes and total chloride as a function of distance will only be established if the chemical and isotopic gradients between the two reservoirs (i.e. porewater and fracture groundwater) along this distance remained constant long enough until steady state conditions with respect to total Cl^- and the chlorine isotopes are achieved (e.g. /Gimmi and Waber 2004/).

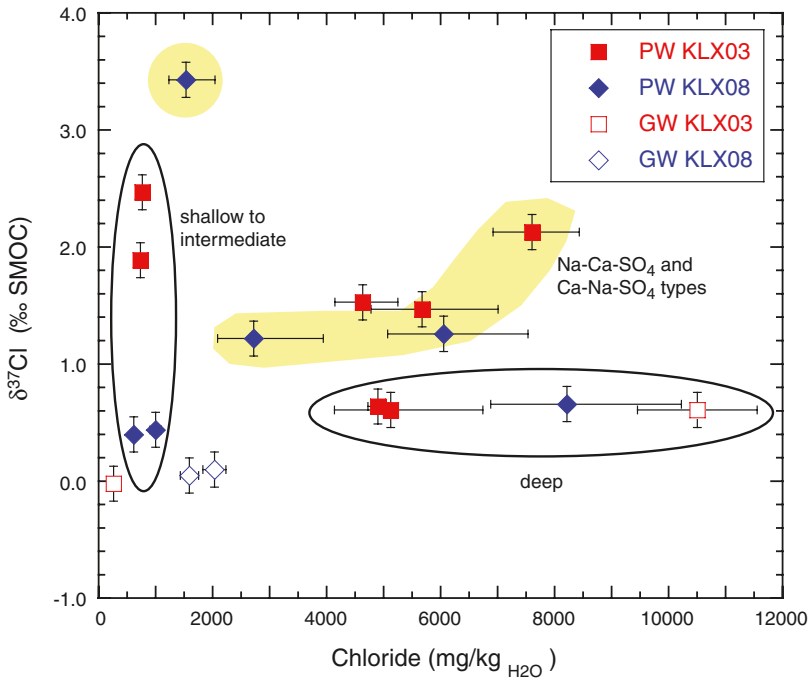

Figure 6-11. *Chlorine isotope ratio, $\delta^{37}Cl$, versus chloride concentration in the porewater (closed symbols) and fracture groundwater (open symbols) in boreholes KLX03 and KLX08. Error bars are ± 0.15‰ for $\delta^{37}Cl$, the cumulated error for Cl in porewater (cf. Table A-3), and ± 10% for Cl in groundwater.*

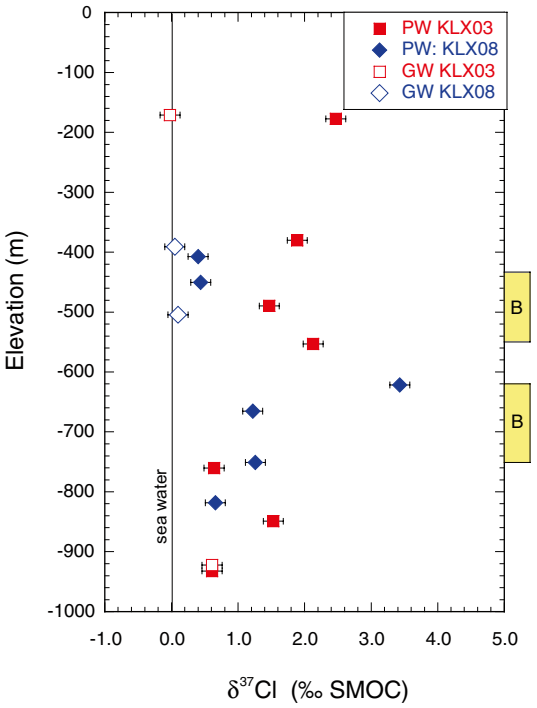

Figure 6-12. *Chlorine isotope ratio, $\delta^{37}Cl$, versus elevation (m.b.s.l.) in the porewater (closed symbols) and fracture groundwater (open symbols) of boreholes KLX03 and KLX08. The bright green bars (B) indicate the occurrence of Na-Ca-SO_4 and Ca-Na-SO_4 type porewater; error bars are ± 0.15‰ SMOC.*

Based on these limited data, the differences in $\delta^{37}Cl$ values between porewater and fracture groundwater in boreholes KLX03 and KLX08 suggest a transient state for the chlorine isotopes at shallow to intermediate depth, although total Cl^- might already be at steady state in certain parts of this depth interval. This would further indicate that the present situation, i.e. steady state with respect total Cl^- and transient state with respect to chlorine isotopes, has not yet been established for a time period long enough to allow equilibration of total Cl^- *and* the chlorine isotopes between porewater and fracture groundwater at these depths. In contrast, such conditions appear to prevail at greatest depths in these boreholes, although this is based only on a single fracture-groundwater sample from borehole KLX03 (Figure 6-12).

6.3.4 Sr-isotope composition

Strontium is chemically reactive and is involved in mineral dissolution reactions during the out-diffusion experiment. The concentration measured in the out-diffusion experimental solutions can, therefore, not be directly extrapolated to a porewater concentration as for chloride. Nevertheless, some insight about the porewater composition and about mineral dissolution reaction during the out-diffusion experiment can be gained from the total Sr concentration and the Sr-isotope ratio, $^{87}Sr/^{86}Sr$.

Depending on the total mineralisation of the *in situ* porewater, the effect of mineral dissolution reactions on the total Sr^{2+} concentration, Sr_{tot}, in the experiment solution will be minimial. This is because Sr^{2+} occurs mainly as a trace element in the matrix minerals of the crystalline rocks of the Laxemar local modal area /Drake and Tullborg 2009a/. As shown in Section 6.3.1, mineral dissolution is limited over the experimental time by the generally low kinetics of major mineral phases, which are also the important carriers of strontium. In contrast to the Sr^{2+} concentration, the effect on the Sr-isotope ratio in the experiment solution is expected to be bigger. This is because radiogenic ^{87}Sr, which is continuously produced by the natural decay of ^{87}Rb, is retained in the minerals unless it gets released by re-crystallisation and/or dissolution processes. During the induced mineral dissolution (e.g. feldspars, biotite, amphibole) in the out-diffusion experiment, the small amounts of Sr^{2+} released from such minerals will thus be highly radiogenic, i.e. have a high $^{87}Sr/^{86}Sr$ ratio.

The comparison of the values for Sr_{tot} and Sr-isotope ratio in the experiment solution and the fracture groundwater might thus reveal different information that depends on the total Sr^{2+} concentration: At low Sr^{2+} concentrations in experiment solution and fracture groundwater equal Sr-isotope ratios would indicate that the isotope ratio in the fracture groundwater is attained rather quickly being derived from the same mineral dissolution reactions that occur during the out-diffusion experiment in the laboratory. In this situation no independent information can be gained for the porewater because the porewater signature is masked by the experiment. At total Sr^{2+} concentration significantly higher than that contributed by mineral dissolution during the out-diffusion experiment, however, the $^{87}Sr/^{86}Sr$ ratio of the experiment solution will be similar to that of the *in situ* porewater. In this situation, information about chemical and isotopic relationships of strontium between porewater and fracture groundwater can be obtained.

Concentrations of Sr_{tot} measured in the experiment solutions by mass spectrometry are generally below 0.5 mg/L, except for the higher mineralised solutions of the general Na-Ca-SO_4 and Ca-Na-SO_4 porewater types where they reach up to 2 mg/L (Table A-4). In all experiment solutions, Sr^{2+} correlates with Ca^{2+}, but is only poorly correlated with chloride (Figure 6-13). This indicates that in the low Sr_{tot} experiment solutions the Sr^{2+} concentration is mainly controlled by mineral dissolution reactions as expected. Because the mineralogy and modal contents of the individual rocks types (i.e. Ävrö granite, quartz monzodiorite, diorite) differ markedly (although being rather homogeneous for an individual rock type), this should result in specific $^{87}Sr/^{86}Sr$ ratios in the experiment solutions of the different rock types, because of the identical experimental conditions for all samples. As shown in Table A-4, this is the case to some degree. The most radiogenic $^{87}Sr/^{86}Sr$ ratios are observed for the experiment solutions of the diorite samples (average = 0.7216 ± 0.0015), followed by the quartz monzodiorite samples (average = 0.7181 ± 0.0021), and the Ävrö granite samples (average = 0.7158 ± 0.0012) with the exclusion of four samples. These four samples represent the chemical Na-Ca-SO_4 and Ca-Na-SO_4 types and have the highest Sr_{tot} concentrations (1.5 ± 0.5 mg/L; Figure 6-13) and the lowest $^{87}Sr/^{86}Sr$ ratios (0.7115 ± 0.0029; Figure 6-14).

/Drake and Tullborg 2009a, b/ describe gypsum together with calcite, fluorite, pyrite, barite, chlorite and mixed layer clay minerals as an infilling mineral in fractures of the Ävro granite from boreholes KLX03 and KLX08. Based on textural and isotope signatures a Palaeozoic age is proposed for this mineral assemblage. Although there are some open questions with respect to the formation temperature (60–150°C according to fluid inclusion investigations and thus too high for gypsum formation), redox conditions (pyrite-gypsum equilibrium?), and thus the absolute age and age relationship of this mineral assemblage, there is no doubt that trace amounts of gypsum occur in some fractures. /Drake and Tullborg op. cit./ report $^{87}Sr/^{86}Sr$ ratios for this fracture gypsum between about 0.7123 and 0.7148, which are lower than those of present-day fracture groundwaters (Figure 6-15). The $^{87}Sr/^{86}Sr$ ratios of fracture gypsum are also lower than most of the experimental solutions. Exceptions are the Ca-Na-SO_4 type experiment solutions of Ävro granite from borehole KLX08, which show similar $^{87}Sr/^{86}Sr$ ratios and the Na-Ca-SO_4 type experiment solutions of Ävro granite from borehole KLX03, which have lower $^{87}Sr/^{86}Sr$ ratios (Figure 6-14). For the Na-Ca-SO_4 type experiment solutions from borehole KLX03 this clearly shows that dissolution of such a type of gypsum during the experiments cannot account for the elevated Sr contents, the $^{87}Sr/^{86}Sr$ ratios and the Ca^{2+} and SO_4^{2-} concentrations. Sample KLX03-8 (–489.64 m elevation), which has a calcite-filled hair fissure (see above), has the overall lowest $^{87}Sr/^{86}Sr$ ratio, far below that of fracture gypsum (Figure 6-14). None of the matrix porewater samples from borehole KLX08 have any visible fractures. It is thus unlikely that the observed fracture gypsum would be the source for Sr^{2+} and $^{87}Sr/^{86}Sr$ ratios in these experiment solutions. If there exists a link between the fracture gypsum and the experiment solutions then the data suggest that this would be more of a genetic link between fracture gypsum formation and *in situ* porewater instead of fracture gypsum and the experiment solution (cf. Chapter 8). The $^{87}Sr/^{86}Sr$ ratios thus support the above observations made based on the chemical composition that most of the Sr in the Na-Ca-SO_4 and Ca-Na-SO_4 type experiment solutions and their $^{87}Sr/^{86}Sr$ ratio is derived from the porewater.

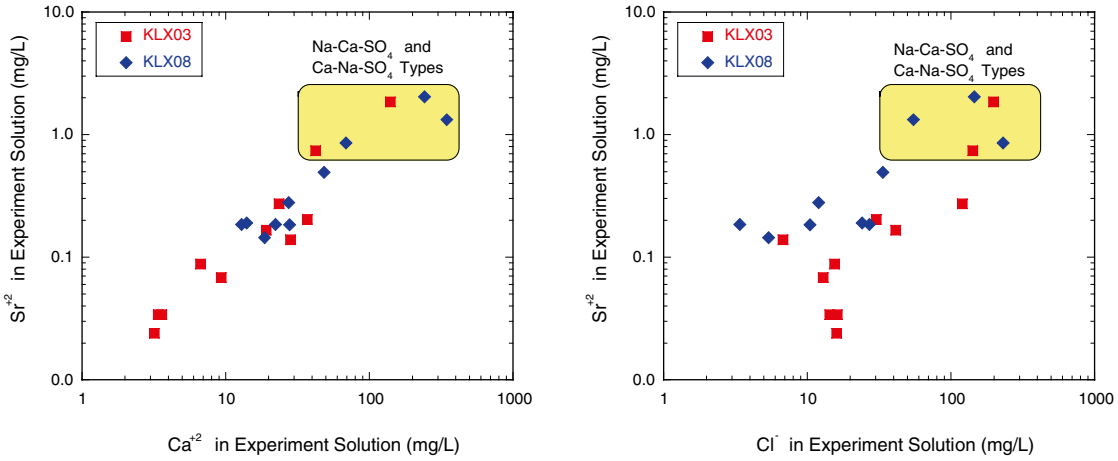

Figure 6-13. *Concentrations of Sr^{2+} versus Ca^{2+} (left) and Cl^{-} (right) in experiment solutions of the out-diffusion experiment at equilibrium with respect to Cl^{-}. Note the log scale and the elevated Sr^{2+} concentrations in the Na-Ca-SO_4 and Ca-Na-SO_4 type solutions.*

In conclusion, the Sr concentrations and the $^{87}Sr/^{86}Sr$ ratios in the experiment solutions clearly support the different character and genesis of the Na-Ca-SO_4 and Ca-Na-SO_4 general type porewaters in the Ävro granite from boreholes KLX03 and KLX08, in spite of Sr being a reactive element (note that there are no Sr-data available for KLX17A). In addition, the $^{87}Sr/^{86}Sr$ ratios in the experiment solutions of the remaining Ävro granite samples and the quartz monzodiorite samples are similar to those measured in fracture groundwaters at similar depths (Figure 6-14). This suggests that the fracture groundwaters derive their strontium signature essentially from the rock from which they were sampled. The only exception of the small dataset is the fracture groundwater sampled in thin intercalated dioritic rock in borehole KLX08, which has a $^{87}Sr/^{86}Sr$ ratio signature typical for Ävro granite.

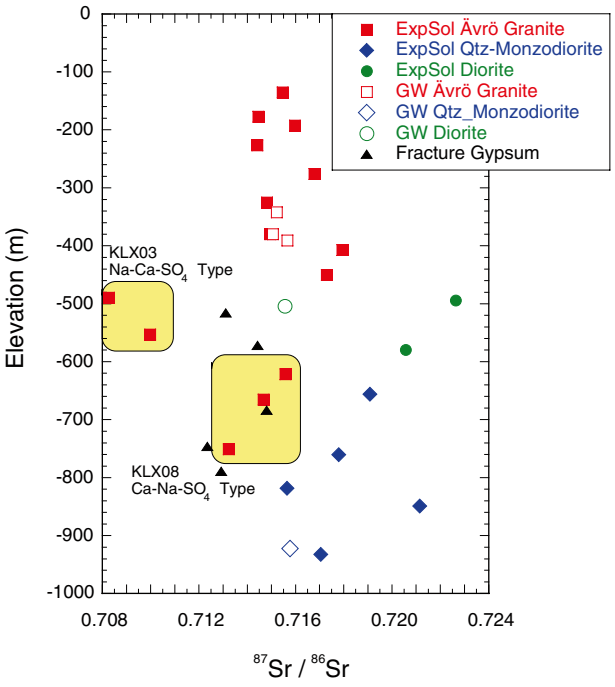

Figure 6-14. *Strontium isotope ratio, $^{87}Sr/^{86}Sr$, in experiment solutions of out-diffusion experiments (closed symbols) and fracture groundwater (open symbols) as a function of rock type and sample elevation in boreholes KLX03 and KLX08 (error bars for $^{87}Sr/^{86}Sr$ are in the size of the symbols; groundwater data from /Laaksoharju et al. 2009/; fracture gypsum data from /Drake and Tullborg 2009a/).*

6.4 $\delta^{18}O$ and $\delta^{2}H$ of porewater

The water isotope composition of the porewater, expressed as $\delta^{18}O$ and $\delta^{2}H$, has been determined by the diffusive-exchange technique. During the course of the Laxemar site investigation programme, the propagated error of the isotope diffusive-exchange technique could be significantly reduced from the first samples collected from borehole KLX03 to the last ones collected from borehole KLX17A (cf. Section 3.2.3). Yet, the overall uncertainty attached to these data is still at the upper end of that attached to the chloride content, certainly for deuterium.

The ratio of the stable isotopes of infiltrating water is, among others, dependent on the temperature and moisture source. This makes the stable isotopes valuable indicators of possible different origins of waters that have similar Cl^- concentrations such as glacial water and present-day infiltration. In contrast to the chloride isotopes, no fractionation is yet known for the oxygen and hydrogen isotopes during diffusion of water through the matrix of a crystalline rock. From the chemical point of view, the interaction between porewater and fracture groundwater can thus be treated for the stable isotopes of water the same way as for the conservative solute Cl^-. From the physical point of view, however, the water isotopes appear to diffuse faster than dissolved Cl^- in low-permeability rock environments up to a factor of about 2 due to the different accessible porosity for the two components /Gimmi and Waber 2004, Mazurek et al. 2009/. During the interpretation of water isotope and chloride porewater data, it has to be kept in mind that changes in the fracture groundwater composition might strongly affect the porewater $\delta^{18}O$- and $\delta^{2}H$-values, but not the chloride in the porewater (e.g. glacial versus meteoric) and vice versa (e.g. Littorina versus Baltic Sea water, brine versus warm-climate meteoric).

Repeating climatic cycles with similar or identical isotope composition in the fracture groundwater will also leave their traces in the porewater and superimpose on each other. Porewater isotope signatures obtained from individual samples collected at large intervals (about 50 m in KLX03 and KLX08) might therefore not resolve a single event during the palaeohydrogeologcal evolution of the system. Exceptions are locations where extreme signatures that can be related to a unique source (e.g. glacial melt water) would have been preserved under certain circumstances. In contrast, a higher resolution and more information about the palaeohydrogeologcal evolution can be gained from porewater samples collected along a continuous profile as collected in borehole KLX17A (cf. Chapter 7).

The water-isotope composition of matrix porewater in rocks of the Laxemar subarea covers a large range of $\delta^{18}O$-values between –14.3‰ and –1.8‰ VSMOW and $\delta^{2}H$-values between about –120‰ and –22‰ VSMOW (Table A-3). In the conventional $\delta^{18}O$-$\delta^{2}H$ diagram, most of the porewater compositions plot along two trend lines, which run essentially parallel to the Global Meteoric Water Line (GMWL; Figure 6-15, top). Trend line ‘A’ is given by the meteoric reference water compositions of the Laxemar subarea, whereas trend line ‘B’ is given by porewaters that plot further to the right, but still parallel to the GMWL. The oxygen and hydrogen composition of the porewater indicates, therefore, a meteoric origin for these waters. Those plotting along trend line ‘A’ suggest a derivation from fracture groundwater that infiltrated under present-day climatic conditions, whereas the porewaters plotting along trend line ‘B’ appear to have been derived from fracture groundwater that infiltrated under warmer climatic conditions and from a different major moisture source than that prevailing today. It is interesting to see that trend line ‘B’ is mainly defined by samples from borehole KLX08, and only few samples from borehole KLX03 and KLX17A fall on this line. These latter samples were collected at large distances to the nearest water-conducting fractures (Figure 6-15, bottom). In contrast, samples from borehole KLX08 represent large and short distances from the nearest water-conducting fractures.

In the $\delta^{18}O$-$\delta^{2}H$ diagram only a few samples plot to the left of the GMWL (Figure 6-15). While this might indicate extended water-rock interactions for deep-seated porewater samples at great distances from water-conducting fractures, the $\delta^{2}H$-values of these samples are less reliable and interpretation limited.

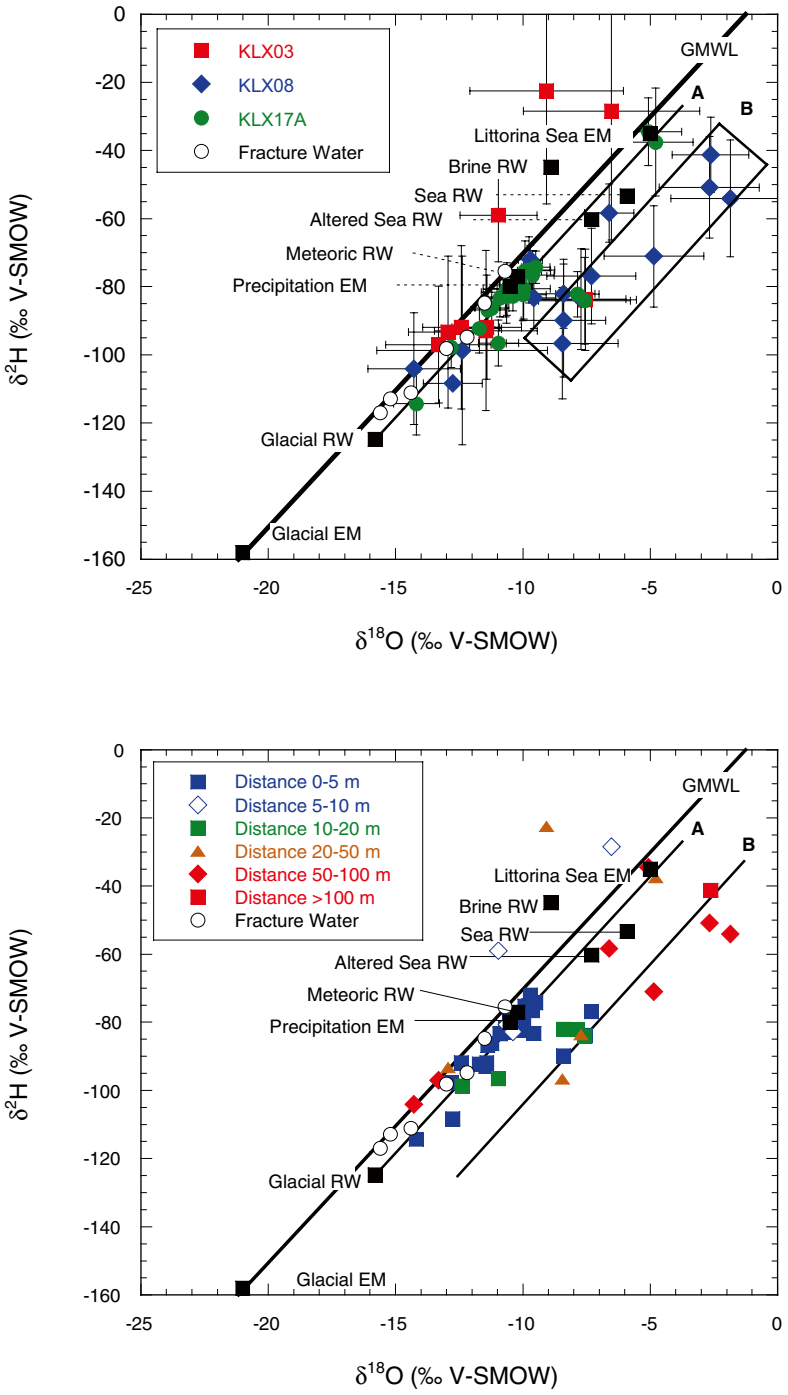

Figure 6-15. *$\delta^{18}O$-$\delta^{2}H$ diagram of porewater as a function borehole or geographic location, respectively (top), and the distance between the porewater sample and the nearest water-conducting fracture. The isotope composition of end-member and reference fracture groundwaters is given for comparison, GMWL: Global Meteoric Water Line; 'A', 'B': trend lines given by the porewater data. Error bars give propagated errors calculated according to Gauss (omitted in lower graph for better legibility).*

Considering the relationships of $\delta^{18}O$ and $\delta^{2}H$ in porewater, their absolute values, the distance between porewater samples and nearest water-conducting fracture, and the Cl^- concentration and chemical type of the porewater, eight different groups of porewater can be distinguished (Table 6-1). As shown in Chapter 5, porewater in a sample located centrally between two 20 m spaced water-conducting fractures would become equilibrated with a fracture groundwater within about 12,000 years given the transport properties of the rocks in the Laxemar subarea and constant fracture-groundwater composition. Based on this, a distance of less or more than 10 metres to the nearest water-conducting fracture in the borehole is used to qualitatively classify the porewater as 'young' and 'old', respectively. The terms 'young' and 'old' thus largely correspond to 'post' and 'pre' last ice coverage of the area.

Because most of the water isotope compositions of porewater appear to plot along lines which run parallel to the GMWL, the trends for $\delta^{18}O$ and $\delta^{2}H$ with depth will be similar and so only the $\delta^{18}O$ values will be plotted against depth and discussed in detail All $\delta^{18}O$ and $\delta^{2}H$ data are relative to VSMOW.

6.4.1 Spatial distribution and relationship to structural features

In common with chloride, the stable isotope composition of porewater shows certain regularities in the lateral and vertical distribution. In spite of the differencies of the boreholes with respect to the major tectonic and deformation zones (Figure 2-1), there exist similarities in the porewater isotope composition in boreholes KLX03 and KLX17A, which differ from those in borehole KLX08. Common to all three boreholes, however, is the dependency of porewater compositions on the frequency of water-conducting fractures and their transmissivity as identified by the downhole differential flow logging.

Porewater $\delta^{18}O$ and $\delta^{2}H$ values and their vertical distribution show greater similarity between boreholes KLX03 and KLX17A when compared to those in borehole KLX08 (Figure 6-16 to 6-18). Unlike the porewater Cl^- concentration profile, however, the isotope concentration profile in borehole KLX08 is not simply shifted to greater depth, but is generally more complex.

Table 6-1. Groups of porewater according to the water-isotope composition, distance to water-conducting fracture and Cl^- concentrations and chemical type of porewater.

Group	Climate	Relative age	Distance to nearest fracture (m)	$\delta^{18}O$ $\delta^{2}H$ (‰ VSMOW)	$\delta^{18}O$-$\delta^{2}H$ Trend line	Cl in porewater (mg/L)	Chemical type
1	present-day		<10 m	–9.5 to –12 –74 to –93	A	70–770	Na-HCO_3
2	warm-climate	young	<10 m	–7 to –9 –75 to –90	B	390–710	Na-HCO_3
3	warm-climate / different moisture source	old	>10 m	–7 to –8.5 –82 to –85	B	120–690	Na-HCO_3
4	cold-climate	young	<10 m	–12 to –14.3 –91 to –114	A	240–820	Na-HCO_3
5	cold-climate	old	>10 m	–12 to –14.3 –91 to –114	A	620–1,000	Na-HCO_3
6	cold ? [1]	young	<10 m	–7.6 to –9.7 –72 to –83	– [3]	1,380–2,760	Ca-Na-SO_4
7	cold ? [1]	old	>10 m	–1.8 to –13.3 –34.5 to –97	– [3]	1,530–7,600	Ca-Na-SO_4 & Na-Ca-SO_4
8	– [2]	old	>>10 m	–2.5 to –6.5 –28 to –58	– [3]	3,040–8,220	Na-Cl-(HCO_3)

[1] The porewater chemical composition suggests an evolution including permafrost-related processes.

[2] Porewater is modified by water-rock and/or deep-seated brine interaction.

[3] The complex porewater evolution excludes a relation to meteoric water types.

In boreholes KLX03 and KLX17A, the porewater isotope composition of group 1 with $\delta^{18}O$ values of porewater between about –9.5‰ and –12.0‰ VSMOW occur down to 412 m and 123 m borehole length, respectively (–380 m and –80 m elevation) where a high frequency of highly transmissive fractures occurs (Figure 6-16 and Figure 6-18). The isotope composition of these porewaters falls along trend line 'A' in the $\delta^{18}O$-$\delta^{2}H$ diagram close to that of modern groundwater (Figure 6-15). What all these samples have in common is that they are located within a short distance (commonly less than 5 m) to the nearest water-conducting fracture (Figure 6-19). Together with the Cl^- content and the chemical type, this indicates a meteoric origin for these porewaters from waters that infiltrated into fractures under present-day climate conditions.

At several depth locations, this general pattern at shallow to intermediate depths is interrupted by porewater that is depleted in ^{18}O (and ^{2}H). Furthermore, these isotope compositions also plot along trend line 'A' in the $\delta^{18}O$-$\delta^{2}H$ diagram. In borehole KLX03 such depleted isotope compositions with $\delta^{18}O$ values of less than –12‰ VSMOW occur at about 160 m borehole length, a distance of about 5 m to the nearest water-conducting fracture, and at 355 m borehole length, a distance of about 25 m to the nearest water-conducting fracture (Figure 6-16). In borehole KLX17A, similarly depleted isotope signatures occur at 332 m and 435 m borehole length (–261 m and –349 m elevation) at a distance of less than 4 m to the nearest water-conducting fracture (Figure 6-16). In addition, depleted isotope signatures indicative of a younger influence are present between 116 m and 118 m borehole length (–74 to –75 m elevation) within the continuously sampled fracture profile, i.e. inbetween present-day type porewater isotope signature (cf. Chapter 7). Based on the distance between pore-water sample and the nearest water-conducting fracture and consistent with the porewater chemical composition, the depleted isotope signature was produced during different time periods. Samples located close to water-conducting fracture (i.e. group 4) experienced a more recent influence of fracture groundwater that infiltrated during a cold-climate period compared to those samples located at greater distance (i.e. group 5).

In borehole KLX017A, samples with isotope compositions enriched in ^{18}O were collected between about 128 m and 134 m borehole length (Figure 6-18). These samples are located more than 10 m from the nearest water-conducting fracture and their isotope compositions plot along trend line 'B' in the $\delta^{18}O$-$\delta^{2}H$ diagram (Figure 6-15). Combined with the low Cl^- concentration of these pore-waters, this suggests a component in the porewater that infiltrated long ago as fracture groundwater under warmer climatic conditions and from a different major moisture source than the present ones (group 3). In borehole KLX03, one porewater sample with similar characteristics is observed at 695 m borehole length (Figure 6-16). The $\delta^{2}H$ value of this sample is, however, not very reliable and an unequivocal assignment to group 3 cannot be made.

In borehole KLX08, the zone with a high frequency of highly transmissive fractures extends deeper down to about 750 m borehole length (about 620 m depth; Figure 6-17). In this borehole, porewater of group 1 that was derived from meteoric water that infiltrated into fractures under present-day climate conditions is only recorded in the shallowest sample at 200.26 m borehole length (–149.07 m elevation). Downwards to 347.1 m borehole length (–275.9 m elevation) porewater enriched in ^{18}O and ^{2}H occurs. The isotope composition of all these samples plots on trend line 'B' in the $\delta^{18}O$-$\delta^{2}H$ diagram (Figure 6-15). Whereas such isotope compositions correspond to those found in KLX17A between about 128 m and 134 m borehole length, the sample in KLX08 at 200.26 m borehole length (–149.07 m elevation) and 660.03 m borehole length (–544.12 m elevation) are located less than 4 m from the nearest water-conducting fracture (Figure 6-19). Therefore, the porewater isotope compositions of these samples suggest a more recent influence of warm climate fracture groundwater (i.e. group 2) compared to the group 3 compositions located at much greater distance from a water-conducting fracture. As shown in Chapter 8, further evidence for such circulation of warm climate fracture groundwater following the retreat of the last ice cover is also indicated in the continuous fracture profile sampled in borehole KLX17A.

Porewater depleted in ^{18}O (and ^{2}H) also occurs in borehole KLX08, but at greater depth compared to the other boreholes. Plotting along trend line 'A' in the $\delta^{18}O$-$\delta^{2}H$ diagram, the depleted isotope compositions occur at 395.65 m and 601.68 m borehole length (–317.63 m and –494.21 m elevation) at a distance of less than 10 m (i.e. group 4) from the nearest water-conducting fracture, and at 550.23 m borehole length (–450.17 m elevation) at a distance of more than 50 m (i.e. group 5).

This latter sample has the most depleted isotope composition ($\delta^{18}O$ = –14.3‰ VSMOW) of all porewater samples. Thus, in borehole KLX08 there also occurs porewater that was modified by different events of cold climate groundwater circulation in the fractures with the most recent such modification (i.e. group 4) extending down to almost 500 m depth.

Common to all three boreholes is the occurrence of brackish Na-Ca-SO_4 and Ca-Na-SO_4 gneral type porewaters at around 430 m depth in KLX03 and KLX17A and about 620 m in KLX08. The change to this chemical porewater type appears to put a lower limit to the alternation of present-day, warm climate and cold climate signatures recorded in the upper porewater samples. Exceptions might include two samples from borehole KLX03 with group 1 and group 3 porewater isotope signatures. However, the δ^2H values of these samples are not very reliable and an unequivocal assignment to a group cannot be made. As already indicated, the brackish Na-Ca-SO_4 and Ca-Na-SO_4 general type porewaters have a highly variable isotope composition with $\delta^{18}O$ values that vary between –7.5‰ and –13.3‰ VSMOW in borehole KLX03 and KLX17A (Figure 6-16 and Figure 6-18) and between –1.8‰ and –9.7‰ VSMOW in borehole KLX08 (Figure 6-17). Unlike the other porewater samples, no clear dependency between isotope composition, chemical composition and distance to the nearest water-conducting fracture is established. It seems more likely that the variable isotope composition is related to the genesis of these anomalous porewaters and the water-isotope composition does not clearly discriminate these porewater types compared to the chemical composition and other isotopes (see above).

With increasing depth, the differences in porewater isotope compositions between the boreholes become less and a trend towards compositions more enriched in ^{18}O and ^2H is observed. At greatest depth, the most saline porewaters in boreholes KLX03 and KLX08 have $\delta^{18}O$ values between about –2‰ and –6‰ VSMOW and δ^2H values of about –28‰ to –58‰ VSMOW (Figure 6-16 and Figure 6-18).

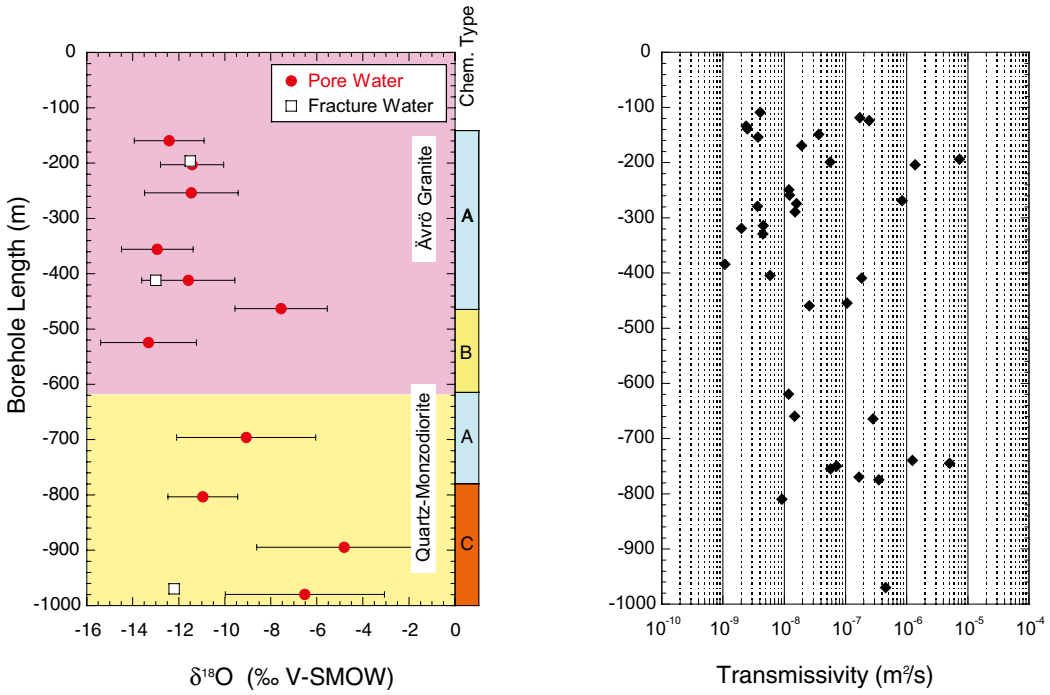

Figure 6-16. *Borehole KLX03: $\delta^{18}O$ of porewater and fracture groundwater as a function of sampling depth (left) compared to the measured hydraulic transmissivity of water-conducting fractures (right, data from /Rouhiainen et al. 2005/). Error bars give propagated error calculated according to Gauss. General chemical types of porewater as in Figure 6-1.*

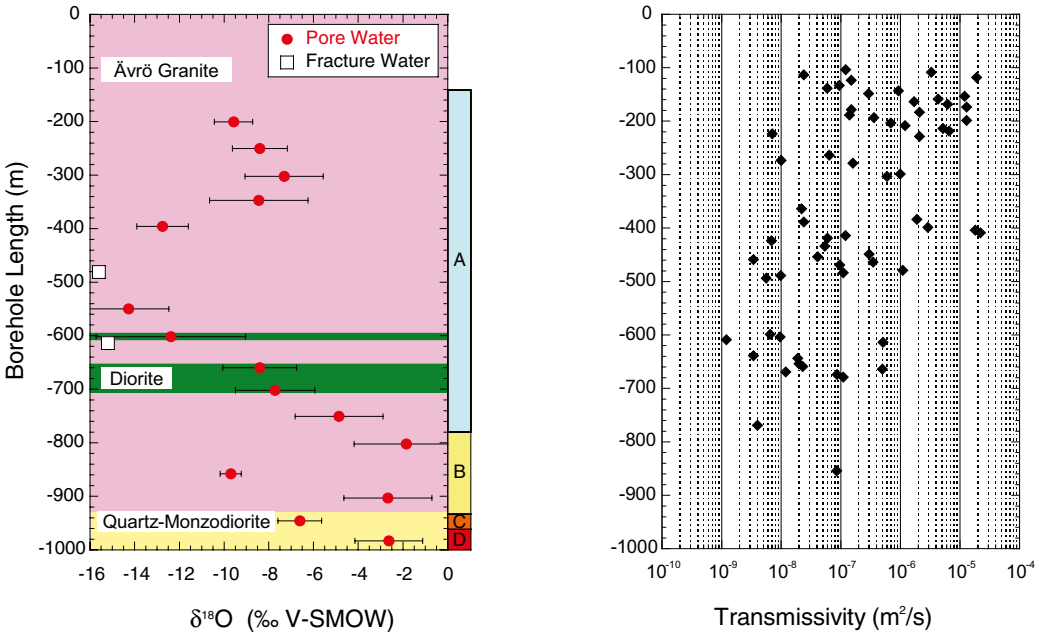

Figure 6-17. *Borehole KLX08: $\delta^{18}O$ of porewater and groundwater as a function of sampling depth (left) compared to the measured hydraulic transmissivity of water-conducting fractures (right, data from /Sokolnicki and Pöllänen 2005/). Error bars give propagated error calculated according to Gauss; general chemical types of porewater as in Figure 6-1.*

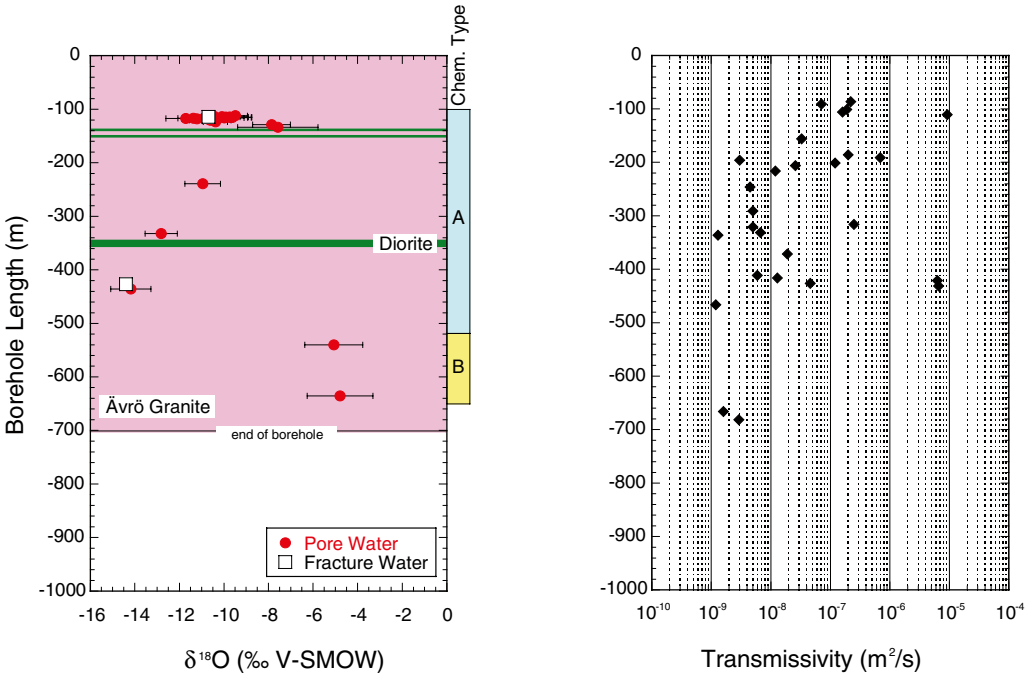

Figure 6-18. *Borehole KLX17A: $\delta^{18}O$ of porewater and groundwater as a function of sampling depth (left) compared to the measured hydraulic transmissivity of water-conducting fractures (right, data from /Pöllänen and Kristiansson 2007/). Error bars give propagated error calculated according to Gauss; general chemical types of porewater as in Figure 6-1.*

6.4.2 Relation between porewater and fracture groundwater

In boreholes KLX03 and KLX17A, porewater samples of the dilute Na-HCO_3 type and located closer than 5 m to the nearest water-conducting fracture have $\delta^{18}O$ and $\delta^{2}H$ values equal to that of fracture groundwater from about 70 m to 230 m depth (Figure 6-19). In this depth interval the exchange of water isotope between porewater and groundwater circulating in the fractures is at steady state as already observed for dissolved chloride (Figure 6-4). Porewater in borehole KLX08 is enriched in ^{18}O and ^{2}H compared to porewater and fracture groundwater from the other two boreholes, except for the shallowest samples. The lack of fracture groundwater data from this interval in borehole KLX08, however, does not allow a statement about the relationship between porewater to fracture groundwater.

Between about 260 m and 350 m of depth in boreholes KLX03, KLX08 and KLX17A, and again between about 450 and 500 m depth in borehole KLX08, there occur cold climate influenced Na-HCO_3 type porewater of group 4 and 5. In the upper interval the fracture groundwater in borehole KLX17A is equally depleted in ^{18}O and ^{2}H compared to modern infiltration (Figure 6-19). A steady state situation between porewater and fracture groundwater is established for the water isotopes, as also observed for dissolved chloride (Figure 6-4).

Fracture groundwaters depleted in ^{18}O and ^{2}H also occur in boreholes KLX03 and KLX08 at about 380 m and 390 m depth, respectively. These fracture groundwaters have, however, high Cl^- concentrations, which are twice as high compared to the porewater, which is more of a group 1 type at these depths in borehole KLX03, i.e. a present-day climate type isotope signature. Therefore, a transient state between porewater and fracture groundwater is established between about 350 m and 400 m depth in boreholes KLX03 and KLX08.

In borehole KLX08, fracture groundwater depleted in ^{18}O and ^{2}H extends down to about 500 m depth. The two Na-HCO_3 type porewaters located at –450 m and –494 m elevation have, within the uncertainty band, similarly depleted isotope signatures and a steady state situation appears to be indicated with respect to the stable isotope signature (Figure 6-19). However, the two porewaters (in one dimension) record greatly different distances to the nearest water-conducting fractures (i.e. groups 4 and 5 isotope signatures) and have Cl^- concentrations that are lower by a factor of 2–10 compared to the fracture groundwater (Figure 6-4). This suggests a very complex genetic relationship between the two porewater samples and the sampled fracture groundwater, if any at all.

No fracture groundwater samples are available from the depth interval between about 430 m and 550 m in boreholes KLX03 and KLX17A, or from between about 620 m and 750 m depth in borehole KLX08 where porewaters of the general Na-Ca-SO_4 and Ca-Na-SO_4 chemical type occur. Based on the fact that some of these porewater samples (group 6) occur at short distances from water-conducting fractures identified by differential flow logging, similar compositions in the fracture groundwater would be expected. Knowledge of the groundwater composition at these depths would certainly contribute greatly to the understanding of the evolution of the porewater composition. However, this remains unresolved at present.

Below 500 m at greater depth, the only fracture groundwater sample available is from borehole KLX03. It has a similar isotopic composition to present-day shallow groundwater; however, this contrasts with the isotope composition of the porewaters, which are enriched in ^{18}O and ^{2}H at these depths in boreholes KLX03 and KLX08 (Figure 6-19). Based on the isotopic composition a transient state is established between the brackish Na-Ca-Cl-(HCO_3) type porewater and this KLX03 fracture groundwater, and this is supported by the Cl^- concentration (Figure 6-4). Interestingly, the differences in isotope composition and Cl^- concentration between the porewater and fracture groundwater diverge in that the porewater is enriched in ^{18}O and ^{2}H, but has a Cl^- concentration that is lower compared to the fracture groundwater.

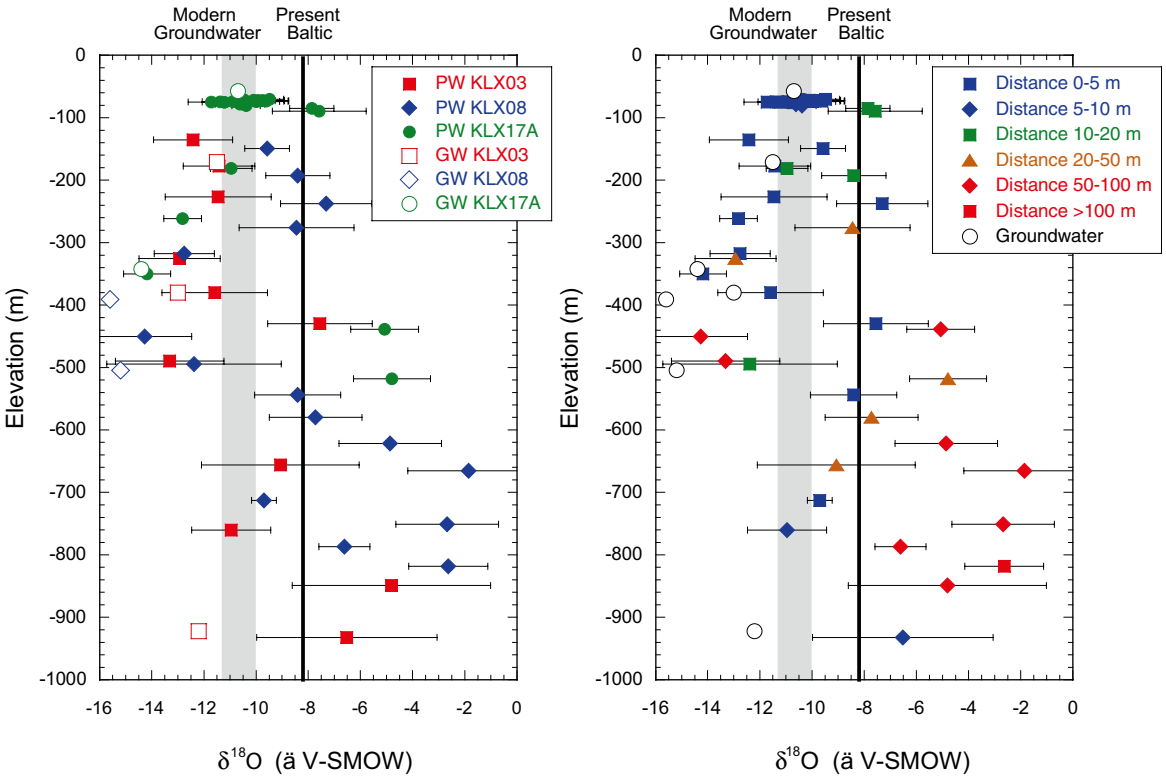

Figure 6-19. *$\delta^{18}O$ of porewater (closed symbols) as a function of borehole from which the core sample was collected (left) and the distance between the porewater sample and the nearest water-conducting fracture (right) versus the sample elevation. The isotope composition of fracture groundwater (open symbols) collected from the same boreholes is given for comparison /Laaksoharju et al. 2009/.*

7 Evolution of porewater tracer profiles

The concentration patterns established for the natural tracers Cl^-, ^{18}O and ^{2}H in porewater located at some distance in low permeability rock from a water-conducting zone, carry information about the long-term interaction between porewater and fracture groundwater. To unravel this interaction at high resolution, possibly allowing the reconstruction over Holocene into Pleistocene times, a continuous profile of drillcore has been collected from a water-conducting fracture into the adjacent intact rock matrix in borehole KLX17A and subjected to porewater investigations.

7.1 Fracture profile in borehole KLX17A

Borehole KLX17A is located in fracture domain FSM-W close to the middle of north-south trending deformation zones ZSMNS001C and ZSMNS059A (Figure 2-1). Prior to drilling into the Ävrö granite and based structural data from boreholes drilled in the neighbourhood, a high frequency of water-conducting fractures was expected to occur at around 100 m below surface in the east-west trending deformation zone ZSMEW900A. This prediction was realised and during further drilling porewater samples were sampled along a continuous drillcore profile extending from the base of this deformation zone at about 112 m, and down into the intact rock matrix according to the concept shown in Figure 7-1 /Waber and Smellie 2008b/. The fracture profile was sampled from 111.90 m to 118.98 m borehole length and additional samples were taken at intervals of about 1 m to 2 m down to the end of the profile at 123.9 m borehole length. This was followed by 5 samples taken at regular depth intervals of about 100 m down to the bottom of the borehole at about 636 m.

Borehole KLX17A is located 27.6 m above sea level and in terms of reference elevation the borehole length corresponds to a porewater profile from –70.4 m to –80.9 m.

7.1.1 Rock texture and structure

Macroscopically, the rock encountered in the fracture profile of borehole KLX17A is generally medium-grained, with an equigranular matrix composed of quartz, K-feldspar, plagioclase, and biotite. Feldspar phenocrysts of 1–3 cm in diameter are randomly distributed in the matrix and display a variably intense reddish hue from hematite staining. A foliation is generally absent or only weakly developed.

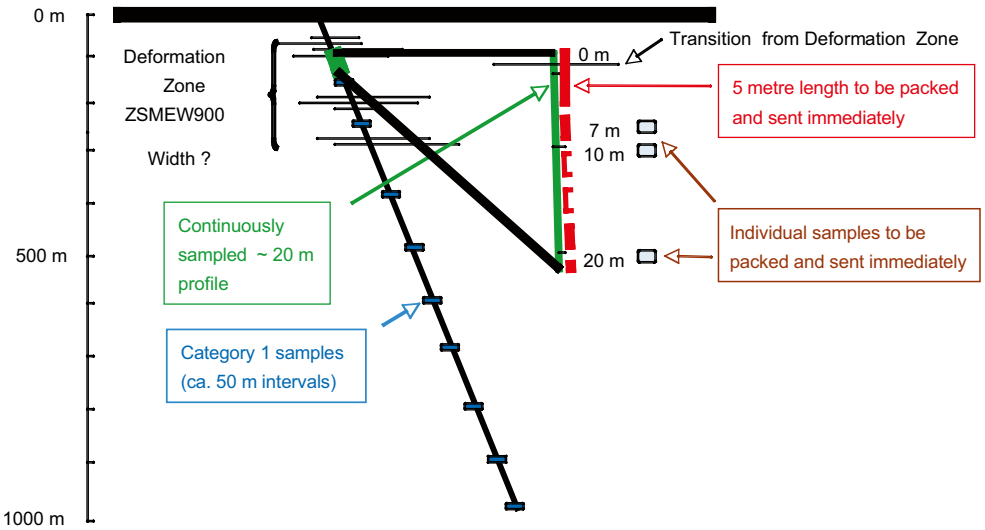

Figure 7-1. Schematic concept of sampling strategy for porewater investigations in borehole KLX17A illustrating the different sample type for the large-scale profile (category 1 samples) and the continuous profile sampled away form the deformation zone into the intact rock matrix /Waber and Smellie 2008b/.

The frequency of closed fissures and hair fissures decreases with increasing depth, i.e. with increasing distance from the deformation zone. In the first six samples, such features are rather abundant (up to three fractures per 20 cm sample length) except for the fourth core sample (KLX17A-4), which is free of fissures. Small, partly open, hair fissures are observed in samples KLX17A-1 to KLX17A-5 and again in KLX17A-10 and KLX17A-14. Especially in the deeper samples outside the main deformation zone, the small nature of these partly open fissures makes it difficult to tell if they are natural or (drilling) induced. Below 117.3 m (sample KLX17A-13) borehole length, hair fissures and similar features become rare, are all closed and are finally absent down to the end of the profile at 123.9 m (sample KLX17A-18).

7.1.2 Hydraulic situation

In borehole KLX17A, highly transmissive intervals occur between about 108 m and 111 m borehole length as recorded by the differential flow logging. Major responses in the flow rate and single point resistance log occur at borehole lengths 108.8–109.4 m (not sampled in the fracture profile), 100.2–100.4 m, 111.2–111.4 m and 113.0–113.2 m. At these depths, the transmissivity measured at one metre intervals ranges from 6.1×10^{-6} and 1.4×10^{-7} m^2/s /Pöllänen and Kristiansson 2007/. The borehole image processing system (BIPS) reveals a strongly tectonised and fracture interval between 108.4 m and 110.5 m borehole length /Gustafsson and Gustafsson 2007/. An accumulation of fractures occurs again between 111.2 m and 111.4 m borehole length and it appears that these fracures are water-conducting and responsible for the elevated transmissivity. Down to about 113 m borehole length where an open fracture is visible in the BIPS log, the rock is unfractured and has no hair fissures; this fracture is also visible in the drillcore sample KLX17A-3 used for porewater investigations. The hydraulic transmissivity of the one metre interval containing this fracture is 7.4×10^{-8} m^2/s /Pöllänen and Kristiansson 2007/.

Further down the borehole the hydraulic transmissivity was below detection ($<10^{-9}$ m^2/s) to about 160 m borehole length, and the rock also seems intact for at least 30 m (BIPS log) before an accumulation of closed fractures is visible. The resolution of the BIPS log is, however, limited with respect to the detection of small open hair fissures. In turn, such partly open fissures are recognised in the drillcore samples around 113.8–114.0 m, 116.0–116.2 m and 117.2–117.5 m borehole length (samples KLX17A-4, KLX17A-10 and KLX17A-14, respectively). Across all these intervals responses in the single point resistance log occur, whereas they are not resolved by the flow rate log /Pöllänen and Kristiansson 2007/.

7.1.3 Water content, water-loss porosity, transport properties

The water content of samples collected from within the deformation zone is about twice as high compared to that of samples further distant from the deformation zone (Figure 7-2). High water contents coincide with a higher degree of alteration of the rock and a higher frequency of partly open and closed fissures in the rock samples. Water contents of samples outside the deformation zone are between about 0.2 and 0.3 wt.% and thus within the range typical for non-deformed, weakly altered Ävrö granite (Table A-1).

The water-loss porosity mimics the profile of the water content because of the similar density of the samples (Figure 7-2). The unusually high water-loss porosity of 2.9 Vol.% in sample KLX17A-3 is due to the intense argillaceous alteration of this sample around the open fracture.

Pore diffusion coefficients were derived for individual samples from the out-diffusion experiments. The fracture profile in borehole KLX17A is located at shallow depth roughly 100 m below the surface in the zone of dilute fracture groundwater and porewater. As a consequence, Cl^- concentrations in the final experiment solutions, i.e. after equilibration, were low for all samples with most below 5 mg/L. In the course of the out-diffusion experiments, time series of Cl^- concentration have been collected for 13 out of the 18 samples describing the fracture profile. Because of the low salinity of the porewater in these depths, the Cl^- concentration of the first time-series sample taken during the first days of out-diffusion is only around 1 mg/L for most samples. Furthermore, the concentration increments in the 0.5 mL of test water collected for the time series are mostly in the range of a few tens of milligrams. Such low concentrations are very susceptible to contamination

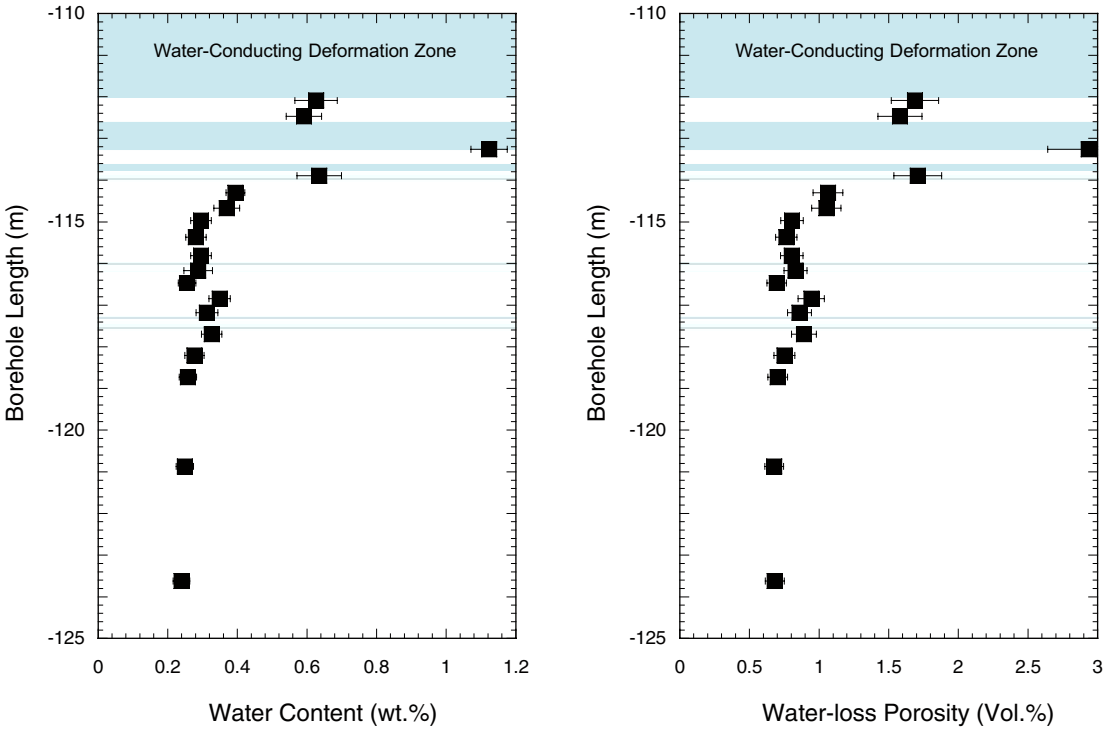

Figure 7-2. *Water content (left) and water-loss porosity (right) of samples collected along a profile away from the water-conducting deformation zone ZSMEW900A into the intact rock matrix. The solid background colour indicates zones with a hydraulic transmissivity of 10^{-7} m²/s to 10^{-8} m²/s. The fine lines indicates small conductive zones with hydraulic transmissivity at detection limit, i.e. $<10^{-9}$ m²/s, data from /Pöllänen and Kristiansson 2007/.*

and/or modification by evaporation of the small sample volumes. In addtion, the small concentration differences are at the accuracy limit of the applied analytical technique. In spite of these experimental and analytical limitations, the chloride time-series data of the out-diffusion experiments display diffusion-type curves. However, not all Cl^- time series were suited for modelling Cl^- diffusion coefficients because of the limitations mentioned above.

The chloride time-series data suited for modelling indicate that diffusion is the dominant transport mechanism for Cl^- during the out-diffusion experiments. This also accounts for the samples from within the deformation zone, in spite of their hair fissures and elevated water-loss porosity values. Differences in the out-diffusion of Cl^- exist, however, among individual samples as indicated by visible changes in slope during the first days of out-diffusion of Cl^- (Figure 7-3). Modelling of the Cl^- data has been performed assuming homogeneous properties across the entire drillcore (cf. Chapter 5). For the tectonised drillcore samples from the deformation zone this results in a somewhat higher uncertainty in the derived pore diffusion coefficient for Cl^- compared to non-tectonised samples. Improvement of the obtained pore diffusion coefficients could be obtained by modelling the data assuming heterogeneous diffusion properties.

For Ävrö granite samples collected from the fracture profile in borehole KLX17A, the modelled pore diffusion coefficients range between about 1.7×10^{-11} m²/s to 6.9×10^{-11} m²/s. The samples are thus within the range of the chloride diffusion coefficient derived for Ävrö granite drillcore samples from other boreholes (5.8×10^{-11} m²/s ± 2.7×10^{-11} m²/s, Chapter 5).

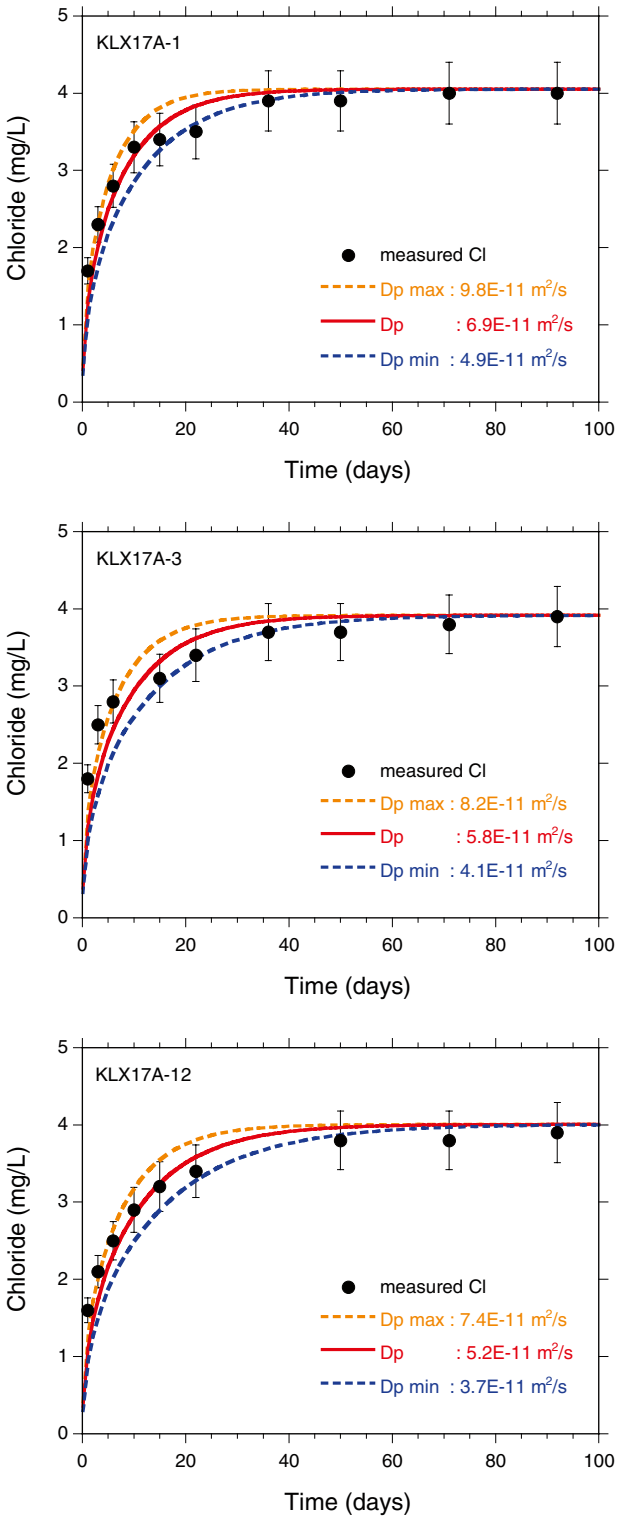

Figure 7-3. *Typical patterns of chloride time series of samples collected in the fracture profile: samples KLX17A-1 and KLX17A-3 come from within the main deformation zone, sample KLX17A-12 comes from the intact rock matrix. Note the steeper slopes in the first days of Cl^- out-diffusion in the samples from the deformation zone. The uncertainty range (D_p min and D_p max) is given by a factor of 2 around the best fit value (red curves).*

7.2 Natural tracer concentrations

7.2.1 Chloride

Chloride concentrations in the porewater along the fracture profile are low, being less than 300 mg/kg_{H2O} even in the undisturbed rock matrix. Nevertheless, they show a distinct, but complex pattern with increasing distance from the deformation zone ZSMEW900A. Chloride concentrations in the porewater vary by more than a factor of three over a few metres from the deformation zone into the undisturbed rock matrix (Figure 7-4). They are lowest in the first four samples within the deformation zone where similar Cl^- concentrations of around 80–90 mg/kg_{H2O} occur. Further into the rock matrix, the concentrations increase uniformly to about 250 mg/kg_{H2O} at 115.5 m borehole length, drop again to about 150 mg/kg_{H2O} at 117.1 m before increasing again to around 275 mg/kg_{H2O} which corresponds, within the uncertainty band, to about the background value (Figure 7-4).

It is interesting to note, although not surprising, that the changes in Cl^- concentration correspond to the water-conducting intervals as identified by differential flow logging and tectonised zones with hair fissures in the drillcores and the BIPS logging (cf. Section 7.1.2). Maybe the only exception is the section between 116.0–116.2 m borehole length represented by sample KLX17A-10. Although the Cl^- concentrations (and $\delta^{18}O$ and δ^2H values, cf. Section 7.2.2) show a slight deviation from the concentration pattern given by the surrounding samples, the difference is within the analytical uncertainty and thus not well defined. In a first assumption, therefore, this zone has been neglected as a significant water-conducting zone in the quantitative interpretation.

The Cl^- concentration profile can be divided into four hydraulic zones that extend from deformation zone ZSMEW900A into the intact rock matrix (Figure 7-4). Zone A comprises samples KLX17A-1 to -4 and represents the highly transmissive zone down to 114 m borehole length. Zone B represents an intact, homogeneous rock portion from 114 m to 117.2 m borehole length and comprises samples KLX17A-5 to -13. Zone C describes the tectonised section from 117.2 m to 117.5 m as identified from the single point resistance log and drillcore mapping. Due to the sample length required for out-diffusion and diffusive isotope-exchange experiments, no porewater sample represents the centre of this zone and samples KLX17A-13 and KLX17A-14 come from the upper and lower border of

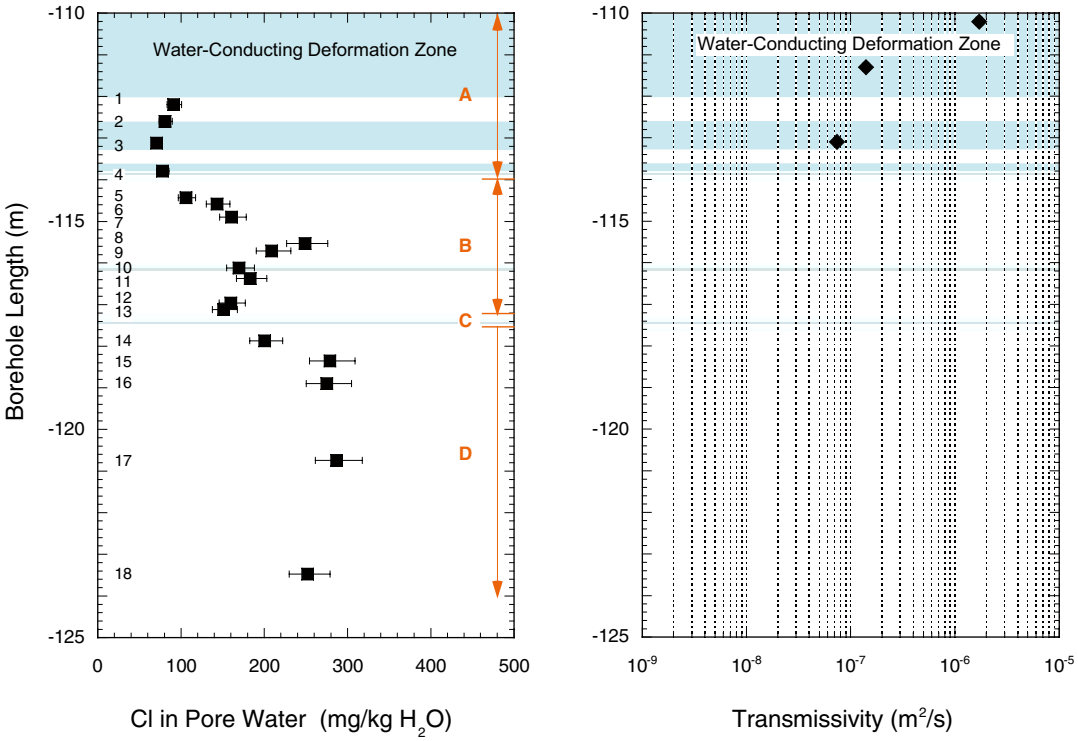

Figure 7-4. *Chloride concentrations in matrix porewater of Ävrö granite samples in borehole KLX17A as a function of distance to the water-conducting deformation zone (left) and the measured transmissivity of 1 m intervals (right, data from /Pöllänen and Kristiansson 2007/). Numbers in the left-hand plot indicate sample numbers and letters refer to the different hydraulic zones (see text).*

zone C. Finally, zone D represents the intact, homogeneous rock matrix further away from the water-conducting deformation zone. According to the differential flow logging, BIPS logging and drillcore mapping, this section extends for about 30 m further into the rock matrix.

In hydraulic zone A, the similarity of Cl^- concentrations of the first four samples suggests that they are at steady state with the groundwater present in the identified fractures. For confirmation, however, a groundwater sample would be needed from a packed-off interval between about 110 m and 113 m borehole length. Unfortunately, the only groundwater sample collected so far is an open-hole tube sample with a mixed composition and the analysis is not representative for this section of deformation zone ZSMEW900A. Fracture fresh groundwater sampled from similar depths in other boreholes in the area show chloride concentrations between 70 mg/L to 120 mg/L (cf. Sicada dataset, Extended data freeze Laxemar 2.3) indicating that the porewater and groundwater in zone A might indeed be in steady state with respect to Cl^-.

The continuation of the profile is complex and cannot be interpreted based on the Cl^- signatures in the porewater alone. This is because different scenarios may explain the observed concentration profile depending on the preferences made based on present knowledge on the palaeohydrological evolution and hydraulic conditions of the site. Based on the Cl^- data, for example, one might argue that only fracture groundwater circulating in zone A forms a boundary condition of the system and the observed profile represents the superposition of multiple step changes in fracture-groundwater composition. On the other hand, fracture groundwater might also circulate in zone C. In this case it is necessary to discern between scenarios where changes in the fracture groundwater composition of zones A and C have occurred at the same time, and scenarios where such changes have occurred with a time delay in fracture groundwater in zone C due to the indicated lower transmissivity of this zone compared to zone A. In both cases, the chloride data cannot discern between a single step change or multiple step changes in the boundaries (i.e. changes in the fracture-groundwater composition in zones A and C). As shown below, some discrimination between these scenarios can be made based on the isotope composition of porewater.

7.2.2 Water isotopes ($\delta^{18}O$ and $\delta^{2}H$)

All porewaters in the fracture profile samples collected from borehole KLX17A are of meteoric origin as indicated by their $\delta^{18}O$ and $\delta^{2}H$ values. These plot parallel to the GMWL on trend line 'A' (Figure 7-5), in common with most other porewaters and also the reference water compositions (cf. Section 6.4). The range of isotope ratios covered by the samples is smaller compared to that of present-day annual precipitation ($\delta^{18}O$ approximately –6.9‰ to –17‰ VSMOW /Laaksoharju et al. 2009/). Smoothing of the extreme isotope signatures is typically observed as a result of dispersion during infiltration of groundwater. In porewater, therefore, an even smoother isotope signature would be expected because of the slow exchange between porewater and fracture groundwater. Nevertheless, the largest difference between porewater samples is 2.5‰ VSMOW for $\delta^{18}O$ and 18‰ VSMOW in $\delta^{2}H$, which falls outside the cumulated analytical error and suggests that different climatic signatures are still preserved in the porewater.

The $\delta^{18}O$ and $\delta^{2}H$ values show an almost identical pattern as a function of the distance from the water-conducting deformation zone (Figure 7-6). The patterns are also similar to that obtained for the Cl^- concentrations with maximum and minimum values occurring at the same positions (Figure 7-4 and Figure 7-6). However, the relative difference between maximum and minimum values differ for the $\delta^{18}O$ and $\delta^{2}H$ values and the Cl^- concentrations, and there exists no correlation between Cl^- concentrations and $\delta^{18}O$ and $\delta^{2}H$. For example, samples collected within zone A (i.e. the conducting deformation zone) have identical isotopic composition when compared to the background compositions in zone D comprising intact rock matrix, whereas Cl^- concentrations are lower in zone A. Similarly, porewater isotope compositions in the centre of zone B are enriched in ^{18}O and ^{2}H compared to the background compositions in zone D, whereas Cl^- concentrations are similar. And finally, porewater isotope compositions of samples KLX17A-13 and -14 surrounding the potentially conductive zone C are most depleted in ^{18}O and ^{2}H compared to all samples, whereas Cl^- concentrations are intermediate between those of zone A and zone D. This latter observation bears consequences on the possible scenarios mentioned above in that these scenarios cannot be resolved based on Cl^- concentrations alone. The isotopic composition of the porewater clearly indicates that there must be a fracture groundwater flow in zone C and that in this zone relicts of water are still present that infiltrated during colder climatic conditions.

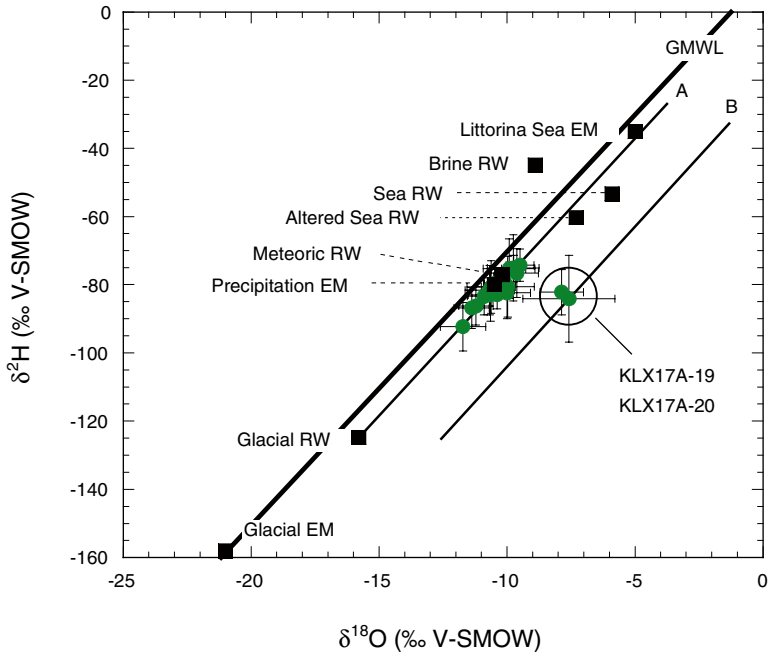

Figure 7-5. *$\delta^{18}O$ vs. $\delta^{2}H$ of porewater of Ävrö granite samples collected along the fracture profile in borehole KLX17A. Note the different signatures of samples KLX17A-19 and -20, which are located along the profile further into the intact rock matrix (error bars give propagated error calculated according to Gauss).*

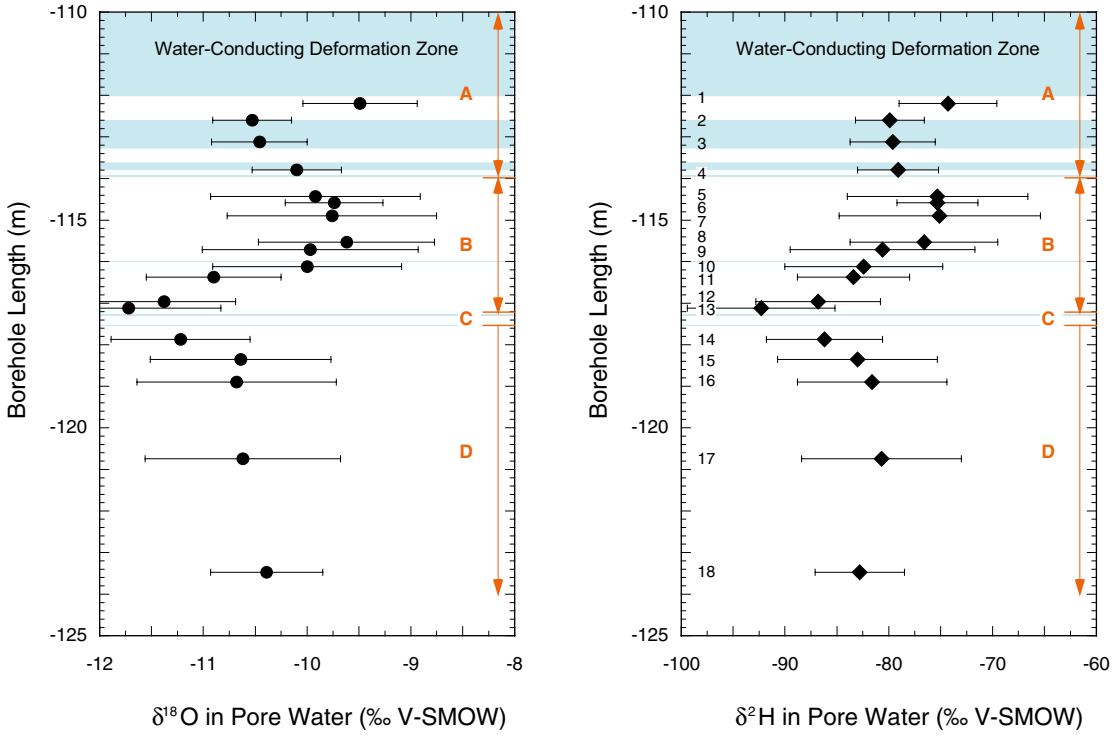

Figure 7-6. *$\delta^{18}O$ (right) and $\delta^{2}H$ (left) of porewater of Ävrö granite samples collected along the fracture profile in borehole KLX17A as a function of distance to the water-conducting deformation zone. Error bars give propagated error calculated according to Gauss. Numbers in the right-hand plot indicate sample numbers and letters in both plots refer to the different hydraulic zones (see text).*

Another interesting palaeohydrogeological aspect comes from the isotopic composition of samples KLX17A-19 and -20 collected some 5 m and 10 m even further into the intact rock matrix. These samples were not considered in the quantitative interpretation of the fracture profile due to the large spacing between the samples, which makes it difficult to quantify the observed large concentration gradient adequately. Moreover, the differential flow log, single resistance log, BIPS logging and borehole mapping failed to indicate a water-conducting zone in the borehole down to these depths, which suggests that these samples might well represent the continuation of the fracture profile. The samples have similar low Cl^- concentrations (213–310 mg/kgH_2O) as the deepest samples of the fracture profile, but differ greatly in their isotopic composition. They are enriched in ^{18}O and ^{2}H and plot on trend line 'B' in the $\delta^{18}O$-$\delta^{2}H$ diagram (Figure 7-5) suggesting an origin from fracture groundwater that infiltrated during warmer climatic conditions (cf. Section 6.4). In comparison with the upper part of the profile, the preservation of such isotopic and Cl^- signatures indicates that water-conducting zones similar to that of deformation zone ZSMEW900A, where changes in infiltration arrive rapidly, are not present close to these these samples. Therefore, the chemical and isotopic signatures, combined with the indicated large distances to the nearest water-conducting fracture, suggest that these porewaters are derived from meteoric water that infiltrated before the Weichselian glacial cycle during a long-lasting warm climate period characterised by a different major moisture source.

7.2.3 Qualitative interpretation of the tracer profiles

For the interpretation of the profiles described by the natural tracers Cl, $\delta^{18}O$ and $\delta^{2}H$ in the porewater of the Ävrö granite the following questions need to be answered:

1) Are the profiles only affected by the upper fracture zone A? Or are they also affected by the lower water-conducting zone C (Figure 7-4 and Figure 7-6) or even by other water-conducting features not visible in the borehole?
2) Do the water-conducting zones A and C at the borehole location have the same chemical signatures at present or do they differ, possibly because of different transmissivity as suggested be the difference flow log? In the second case, it would result in a time lag of a specific chemical and isotopic signature.
3) Can the profiles be explained by a single step change from the initial compositions as observed in zone D to the present-day fracture-groundwater composition in the water-conducting zones (zones A and C)? Such a scenario would describe only the most recent part of the evolution.
4) Does a more complex palaeohydrogeological evolution represented by several subsequent step changes of the fracture groundwater composition have to be invoked? Such a scenario would look further back into the past including several compositional changes of groundwater in the fracture(s).

Attempts to define possible evolution scenarios can be undertaken to investigate the differences in the relative tracer concentration changes along the profile. The comparison of the datasets reveals the following answers to the above questions:

- Both fracture zones A and C appear to affect the Cl^- and the stable isotope profiles. This becomes evident from the sharp decrease in both the Cl^- concentrations and $\delta^{18}O$ and $\delta^{2}H$ values towards zone C, which seems inconsistent with a simple diffusive propagation of compositional changes in zone A towards greater depth.
- The lower fracture zone C has a higher Cl^- concentration than the upper fracture zone A, but more depleted water isotope values (Figure 7-4 and Figure 7-6) indicating that the composition of the water in zone C must be different compared to that in zone A. This can be associated to the different hydraulic conductivity in the two zones being much lower in zone C. Consequently, the same chemical or isotopic signature in zone A will arrive at the borehole location in zone C with a time lag resulting also in a delayed modification of the porewater.
- A link between the maximum values in the centre of zone B and a nearby water-conducting zone not visible in the borehole cannot be excluded. In the absence of any data supporting such a feature this was, however, not further considered as a possible scenario.

- Isotope composition in the porewater of samples from zone B are more enriched in $\delta^{18}O$ and $\delta^{2}H$ compared to the background composition in zone D and also different from the boundary conditions in zone A. This indicates that at least on one occasion during the evolution, the fracture zones A (and possibly C) must have conducted water with an enriched isotope composition compared to that circulating there today. In addition, the depleted isotope signatures in the porewater of zone C are also different from the background and the present-day fracture groundwaters in zone A.
- Thus, at least three different fracture-groundwater compositions appear to have influenced the porewaters in zones B and D: the present-day water in zone A, a water enriched in ^{18}O and ^{2}H, and a water depleted in ^{18}O and ^{2}H. This latter water also appears to have had a low Cl^- concentration.

Combining the information gained from the Cl^- concentrations and the porewater isotopic signatures, it appears that the background conditions down to 125 m borehole length have developed under a moderately warm climate (similar to today) and with moderately mineralised groundwater (Cl^- about 300 mg/L) circulating in the fractures for a very long time (i.e. in the order of $>10^4$ years). For a short time period (approximately 10^3–10^4 years), dilute water of a colder climate origin must have circulated in the fracture. These signatures are still preserved in the depleted isotope composition and the low Cl^- concentration in zone C at 117.2–117.5 m along the profile (Figure 7-6 and Figure 7-4). This was followed by chlorine-rich water that was enriched in the heavy isotopes ^{18}O and ^{2}H as observed in the porewater in zone B between 114 m and 116 m along the profile. Based on these data alone, it cannot be resolved if this groundwater was saline in origin (e.g. seawater) or moderately mineralised water from a warm-climate period, warmer than today. The fact that the Cl^- concentrations in the porewater in this interval are below the background concentration in zone D, however, supports more the second possibility. The final step in the evolution is then the change to present-day conditions in the fracture slowly modifying the established signatures to those observed today.

7.3 Numerical simulations

A series of numerical simulations were performed in order to quantify the different and complex tracer profiles and the exchange between rock matrix porewater and fracture groundwater in terms of solute transport processes. In agreement with the determined transport properties of the rock matrix, diffusion was regarded as the dominant transport mechanism for solutes dissolved in the porewater of the rock matrix in all simulations. In contrast, the water-conducting zones were treated as mixing cells with constant concentrations over a specified time interval.

In the initial simulations the transport calculations were based on the one-dimensional advective-dispersive equation with constant coefficients. The porosity, θ, or water content was assumed to be constant throughout the rock matrix and therefore could be eliminated from the equations. For zero or very low advective velocities as considered for the simulations, dispersion in the rock matrix is dominated by diffusion as given by the pore diffusion coefficient D_p. A semi-analytical solution was used to solve the advective-dispersive equation for constant concentrations in the water-conducting zone on one side of the domain (zone A) and zero gradient in the rock matrix (zone D), or constant concentrations in the water-conducting zones on both sides (zones A and C) of the domain (zone B) and zero gradient in the rock matrix (zone D). The solutions were obtained in Laplace space and inverted back numerically with the Talbot algorithm (cf. /Gimmi and Waber 2004/ and /Gimmi et al. 2007/ for details). In these simulations each tracer had to be calculated separately.

For later simulations the numeric code FLOTRAN /Lichtner 2004/ was used. This code has recently been benchmarked and used for the numerical simulation of concentration profiles across nine different sedimentary formations of low-permeability in Belgium, France, Switzerland and United Kingdom /Mazurek et al. 2009/. The modelled natural tracers in porewater included Cl^-, $\delta^{37}Cl$, $\delta^{18}O$, $\delta^{2}H$ and He. All these formation are either considered as potential host rocks or research sites for the geological disposal of radioactive waste.

FLOTRAN can simulate time-dependent, coupled thermal-hydrological-chemical processes in variably saturated, non-isothermal porous media in up to three dimensions. It calculates multi-component reactive transport involving aqueous, mineral or gaseous species. It can also be used for for systems consisting of fractured porous media and for systems involving two-phase flow (i.e. liquid and gaseous phase). Both Cartesian and cylindrical model geometries can be used. FLOTRAN consists of two distinct modules: The first module (FLOW) solves the flow equation for water and (optionally) gas, and the heat transport equation. The second module (TRANS) solves the mass conservation (i.e. transport) equations for a multi-component geochemical system. In simulations performed with FLOTRAN all tracers (i.e. Cl^-, $\delta^{18}O$ and δ^2H) were calculated simultaneously.

In stand-alone mode, the TRANS module incorporates advective/dispersive and diffusive transport in the liquid or both gaseous and liquid phase. TRANS may use a constant flow velocity or an externally calculated steady state flow field for simulating one- or three-dimensional problems, respectively. The diffusion coefficient is temperature dependent and optionally species dependent. The tortuosity is allowed to vary in space and to be isotropic or anisotropic. Consequently, the pore diffusion coefficient, D_p, can be spatially heterogeneous or can vary in the principal coordinate directions. TRANS uses a range of solution algorithms based on the finite difference method in which the model domain (i.e. the spatial representation of the natural system) is separated into a grid of rectangular blocks. In each of these representative elementary volumes (REV) material and system properties, such as porewater composition, mineralogy, porosity, permeability, temperature, pressure etc. are assumed to be uniform. TRANS can use implicit, explicit or the operator-splitting method to solve transport and chemistry sequentially, i.e. it splits each time step into a transport time step and a reaction time step. Boundary conditions are handled in TRANS as Dirichlet-type conditions (constant concentration) or zero-flux type boundary conditions. When diffusion is the only transport mechanism in the system, diffusive mass transfer can occur across the boundary and depends on the concentration gradient across the boundary. If advection occurs into the system at this boundary, the fluid entering the system has the composition specified by that boundary condition. In contrast, if a zero-flux condition is specified, the concentration gradient across that boundary is zero and the boundary is closed with respect to mass transport. In the present simulations, a slightly modified version of FLOTRAN was used that allows also to consider time-dependent boundary conditions and the specification of properties such as concentrations at internal nodes at given times.

Note: For modelling purposes it is inconvenient to use 'BC' as a time annotation and conversion of absolute times to 'BC' in the many model runs and plots bears the risk of easily introducing mistakes. Therefore, the time annotation used here is 'BP' which refers to 'before the year of 2008', the time the model calculations have been performed.

7.3.1 Climatic and hydrological issues

The qualitative interpretation of the porewater data suggests that the concentration profiles of Cl^-, $\delta^{18}O$ and δ^2H are the product of at least three different types of fracture groundwater that subsequently circulated in the fractures of deformation zone ZSMEW900A (Section 7.2.3). The evolution of the tracer concentration profile and the initial conditions of porewater deep within the rock matrix must thus be brought into context with the known climatic and hydrological conditions of the Laxemar subarea.

Climate

During Quaternary times, the Laxemar subarea was glaciated several times during the major glacial cycles Elster (Marine Isotope Stage MIS12 or 10), Saale (MIS 6) and Weichsel (MIS 5d–2). These glacial cycles were interrupted by the interglacial periods of Holstein (MIS 11, 400,000 years or possibly MIS 9, 325,000 years BP) and Eemian (MIS 5e, 130,000–115,000 years BP). During the Eemian interglacial, the climate in Sweden was periodically warmer by 1°–2°C compared to today (/Söderbäck 2008/ and references therein). During the first two stadials of the Weichselian glacial cycle from about 115,000–100,00 years BP and from 90,000–80,000 years BP the Laxemar subarea appears not to have been covered by ice and tundra type vegetation was developed instead. The climate during these glacial stadials and their ice-free interstadials was, however, considerably colder than the present and permafrost conditions prevailed in large parts of Sweden /Söderbäck

2008/. The last glacial phase of the Weichselian glaciation began about 70,000 years ago and larger parts of Sweden were thereafter covered by ice until the last deglaciation /Lundqvist 1992/. More recent climate data and models sugggest, however, that also ice free conditions prevailed in southern and central Sweden during this period especially during parts of MIS 3 (e.g. between about 44,000–24,000 years; /cf. Wohlfarth 2009, Kjellström et al. 2009/). The ice sheet reached its maximum extent during the Last Glacial Maximum (LGM, about 20,000 years BP) before the ice began to retreat at a change towards warmer climatic conditions about 18,000 years BP.

The Laxemar area became ice free about 14,000 years BP /Lundquist and Wohlfarth 2001/. The retreat was interrupted during the cold period of the Younger Dryas (about 12,850–11,650 years BP) and at some locations the ice sheet advanced again. According to present knowledge, the Laxemar subarea was covered with water during this cold phase suggesting that it was not affected by permafrost at this time /Söderbäck 2008/. The climate finally changed to warmer conditions at the end of the Younger Dryas, which marks the onset of the present Holocene interglacial.

During the Holocene the climate in Sweden displays several small oscillations of about 1°C between warmer and colder periods compared to present /Karlén et al. 1995/. The most pronounced oscillation was during the Holocene thermal maximum between about 7,000 and 4,000 years BP when the mean annual temperature was between 1.5°C and 3°C higher than at present /Heikkilä and Seppä 2003, Antonsson et al. 2006, Antonsson and Seppä 2007/. After this period the oscillations were again more moderate (or only short-termed) until the present.

Palaeohydrology

The palaeohydrological situation at the Laxemar subarea is fairly well understood over the last 14,000 years BP, i.e. the period since the retreat of the last ice sheet, but little is known about the situation during late Pleistocene times. Some information exists about the Eemian interglacial (130,000–115,000 years BP) during which the sea level was at least periodically higher than at present resulting in a recurrent submersion of the Laxemar subarea (/Söderbäck 2008/ and references therein). The salinity of the Eemian Sea varied between brackish and marine and at least periodically appears to have been 5–10‰ more saline compared to all Holocene Baltic sea types.

Since the last glaciation the regional groundwater flow in the Laxemar subarea is driven by topography with a general gradient from the elevated areas in the west to the Baltic Sea in the east. The flow pattern is largely governed by the mutual connections of the deformation zones, which characterise the region /Rhén et al. 2008/. In the same period, the Baltic Sea has been characterised by a series of fresh water and brackish stages, which have been caused by interplay between variations in the relative sea level and the isostatic uplift. The evolution can be divided into four main stages: Baltic Ice Lake, Yoldia Sea, Ancylus Lake, and Littorina Sea (/Söderback 2008/ and references therein). The timing and salinity ranges of these stages in the Laxemar area are given in Table 7-1. The Laxemar site has experienced at least two periods of transgressions. The first transgression took place during the Ancylus Lake stage and was a lacustrine transgression. The more recent transgression caused by the increased global sea level took place during the early part of the Littorina Sea stage when the seawater was saline. More recent sediment stratigraphic studies from north and south of the Laxemar area suggest even more transgressive cycles and it is likely that the area was at least partly subjected to several (short-termed) transgressions during the Littorina Sea stage (/Söderback 2008/ and references therein). The most saline period during the Littorina Sea stage occurred approximately 6,500 to 5,000 years BP when the surface water salinity in the Littorina Sea was 9‰ to 14‰ compared with approximately 5‰ today in the Baltic Sea /Westman et al. 1999/. There are signatures of Littorina type water present in fracture groundwaters of the basement at Laxemar /Gimeno et al. 2009, Laaksoharju et al. 2009/. The signatures are, however, not as strong as could be expected. This is attributed to: a) only partial submersion of the Laxemar subarea during Littorina transgression(s), b) restricted access of the Littorina Sea along valley systems and over relatively short time intervals, and c) the Littorina Sea water in the valleys was diluted continuously by meteoric recharge water. Combined, this resulted in a diluted Littorina end-member water which was limited in the extent of infiltrating into the bedrock.

Table 7-1. Major evolutionary stage of the Baltic Sea during the Holocene (adapted from /Söderback 2008/).

Baltic stage	Years BP	Salinity	Environment in Laxemar
Baltic Ice Lake	15,000 to 11,500	Glacio-lacustrine	Covered by inland ice.
Yoldia Sea	11,500 to 10,800	Lacustrine/Brackish /Lacustrine	At the rim of the retreating inland ice.
Ancylus Lake	10,800 to 9,500	Lacustrine	Regressive shoreline .
Littorina Sea (→ Baltic Sea)	9,500 to present	Brackish	Regressive shoreline Most saline period 6,500–5,000 BC. Present-day Baltic Sea conditions have prevailed during the last ca. 2,000 years.

7.3.2 Initial and boundary conditions

In the present simulations, the evolution of the porewater tracer profiles started between 14,000 and 11,000 years BP. This time span was chosen because the Laxemar subarea was still covered by ice during the first part of the Baltic Ice Lake period and circulation of glacio-lacustrine water might not have started before about 14,000 years BP. The modelled domain in the KLX17A porewater profile extends from the deformation zone at about 112 m borehole length to the intact rock matrix at about 125 m borehole length. The homogeneous initial conditions are given by the matrix porewater composition that still prevails at the end of the modelled domain where a zero flux boundary was assumed. The boundary conditions at the upper end of the profile in zone A, or within zone C are given by the circulating fracture groundwater compositions and step-wise and gradual changes were tested. The shape of the concentration profile then gradually evolved as a function of the chemical gradient established between porewater and fracture groundwater, the latter changing its composition as a function of palaeohydrological changes.

Homogeneous initial conditions in the rock matrix were assumed corresponding to the porewater concentrations of Cl^-, ^{18}O and ^{2}H for the last sample of the profile, i.e. KLX17A-18 at 123.5 m borehole length (–80.5 m elevation). In the first batch of simulations the final water content of the samples was not yet available and these simulations have been performed based on slightly higher initial Cl^- concentrations than the final simulations. Over the modelled time period this slight difference had, however, only marginal influence.

Unfortunately, no CCC (Complete Chemical Characterisation) groundwater analyses exist from the highly conducting deformation zone ZSMEW900A in borehole KLX17A so that even the present-day boundary conditions of the model domain had to be assumed. The Cl^- concentrations in the porewater in zone A (first four samples) are similar suggesting that they might be in equilibrium with present-day fracture groundwater. However, the isotope composition of the first sample KLX17A-1 differs significantly from the subsequent samples (Figure 7-6) and a closer look at the Cl^- concentrations also shows a higher concentration for this sample just outside the uncertainty band (Figure 7-4). Nevertheless, zone A was treated in the modelling as being homogeneous and, in the absence of measured fracture groundwater data, being representative for the present-day water circulating there. The effect of the (small) variability shown by the data was then explored by using the compositions of samples KLX17A-1 and KLX17A-4 at 112 m and 114 m borehole length, respectively, as present-day boundary conditions.

The set of transient palaeo-boundary conditions was kept simple in the first batch of simulations and became iteratively complex based on the results of previous simulations. In the first batch it consisted only of a glacial type, a brackish type and present-day type fracture groundwater. These water types were chosen to represent the major stages of the Baltic basin and Laxemar subarea, here simplified to a combined Baltic Ice Lake and Ancylus Lake stage, a Littorina stage and a present-day meteoric water stage. In the final simulations the boundary conditions consisted of six different water types that circulated over a specific time period in the water-conducting deformation zone. All water types are compatible with the palaeo-climatic evolution of the site.

The initial conditions and boundary conditions used in the various numerical simulations are given in Figures 7-7 to 7-13 for each simulation.

7.3.3 Parameter variation

In the model simulations, a homogeneous and heterogeneous domain with respect to boundary conditions and transport properties were considered. In the initial simulations only zone A in the model domain, i.e. the deformation zone ZSMEW900A in nature, was treated as being water-conductive and forming a single boundary condition. Most of the simulations, however also considered zone C between 117.2 m to 117.5 m borehole length as water-conductive, but with an about two orders of magnitude lower transmissivity as indicated by the differential flow logging in the borehole. As a consequence, a compositional change in the fracture groundwater arriving at zone A at a certain time will show up in zone C with a time delay that corresponds to the different transmissivity.

The transport properties were also treated in a homogeneous way across the entire model domain in the first simulations in spite of the differences in, for example, porosity (Figure 7-2) and pore diffusion coefficients for Cl^- (Figure 7-3). To account for such heterogeneities, pore diffusion coefficients for Cl^- were varied and different coefficients were used for the rock matrix zones B and D in the model domain in the later simulations.

Except for one case, only diffusive transport was considered in the simulations. This choice was based on the low hydraulic conductivities of the rock matrix, the out-diffusion experiments and the general shape of the profile data, which hint to diffusion dominated transport. The occurrence of small advective flow cannot be ruled out *a priori*, but the modelling results gave no indication that advection has to be invoked to explain the results.

The system characteristics and transport parameters used in the various numerical simulations are given in Figures 7-7 to 7-13 for each simulation.

7.3.4 Results

As already expected from the qualitative interpretation, model simulations using a homogeneous system with one single water-conducting zone at the top and a simplified palaeohydrological history cannot describe the observed data. Starting with a glacio-lacustrine water type at about 4,500 years BP (Baltic Ice Lake and Ancylus Lake stage), followed by a Littorina stage between 6,500–3,500 years BP with a moderately saline composition (average of present-day Baltic seawater, 3,500 mg/L) and finally present-day conditions over the last 3,500 years results in grossly overestimated Cl^- concentrations that extend between 113 m and 116 m borehole length or down to the end of the model domain depending on the pore diffusion coefficient used in the model (Figure 7-7, left). The reduction of the Littorina stage to between 6,000–5,000 years BP and of the Cl^- concentration to 2,000 mg/L greatly reduced the calculated Cl-concentrations and now the modelled profile shows some similarity with the measured data (Figure 7-7, middle). In this case, a small downward advective velocity was also used to move the concentration maxima to lower depths. For all these simulations the upper limit of the domain, i.e. the water-conducting zone, was set to 112 and 113 m borehole length. In the third simulation (Figure 7-7, right) this upper limit was set to 114 m borehole length to be more consistent with the observations, and the concentration maxima was moved to greater depths. In addition, the time period of Littorina seawater influence was once more reduced to 700 years and 500 years, but ending at 4,000 years BP instead of 5,000 years BP as before, and variations in D_p by a factor of 4 were tested. Again, the observed data are only poorly matched and the change to lower Cl-concentrations around 117 m borehole length, i.e. the potential water-conducting zone, is not developed using such conditions.

Based on these calculations, it can be concluded that the system cannot be described with only one water-conducting zone and with a simplified palaeohydrological history that includes glacio-lacustrine type, Littorina type (with variable salinity) and present-day type fracture groundwater.

In the following simulations the model domain was divided into four zones A to D and included zone C as a second water-conducting zone between 117.2 and 117.5 m borehole length. The palaeohydrological history was still kept simple, but the Littorina stage was now set to its maximum salinity stage with respect to onset and salinity. The time period of the Littorina stage was reduced to 500 years based on the previous results. The transport properties in water-conducting and rock matrix zones B and D were kept constant and the step-wise changes in fracture groundwater occurred simultaneously and with equal compositions. Such a scenario describes the observed

Cl^- concentrations quite reasonably (Figure 7-8, left). Chloride concentrations are first lowered during the Baltic Ice Lake and Ancylus Lake stages with glacio-lacustrine groundwater in the water-conducting zones A and C (blue line in Figure 7-8) before they dramatically increase during the short-term Littorina water input (brown line) followed by dilution to almost presently observed values during present-day type groundwater flow in the fractures over the last 6,500 years (green line). The scenario is, however, not compatible with the observed porewater isotope composition (Figure 7-8, middle and right). The calculated distribution is almost a mirror image of the measured values in that too enriched values occur in the lower water-conducting zone C and too depleted values are present in the rock matrix zone B. This indicates that the modelled decrease corresponding to the glacio-lacustrine fracture groundwater circulating in the lower conducting zone C occurred too early with respect to zone C. With respect to zones B and the top of zone D the depletion in the isotopes is too strong to be compensated later in the rock matrix at distances more than a few decimetres from the conducting zone by subsequent Littorina type and present-day type groundwaters. Such compensation would require, for instance, a stage with heavier isotope values in the fracture groundwater.

A possible source of water enriched in the heavy isotopes could be Yoldia Sea water, which has been neglected so far. For the following simulations, therefore, the palaeohydrological history was essentially made up as presented in Table 7-1, i.e. according to the generally accepted evolution of the Baltic basin. The simulation investigates the possible influence of the Yoldia Sea stage between the Baltic Ice Lake and Ancylus, while the Littorina and present-day stage are treated as in the previous simulations. As shown in Figure 7-9 (left), this results in a worse fit of the observed Cl^- data in that too high concentrations would be present in the porewater in zone B and at the top of zone D. In contrast, the Yoldia stage has only an impact on the isotopic composition of the porewater at early times, but the final modelled profile for $\delta^{18}O$ and $\delta^{2}H$ (Figure 7-9, middle and right) are nearly identical to those without a Yoldia Sea stage (cf. Figure 7-8, middle and right), i.e. they do not fit the data.

All further adjustments of parameters did not result in an improvement of the fit between model results and data. As a conclusion, a time lag between the concentration changes in the water-conducting zone A and that of zone C needs to be taken into account. Such different times of arrival of a specific groundwater composition are consistent with the different transmissivity of the water-conducting zones (cf. Section 7.3.1). In addition, the calculated isotope composition in the porewater of zone B was too depleted in ^{18}O and ^{2}H in all simulations whereas the applied palaeohydrological scenarios could reasonably well describe the Cl^- concentrations (Figure 7-8 and Figure 7-9). It follows that a better fit of the isotope data cannot be obtained from a simultaneous contact in both fracture zones with a known groundwater type that is enriched in ^{18}O and ^{2}H because all these types are brackish or saline waters (Yoldia, Littorina or present-day Baltic) and result in a worse fit for Cl^-.

The previous simulations showed that an influence of the Yoldia Sea is no longer resolved in the present-day concentration profiles if it was ever present at all. From the hydrochemical investigations of the fracture groundwaters /Gimeno et al. 2009, Laaksoharju et al. 2009/ and shoreline reconstructions /Rhén et al. 2008/ it was concluded that also the impact of Littorina seawater was minor in the Laxemar subarea and in the western part probably never present at all. Therefore, based on the model results an alternative palaeohydrological scenario was adapted. It includes meteoric water input from a warm-climate period from 7,500–4,000 years BP, which corresponds to the well-defined Holocene thermal maximum /Heikkilä and Seppä 2003, Antonsson et al. 2006, Antonsson and Seppä 2007/. The isotope composition of this warm-period infiltration was assumed to be enriched by about 2‰ in $\delta^{18}O$ and 16‰ in $\delta^{2}H$ corresponding to a difference in the mean annual temperature of about 1–2°C compared to that of today. As shown by the simulations a short-termed circulation of brackish water is, however, required. This was included as present-day Baltic Sea water that was subsequently replaced in two steps by present-day type meteoric water.

The results of this base case are shown in Figure 7-10. It should be noted that the glacio-lacustrine water arriving in the lower water-conducting zone C was assumed to be a mixture of Baltic Ice Lake and Ancylus Lake type water slightly modified by exchange with matrix porewater. It has thus an isotope composition intermediate between true Baltic Ice Lake and Ancylus Lake type water and a slightly elevated Cl^- content. This is based on the long residence time of this water in the bedrock fracture network allowing dispersive exchange before it arrived in borehole KLX17A. The model

describes the measured Cl^- concentrations reasonably well although deviations occur in the middle part of the rock matrix zone D and the modelled Cl^- peak in the rock matrix zone B seems too broad (Figure 7-10, left). Whereas the deviation in zone D might be due to a too long circulation of low Cl, glacio-lacustrine water in the conducting zone C, the deviation in zone B might be due to a too high pore diffusion coefficient chosen for this zone. In contrast to all previous simulations, however, the general profile shape of the measured isotope composition is simulated although the fit to the data is still poor. Major discrepancies occur around the lower conducting zone C and in zone B where the simulated values are too depleted in ^{18}O and ^{2}H. Thus, also the simulated isotope profiles suggest that a circulation of low Cl, glacio-lacustrine water in the conducting zone C over the last 500 years appears too long.

In the following simulation the circulation time was, therefore, reduced to 200 years (Figure 7-11). In addition, the timing of the circulation of the two present-day type waters in the upper conducting zone A was slightly changed, while all other parameters remained as in the base case. Reducing the flow time in the lower conducting zone C results in a better fit of the isotopic porewater data (Figure 7-11, middle and right), but the Cl^- concentrations become overestimated in zone B and at the top of zone D (Figure 7-12).

A similar situation is obtained when simulating the base case with lower pore diffusion coefficients in the rock matrix zones B and D (Figure 7-12). This results in an improved fit for Cl^- and the isotopes in zone D, whereas no real improvement is obtained in zone B. Figure 7-13 finally shows the results of a simulation in which the Baltic Ice Lake stage was omitted and the meteoric input with a Holocene warm-climate signature was (unrealistically?) extended back to 9,500 years. For Cl^- a similar and reasonable fit is obtained for the base case (Figure 7-13, left). The porewater isotope composition is better described in the rock matrix zone B, but less well at the top of zone D compared to the base case (cf. Figure 7-13 and Figure 7-10 middle and right).

runs 1, 2; 11, 24–26		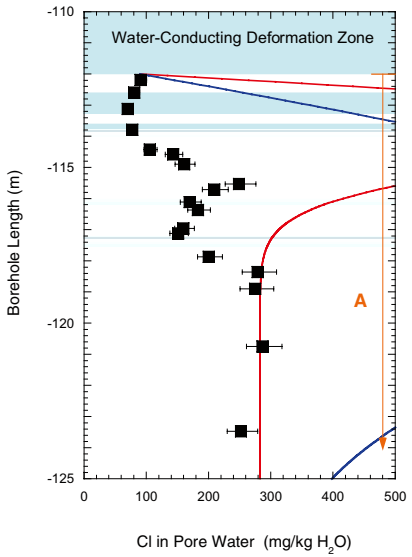		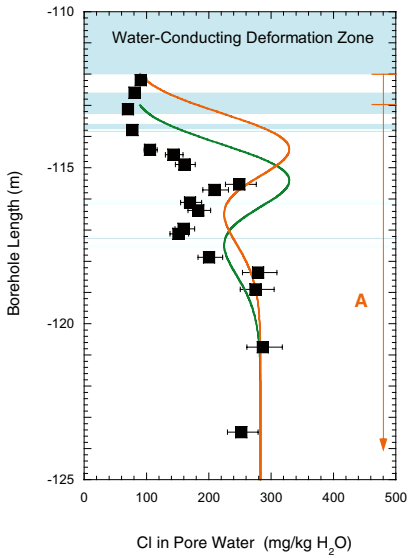		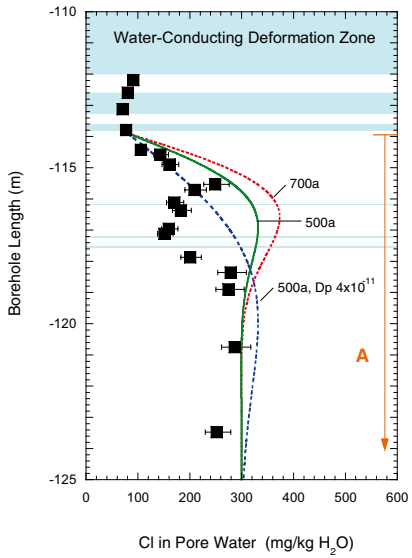	
Domain		1 zone (A), homogeneous properties; fracture water at 112 m		1 zone (A), homogeneous properties; fracture water at 112 m (orange curve) and 113 m (green curve)		1 zone (A), homogeneous properties; fracture water at 114 m	
Initial conditions		>11,000 years	Cl = 280 mg/L	>11,000 years	Cl = 280 mg/L	>11,000 a	Cl = 300 mg/L
Boundary conditions	BIL, AL Litt present	11,000 – 6,500 years 6,500 – 3,500 years 3,500 years – present	Cl = 1 mg/L Cl = 3,500 mg/L Cl = 90 mg/L	11,000 – 6,000 years 6,000 – 5,000 years 5,000 years – present	Cl = 1 mg/L Cl = 2,000 mg/L Cl = 90 mg/L	red : 11,000 – 4,700 years 4,700 – 4,000 years blue & green: 11,000 – 4,500 years 4,500 – 4,000 years all : 4,000 years – present	 Cl = 1 mg/L Cl = 6,500 mg/L Cl = 1 mg/L Cl = 6,500 mg/L Cl = 80 mg/L
Dp (m^2/s)		red : 7×10^{-11}, blue : 7×10^{-12}		green & orange : 4×10^{-12}, v = 1×10^{-11} m/s		red & blue : 1×10^{-11}, green : 4×10^{-11}	

Figure 7-7. *Fracture profile KLX17A: Modelled concentration profiles for Cl^-, assuming homogeneous properties, only one water-conducting zone and a simple palaeohydrological history. Line colours are explained in the table. All dates given represent years BP.*

run 33	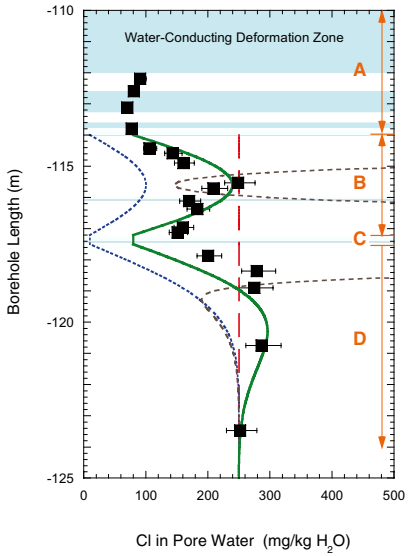		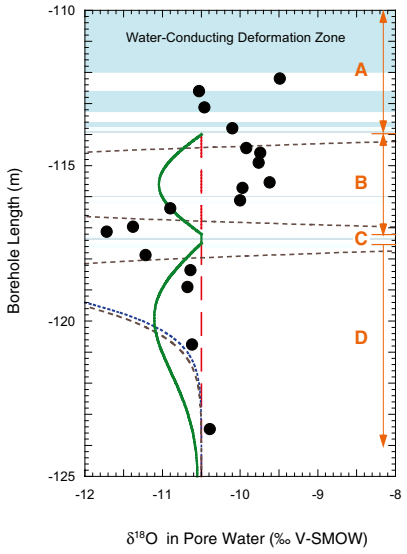		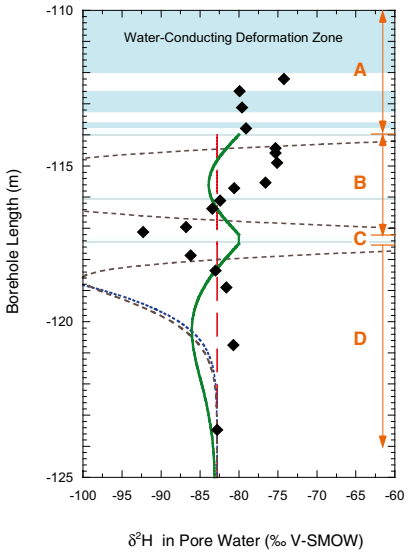	
Domain		4 zones (A to D), homogeneous properties; A, C fracture zones at 112 m and 117.5 m with equal concentration and time of changes		4 zones (A to D), homogeneous properties; A, C fracture zones at 112 m and 117.5 m with equal concentration and time of changes		4 zones (A to D), homogeneous properties; A, C fracture zones at 112 m and 117.5 m with equal concentration and time of changes	
Initial conditions		>11,000 years	Cl = 250 mg/L	>11,000 years	$\delta^{18}O$ = –10.5 ‰	>11,000 years	δ^2H = –82.5 ‰
Boundary conditions	BIL, AL Litt present	11,000 – 7,000 years 7,000 – 6,500 years 6,500 years – present	Cl = 10 mg/L Cl = 6,500 mg/L Cl = 80 mg/L	11,000 – 7,000 years 7,000 – 6,500 years 6,500 years – present	$\delta^{18}O$ = –17 ‰ $\delta^{18}O$ = –4.7 ‰L $\delta^{18}O$ = –10.5 ‰L	11,000 – 7,000 years 7,000 – 6,500 years 6,500 years – present	δ^2H = –125 ‰ δ^2H = –37.8 ‰ δ^2H= –80 ‰
Dp (m^2/s)		1×10^{-11}		1×10^{-11}		1×10^{-11}	

Figure 7-8. *Fracture profile KLX17A: Modelled concentration profiles for Cl^-, $\delta^{18}O$ and δ^2H assuming homogeneous properties, two water-conducting zones with equal arrival times of groundwater and a simple palaeohydrological history. Line colours correspond to: red = initial conditions, blue = combined Baltic Ice Lake and Ancylus stage, black = Littorina Sea stage, green = present-day. All dates given represent years BP.*

run 34		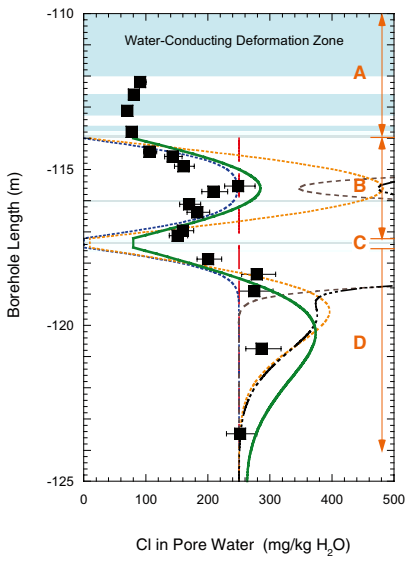		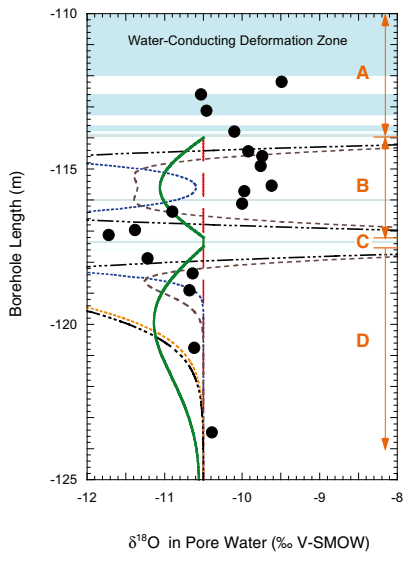		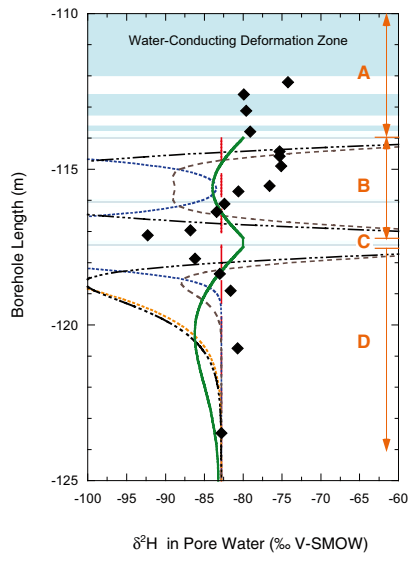
Domain		4 zones (A to D), homogeneous properties; A, C fracture zones at 112 m and 117.5 m with equal concentration and time of changes		4 zones (A to D), homogeneous properties; A, C fracture zones at 112 m and 117.5 m with equal concentration and time of changes		4 zones (A to D), homogeneous properties; A, C fracture zones at 112 m and 117.5 m with equal concentration and time of changes	
Initial conditions		>12,100 years	Cl = 250 mg/L	>12,100 years	$\delta^{18}O$ = –10.5 ‰	>12,100 years	$\delta^{2}H$ = –82.5 ‰
Boundary conditions	BIL YS AL Litt Present	12,100 – 11,600 years 11,600 – 11,000 years 11,000 – 7,000 years 7,000 – 6,500 years 6,500 years – present	Cl = 1 mg/L Cl = 6,500 mg/L Cl = 10 mg/L Cl = 6,500 mg/L Cl = 80 mg/l	12,100 – 11,600 years 11,600 – 11,000 years 11,000 – 7,000 years 7,000 – 6,500 years 6,500 years – present	$\delta^{18}O$ = –21 ‰ $\delta^{18}O$ = –4.7 ‰ $\delta^{18}O$ = –17 ‰ $\delta^{18}O$ = –4.7 ‰ $\delta^{18}O$ = –10.5 ‰	12,100 – 11,600 years 11,600 – 11,000 years 11,000 – 7,000 years 7,000 – 6,500 years 6,500 years – present	$\delta^{2}H$ = –158 ‰ $\delta^{2}H$ = –37.8 ‰ $\delta^{2}H$= –125 ‰ $\delta^{2}H$ = –37.8 ‰ $\delta^{2}H$ = –80 ‰
Dp (m^2/s)		1×10^{-11}		1×10^{-11}		1×10^{-11}	

Figure 7-9. *Fracture profile KLX17A: Modelled concentration profiles for Cl^-, $\delta^{18}O$ and $\delta^{2}H$ assuming homogeneous properties, two water-conducting zones with equal arrival times of groundwater and the standard palaeohydrological history. Line colours correspond to: red = initial conditions, blue = Baltic Ice Lake stage, brown = Yoldia Sea stage, orange = Ancylus Lake stage, black = Littorina Sea stage, green = present-day. All dates given represent years BP.*

run 50		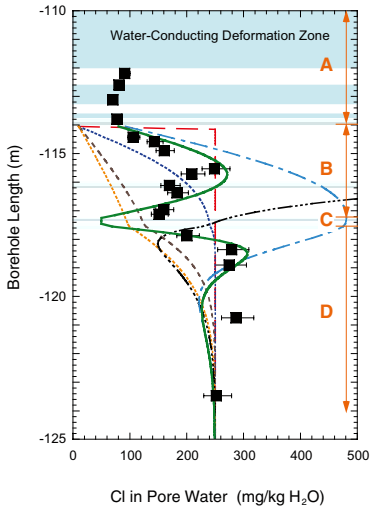		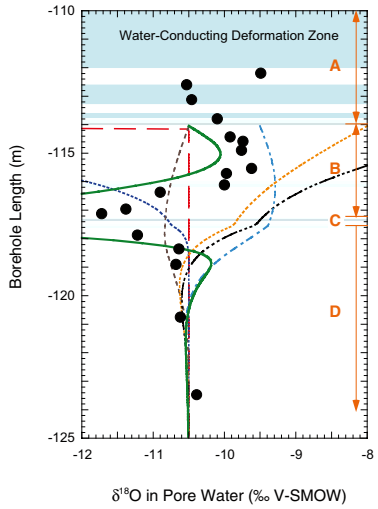		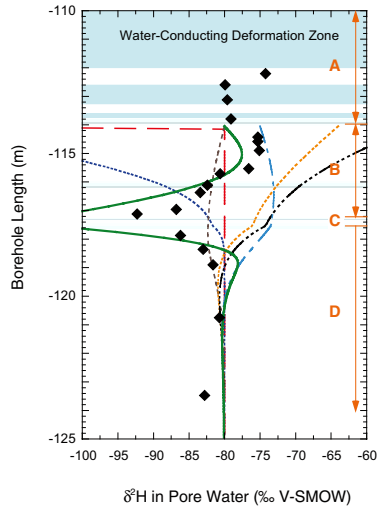	
Domain		four zones (A to D), heterogeneous properties; A, C fracture zones at 112 m and 117.5 m with different concentration/time changes		four zones (A to D), heterogeneous properties; A, C fracture zones at 112 m and 117.5 m with different concentration/time changes		four zones (A to D), heterogeneous properties; A, C fracture zones at 112 m and 117.5 m with different concentration/time changes	
Initial conditions		>14,000 years	Cl = 250 mg/L	>14,000 years	$\delta^{18}O$ = –10.5 ‰	>14,000 years	$\delta^{2}H$ = –80 ‰
Boundary conditions: zone A	BIL	14,000 –13,000 years	Cl = 10 mg/L	14,000 –13,000 years	$\delta^{18}O$ = –17 ‰	14,000 – 13,000 years	$\delta^{2}H$ = –125 ‰
	AL	13,000 – 7,500 years	Cl = 10 mg/L	13,000 – 7,500 years	$\delta^{18}O$ = –10.5 ‰	13,000 – 7,500 years	$\delta^{2}H$ = –80 ‰
	WM	7,500 – 4,000 years	Cl = 10 mg/L	7,500 – 4,000 years	$\delta^{18}O$ = –8 ‰	7,500 – 4,000 years	$\delta^{2}H$= –64 ‰
	Balt	4,000 – 3,000 years	Cl = 3,760 mg/L	4,000 – 3,000 years	$\delta^{18}O$ = –5.9 ‰	4,000 – 3,000 years	$\delta^{2}H$ = –53.3 ‰
	Present	3,000 – 500 years	Cl = 92 mg/L	3,000 – 500 years	$\delta^{18}O$ = –9.5 ‰	3,000 – 500 years	$\delta^{2}H$ = –75 ‰
	Present	500 – present	Cl = 80 mg/l	500 – present	$\delta^{18}O$ = –10.5 ‰	500 – present	$\delta^{2}H$ = –80 ‰
zone C		14,000 – 500 years	not relevant	14,000 – 500 years	not relevant	14,000 – 500 years	not relevant
	BIL&AL	500 years – present	Cl = 50 mg/L	500 years – present	$\delta^{18}O$ = –15 ‰	500 years – present	$\delta^{2}H$ = –105 ‰
Dp (m^2/s)		zone B: 4×10^{-11}; zone D: 1×10^{-11}		zone B: 4×10^{-11}; zone D: 1×10^{-11}		zone B: 4×10^{-11}; zone D: 1×10^{-11}	

Figure 7-10. *Fracture profile KLX17A: Modelled concentration profiles for Cl^-, $\delta^{18}O$ and δ^2H assuming heterogeneous properties, two water-conducting zones with different arrival times of groundwater and the new 'base case' palaeohydrological history. Line colours correspond to: red = initial conditions, blue = Baltic Ice Lake stage, brown = Ancylus Lake stage, orange = Holocene thermal maximum, black =present-day Baltic, bright blue: present-day 'mixed', green = present-day. All dates given represent years BP.*

run 51		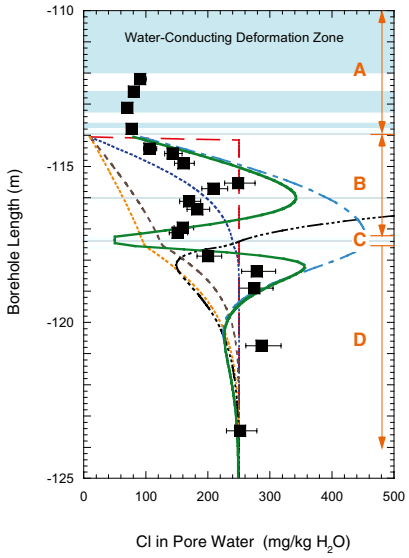		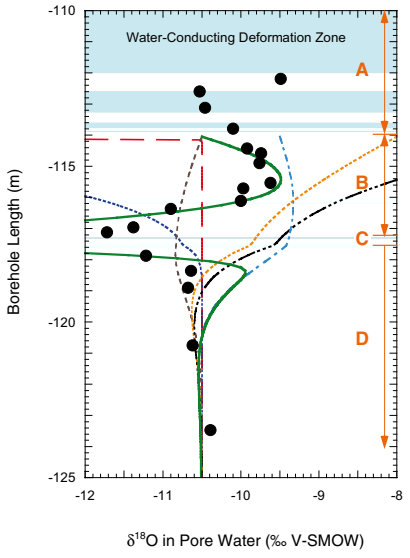		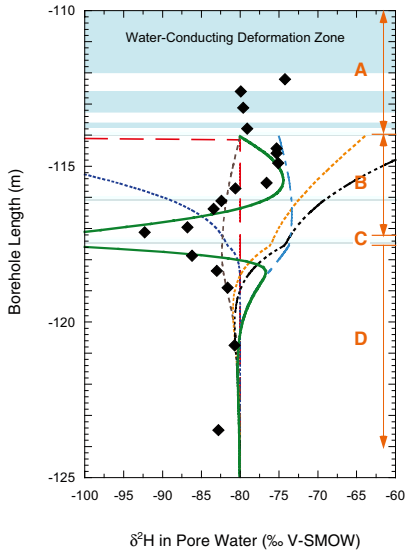	
Domain		four zones (A to D), heterogeneous properties; A, C fracture zones at 112 m and 117.5 m with different concentration/time changes		four zones (A to D), heterogeneous properties; A, C fracture zones at 112 m and 117.5 m with different concentration/time changes		four zones (A to D), heterogeneous properties; A, C fracture zones at 112 m and 117.5 m with different concentration/time changes	
Initial conditions		>14,000 years	Cl = 250 mg/L	>14,000 years	$\delta^{18}O$ = –10.5 ‰	>14,000 years	$\delta^{2}H$ = –80 ‰
Boundary conditions: zone A	BIL	14,000 – 13,000 years	Cl = 10 mg/L	14,000 – 13,000 years	$\delta^{18}O$ = –17 ‰	14,000 – 13,000 years	$\delta^{2}H$ = –125 ‰
	AL	13,000 – 7,500 years	Cl = 10 mg/L	13,000 – 7,500 years	$\delta^{18}O$ = –10.5 ‰	13,000 – 7,500 years	$\delta^{2}H$ = –80 ‰
	WM	7,500 – 4,000 years	Cl = 10 mg/L	7,500 – 4,000 years	$\delta^{18}O$ = –8 ‰	7,500 – 4,000 years	$\delta^{2}H$= –64 ‰
	Balt	4,000 – 3,000 years	Cl = 3,760 mg/L	4,000 – 3,000 years	$\delta^{18}O$ = –5.9 ‰	4,000 – 3,000 years	$\delta^{2}H$ = –53.3 ‰
	Present	3,000 – 200 years	Cl = 92 mg/L	3,000 – 200 years	$\delta^{18}O$ = –9.5 ‰	3,000 – 200 years	$\delta^{2}H$ = –75 ‰
	Present	200 – present	Cl = 80 mg/l	200 – present	$\delta^{18}O$ = –10.5 ‰	200 – present	$\delta^{2}H$ = –80 ‰
zone C		14,000 – 200 years	not relevant	14,000 – 200 years	not relevant	14,000 – 200 years	not relevant
	BIL&AL	200 years – present	Cl = 50 mg/L	200 years – present	$\delta^{18}O$ = –15 ‰	200 years – present	$\delta^{2}H$ = –105 ‰
Dp (m^2/s)		zone B: 4×10^{-11}; zone D: 1×10^{-11}		zone B: 4×10^{-11}; zone D: 1×10^{-11}		zone B: 4×10^{-11}; zone D: 1×10^{-11}	

Figure 7-11. *Fracture profile KLX17A: Modelled concentration profiles for Cl^-, $\delta^{18}O$ and δ^2H assuming heterogeneous properties, two water-conducting zones with different arrival times of groundwater and the new 'base case' palaeohydrological history (Figure 7-10), but a shorter time of groundwater flow in the lower conducting zone C. Line colours as in Figure 7-10. All dates given represent years BP.*

run 58		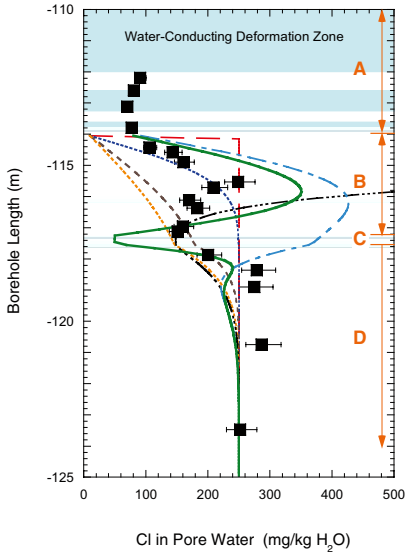		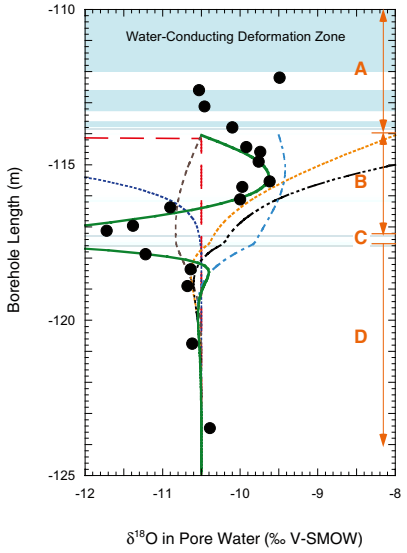		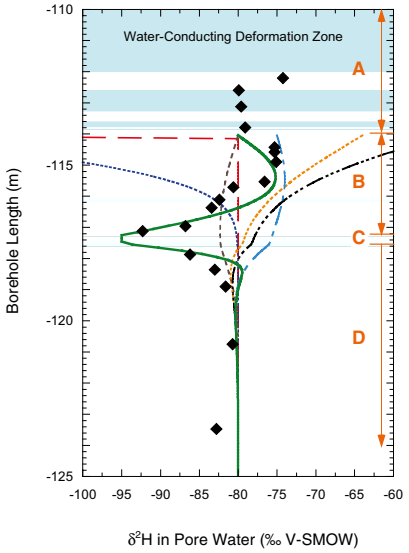	
Domain		four zones (A to D), heterogeneous properties; A, C fracture zones at 112 m and 117.5 m with different concentration/time changes		four zones (A to D), heterogeneous properties; A, C fracture zones at 112 m and 117.5 m with different concentration/time changes		four zones (A to D), heterogeneous properties; A, C fracture zones at 112 m and 117.5 m with different concentration/time changes	
Initial conditions		>14,000 years	Cl = 250 mg/L	>14,000 years	$\delta^{18}O$ = –10.5 ‰	>14,000 years	$\delta^{2}H$ = –80 ‰
Boundary conditions: zone A	BIL	14,000 – 13,000 years	Cl = 10 mg/L	14,000 – 13,000 years	$\delta^{18}O$ = –17 ‰	14,000 – 13,000 years	$\delta^{2}H$ = –125 ‰
	AL	13,000 – 7,500 years	Cl = 10 mg/L	13,000 – 7,500 years	$\delta^{18}O$ = –10.5 ‰	13,000 – 7,500 years	$\delta^{2}H$ = –80 ‰
	WM	7,500 – 4,000 years	Cl = 10 mg/L	7,500 – 4,000 years	$\delta^{18}O$ = –8 ‰	7,500 – 4,000 years	$\delta^{2}H$= –64 ‰
	Balt	4,000 – 3,000 years	Cl = 3,760 mg/L	4,000 – 3,000 years	$\delta^{18}O$ = –5.9 ‰	4,000 – 3,000 years	$\delta^{2}H$ = –53.3 ‰
	Present	3,000 – 500 years	Cl = 92 mg/L	3,000 – 500 years	$\delta^{18}O$ = –9.5 ‰	3,000 – 500 years	$\delta^{2}H$ = –75 ‰
	Present	500 – present	Cl = 80 mg/l	500 – present	$\delta^{18}O$ = –10.5 ‰	500 – present	$\delta^{2}H$ = –80 ‰
zone C		14,000 – 500 years	not relevant	14,000 – 500 years	not relevant	14,000 – 500 years	not relevant
	BIL&AL	500 years – present	Cl = 50 mg/L	500 years – present	$\delta^{18}O$ = –15 ‰	500 years – present	$\delta^{2}H$ = –105 ‰
Dp (m^2/s)		zone B: 2×10^{-11}; zone D: 5×10^{-12}		zone B: 2×10^{-11}; zone D: 5×10^{-12}		zone B: 2×10^{-11}; zone D: 5×10^{-12}	

Figure 7-12. *Fracture profile KLX17A: Modelled concentration profiles for Cl^-, $\delta^{18}O$ and $\delta^{2}H$ assuming heterogeneous properties, two water-conducting zones with different arrival times of groundwater and the new 'base case' palaeohydrological history (Figure 7-10), but lower pore diffusion coefficients. Line colours as in Figure 7-10. All dates given represent years BP.*

run 61		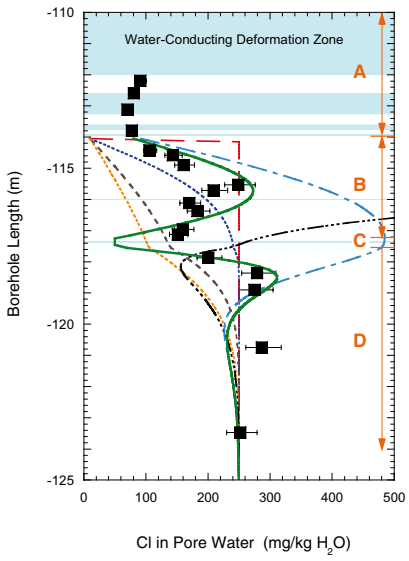		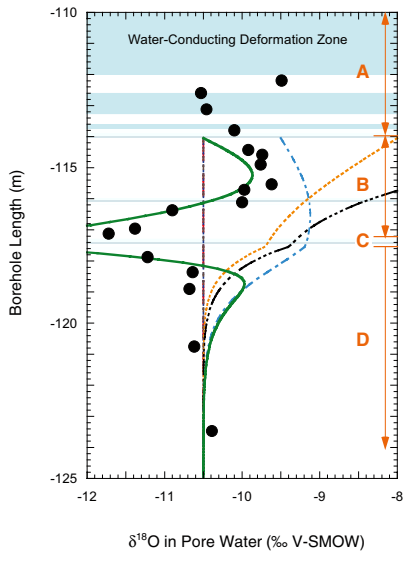		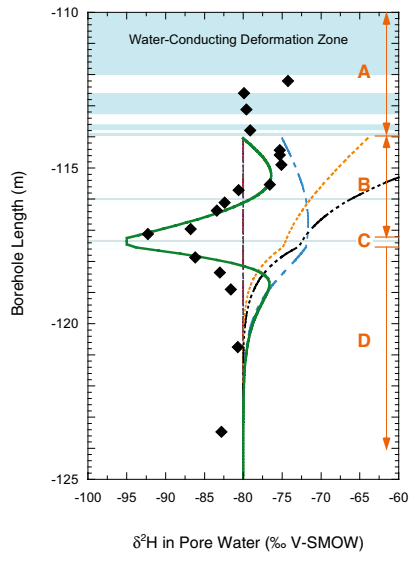	
Domain		four zones (A to D), heterogeneous properties; A, C fracture zones at 112 m and 117.5 m with different concentration/time changes		four zones (A to D), heterogeneous properties; A, C fracture zones at 112 m and 117.5 m with different concentration/time changes		four zones (A to D), heterogeneous properties; A, C fracture zones at 112 m and 117.5 m with different concentration/time changes	
Initial conditions		>13,000 years	Cl = 250 mg/L	>13,000 years	$\delta^{18}O$ = –10.5 ‰	>13,000 years	$\delta^{2}H$ = –80 ‰
Boundary conditions: zone A	AL	13,000 – 9,500 years	Cl = 10 mg/L	13,000 – 9,500 years	$\delta^{18}O$ = –10.5 ‰	13,000 – 9,500 years	$\delta^{2}H$ = –80 ‰
	WM	9,500 – 4,000 years	Cl = 10 mg/L	9,500 – 4,000 years	$\delta^{18}O$ = –8 ‰	9,500 – 4,000 years	$\delta^{2}H$= –64 ‰
	Balt	4,000 – 3,000 years	Cl = 3,760 mg/L	4,000 – 3,000 years	$\delta^{18}O$ = –5 ‰	4,000 – 3,000 years	$\delta^{2}H$ = –45 ‰
	Present	3,000 – 500 years	Cl = 92 mg/L	3,000 – 500 years	$\delta^{18}O$ = –9.5 ‰	3,000 – 500 years	$\delta^{2}H$ = –75 ‰
	Present	500 years – present	Cl = 80 mg/l	500 years – present	$\delta^{18}O$ = –10.5 ‰	500 years – present	$\delta^{2}H$ = –80 ‰
zone C		13,000 – 500 years	not relevant	13,000 – 500 years	not relevant	13,000 – 500 years	not relevant
	BIL&AL	500 years – present	Cl = 50 mg/L	500 years – present	$\delta^{18}O$ = –13 ‰	500 years – present	$\delta^{2}H$ = –95 ‰
Dp (m^2/s)		zone B: 4×10^{-11}; zone D: 1×10^{-11}		zone B: 4×10^{-11}; zone D: 1×10^{-11}		zone B: 4×10^{-11}; zone D: 1×10^{-11}	

Figure 7-13. *Fracture profile KLX17A: Modelled concentration profiles for Cl^-, $\delta^{18}O$ and $\delta^{2}H$ assuming heterogeneous properties, two water-conducting zones with different arrival times of groundwater and the new 'base case' palaeohydrological history (Figure 7-10), but neglecting the Baltic Ice Lake stage. Line colours as in Figure 7-10. All dates given represent years BP.*

7.3.5 Conclusions from modelling of the porewater tracer profile

The measured tracer data of the fracture porewater profile in borehole KLX17A and the numerical simulation of the data allow the following conclusions:

- The observed profiles for Cl^-, $\delta^{18}O$ and δ^2H in the porewater are the product of a complex palaeohydrological evolution during Late Pleistocene and Holocene times that includes various compositional changes in the groundwater circulating in the fractures.
- The initial conditions chosen in the model domain appear to have formed from meteoric water under climatic conditions comparable to those prevailing today. The extension of the profile 10 m further into the non-deformed rock matrix suggests, however, that these initial conditions form a transient state between porewater formed from meteoric fracture groundwater that infiltrated during a warm period and from a different major moisture source during the Pleistocene and different fracture groundwaters of the Late Pleistocene and Holocene history. A possible period for this interaction with warm-climate groundwater would be the Eemian interglacial (MIS 5e, 130,000–115,000 years BP).
- The porewater signatures along the profile are the result of interaction with fracture groundwater that originates from the stages: Baltic Ice Lake, Ancylus Lake, warm-climate meteoric (Holocene thermal maximum), Baltic Sea and present-day meteoric.
- For the given initial conditions, the effect of the Baltic Ice Lake water is limited and glacio-lacustrine water appears to have circulated in the conducting deformation zone ZSMEW900A for less than 1,000 years. A longer circulation of glacio-lacustrine water would result in too depleted $\delta^{18}O$ and δ^2H signatures and too low Cl^- concentrations in the porewater compared to the measured values.
- A short circulation of saline water enriched in ^{18}O and ^2H during the Yoldia stage leads to a worse match with the Cl^- data, but leaves virtually no signature of heavier isotope contents in the porewater (the latter would have been overprinted by the later Ancylus stage). Thus, a circulation of lacustrine-type water seems to have occurred during the Yoldia and the Ancylus stage.
- The lacustrine water during the Yoldia and Ancylus stages appears to have been low in Cl^- and with an isotope composition similar to that of present-day meteoric water. With more depleted isotope values, the measured data cannot be approximated.
- During the Littorina stage no, or only a very shorted-termed (< about 500 years) input of brackish seawater, can have occurred. A circulation of saline water during the most saline stage of the Littorina Sea can be excluded from the observed data.
- The Ancylus stage was more likely followed by circulation of warm-climate meteoric type water in the conducting deformation zone ZSMEW900A. This water had a low Cl concentration and an enriched $\delta^{18}O$ and δ^2H signature compared to present-day meteoric water. The circulation of this fracture-water type coincides with the Holocene thermal maximum.
- A short-termed, maximum 500 years long circulation of brackish water similar to present-day Baltic Sea water appears to have occurred between about 4,000 years and 3,000 years BP before circulation of present-day type meteoric water commenced.
- A more gradual and not immediate decrease of the $\delta^{18}O$ and δ^2H from the brackish Baltic type water at about 3,000 years BP to the present-day water is required to obtain the curved isotope profiles in the uppermost part towards the conducting deformation zone ZSMEW900A. For the Cl^- concentration this effect is negligible (i.e. equally low Cl meteoric water).
- Over a large time interval the lower water-conductive zone was not relevant for the porewater profile evolution as indicated by the data and consistent with its low transmissivity. Over the time scale considered in the models, fracture groundwater flowing in this zone had an impact on the surrounding porewater only during the last 500 years at maximum.

- The fracture groundwater arriving in the lower water-conducting zone has a higher Cl^- concentration and is less depleted in ^{18}O and ^{2}H compared to pure Baltic Ice Lake water. It may represent a mixture of Baltic Ice Lake and Ancylus type water that is diffusively affected by porewater originally present in the rock matrix. Pure Baltic Ice Lake water in the lower conducting zone would lead to a too strong decrease in the isotope composition of the porewater.
- The chosen diffusion coefficients are plausible if compared to the experimentally derived values. A lower D_p in the lower part of the profile, i.e. in the intact rock matrix, results in a better agreement with the measured data compared to a constant D_p throughout the model domain. Larger pore diffusion coefficients tend to decrease and increase the peaks in the upper and lower rock matrix zones, respectively. Lower pore diffusion coefficients result in the opposite effect.

8 Palaeohydrogeological implications

The chemical and isotopic composition of porewater in the rock matrix encountered by boreholes KLX03, KLX08 and KLX17A combined with the quantitative description of the tracer profiles that extends in borehole KLX17A from the water-conducting deformation zone ZSMEW900A into the rock matrix allows the possibility to establish a conceptual model of the palaeohydrogeological evolution of the site. Over most recent times, this model coincides with that derived from the dynamic system of the fracture groundwaters /Laaksoharju et al. 2009/. In addition, hydrogeological events that occurred during Holocene and Pleistocene times and that are no longer resolvable in the fracture groundwater can still be identified in the porewater.

In the shallow and intermediate bedrock zone of the Laxemar subarea, the porewater of most of the samples is of meteoric origin as indicated by their oxygen and hydrogen isotope compositions. The majority of porewater samples from boreholes KLX03 and KLX17A, and a few samples from borehole KLX08 plot along a line defined by the fracture groundwater 'Littorina seawater' to 'Glacial Reference Water' end-member compositions, parallel to, but to the right of the Global Meteoric Water Line, GMWL (Figure 6-15). Porewater samples of this group, located within less than about 5 m metres from the nearest water-conducting fracture, have similar Cl^- concentrations and $\delta^{18}O$ and δ^2H vales and a close to steady state situation between porewater and fracture groundwater is established. These porewaters at short distances to water-conducting fractures are of a dilute Na-HCO_3 chemical type and have evolved during the last few thousand years from present-day type fracture meteoric groundwater.

A second group of porewater samples is covered by most of the shallow to intermediate porewater samples from borehole KLX08, and three samples from KLX17A and KLX03, all of which plot on another trend line parallel to, but further to the right of the GMWL. These samples have been further subdivided according to the distance to the nearest water-conducting fracture in the borehole. Samples from within less than 5 m distance occur only in borehole KLX08, whereas all other samples come from distances greater than 10 m from the nearest water-conducting fracture. This latter group includes two samples from borehole KLX17A, which are located some 15 m further into the intact rock matrix at the end of the continuously sampled tracer profile. The quantitative description of this tracer profile revealed that samples located close to water-conducting fractures and having enriched $\delta^{18}O$ and δ^2H signatures at low Cl^- concentrations have evolved from warm-climate meteoric water that circulated in the fracture system. Consistent with the isotope composition and the distance to the nearest water-conducting fracture, the porewater of these samples evolved from fracture groundwater during the Holocene thermal maximum (about 7,500 to 4,000 years BP). Such signatures are mainly preserved in porewater samples down about 544 m depth in borehole KLX08 and, although superimposed by subsequent exchange with present-day type fracture groundwater, at about 72 m depth in borehole KLX17A.

The other group of porewater samples that plot on this second trend line further to the right of the GMWL, but are located at greater distances from the nearest water-conducting fracture, have evolved from a different fracture groundwater. These samples appear to have evolved from meteoric water of a different major moisture source during the Eemian interglacial (about 130,000–115,000 years BP), consistent with the isotope composition and the distance to the nearest water-conducting fracture. During both these warm-climate periods, the Eemian interglacial and the Holocene thermal maximum, the average annual tempreature was about 1°–3°C higher compared to today /Heikkilä and Seppä 2003, Antonsson et al. 2006, Antonsson and Seppä 2007, Söderbäck 2008/ and it is likely that meteoric water had about the same isotopic signature. In fracture groundwater such differences can no longer be resolved. The greatly different distances of the porewater samples to the nearest water-conducting fracture, combined with the quantitative modelling of the tracer profile, however, allow a distinction between these two events in the porewater.

A similar situation is encountered with porewater samples carrying a meteoric cold temperature isotope signature. Such porewater compositions are observed in all three boreholes again at highly varying distances from the nearest water-conducting fracture. As for the warm climate signatures, porewater samples with depleted $\delta^{18}O$ and δ^2H signatures, low Cl^- concentration and located

close to water-conducting fractures, appear to represent the last cold temperature event, i.e. they evolved from fracture groundwaters of the last deglaciation cycle. Samples within 10 m from the nearest water-conducting fracture carrying such young glacial-lacustrine influenced signatures are observed in borehole KLX08 down to about 500 m depth, in borehole KLX17A to about 350 m and in borehole KLX03 to about 135 m depth. Older, cold temperature signatures, i.e. pre-Last Glacial Maximum, are observed in borehole KLX03 down to about 325 m depth and in borehole KLX08 down to about 450 m depth. From the samples available it cannot be discerned if the cold temperature signature has been established during the early Weichselian period or even during an older glacial cycle.

Most prominent is the change in chemical and isotopic composition of the porewater in the Ävrö granite over a depth interval of about 120 m, starting at about 430 m depth in boreholes KLX03 and KLX17A and about 620 m depth in borehole KLX08. Porewater at these depths is of a general Na-Ca-SO_4 and general Ca-Na-SO_4 (borehole KLX08) chemical type that cannot be explained by interaction with a known type of fracture groundwater and more advanced interaction with the Ävrö granite, but must originate from different processes. Based on ion-ion ratios, Sr-isotope composition, the highly variable $\delta^{18}O$ and $\delta^{2}H$ signatures and geochemical model calculations, the evolution of these porewater types is most probably related to the formation and dissolution of highly soluble sulphates. Possible candidates such as gypsum and mirabilite are low-temperature minerals that are not stable at temperature above about 40°C. A hydrothermal and thus old origin can therefore be excluded. On the other hand such sulphate minerals may form during freezing of a solution. As shown by /Gitterman 1937/ and later experimentally and thermodynamically confirmed by /Marion et al. 1999/ during freezing of seawater mirabilite starts to precipitate at –6.3°C and gypsum at –15° to –22°C (depending on these authors), the latter at the expense of mirabilite dissolution.

It thus appears that freezing processes related to permafrost could have produced these extraordinary types of Na-Ca-SO_4 and Ca-Na-SO_4 type porewaters. Such formation could have occurred essentially in two different ways. As a fist hypothesis, permafrost could have resulted in the formation of cryogenic brines in the upper 100–300 m below the surface from where they migrated downwards to depths between about to 430–750 m by buoyancy effects. The large distance of all but one of the Na-Ca-SO_4 and Ca-Na-SO_4 type porewater samples and the nearest water-conducting fracture suggests that the cryogenic brines must have resided a these depth for a long time (>10–50 ka) and, therefore, that these signatures must have been established a long time ago, certainly before the Last Glacial Maximum (LGM). A second hypothesis would include the occurrence of permafrost down to greater depth where the Na-Ca-SO_4 and Ca-Na-SO_4 type porewaters are observed today. Whereas the first hypothesis asks for a long period of almost stagnant conditions at the depth levels where such porewater signatures are observed, the second hypothesis seems inconsistent with other findings such as heat production of the rocks and duration of possible permafrost events in the past (e.g. /Kjellström et al. 2009, Wohlfarth 2009/). The porewater data alone do not allow neither discerning between these two (or more?) hypotheses nor can they rule out one (ore more) of these hypotheses and more data and models simulations are needed to solve this problem.

With respect to the palaeohydrogeological evolution the chemical and isotopic composition of the porewater, in combination with the occurrence of the porewater samples with respect to depth, the distance to the nearest water-conducting fracture in the borehole and rock type allows the possibility of discerning an evolution from fracture groundwater that infiltrated from different sources and under different conditions. The observed signatures can be explained in terms of exchange with Holocene meteoric water of present-day type, Holocene thermal maximum type, glacial or glacio-lacustrine type and Pleistocene meteoric water of warm climate (possibly Eemian interglacial) and cold climate periods (early Weichselian or older). In addition, old signatures of exchange with pre-LGM permafrost-related fracture groundwater during Pleistocene times may also exist. Only weakly and locally developed are porewater signatures influenced by fracture groundwater related to Baltic Sea water and signatures influenced by fracture groundwater related to Littorina Sea water seem to be almost absent.

9 Conclusions

The information contained in the chemical and isotopic composition of porewater in rock matrix from the Laxemar subarea is the result of a variable but long-lasting exchange between different types of fracture groundwater circulating in the connected fracture network and the porewater in connected porosity of the rock matrix of the crystalline rock combined with water-rock interactions. The exchange between fracture groundwater and porewater has been identified to occur mainly by diffusion. Diffusive processes are much slower than the mixing processes in the dominant fracture-groundwater system characterised by advection. Therefore, the porewater composition represents an archive of the palaeohydrogeological evolution of the site. In this archive, information is still preserved with respect to palaeo-fracture groundwater compositions that are no longer resolvable in the present-day fracture groundwaters.

The quantitative interpretation of the porewater-fracture groundwater interaction as a function of time is complex and depends on many factors such as the transport properties in the rock matrix, the distance to the nearest water-conducting fracture, and the time period of fracture groundwater circulation with constant chemical and isotopic conditions, etc. Most demanding in such an interpretation is the case if a transient state (i.e. a difference in the chemical and isotopic composition between porewater and fracture groundwater) is established because of the unknown conditions at the start of the interaction (initial conditions). In the situation of a steady state, on the other hand, at least a minimum and maximum time of interaction can be deduced more easily. In both cases, however, changes in the boundary conditions (i.e. the fracture groundwater composition) might become masked and superimposed in the course of the interaction. Furthermore, changes in the boundary conditions might not be equally present for all components. For example, the Cl^- concentration in fracture groundwater might grossly change with time while the water isotope composition remains similar as, for example, in the case of Littorina and Baltic Sea water, or the Cl^- concentration might remain similar whereas the water isotope composition changes dramatically as, for example, in the case of present-day infiltration and glacial meltwater. For the quantitative interpretation of the porewater-fracture groundwater interactions, observations from several independent natural tracers (such as Cl^-, ^{18}O, ^{2}H, noble gases etc) are required. In addition, the limitations of borehole observations with respect to the 3-dimensional distribution of water-conducting fractures and rock matrix transport properties have to be respected.

Based on the conducted characterisation of the porewater chemical and isotopic composition, geochemical modelling and the quantitative description of natural tracer profiles in porewater from rocks of the Laxemar subarea, the following conclusions emerge:

- Porewater acts as an archive of the past hydrogeological history at the Laxemar subarea and its composition puts constraints on the interpretation of the palaeohydrogeological evolution of the site.
- Solute transport in the intact rock matrix appears to be dominated by diffusion, and matrix diffusion was identified to occur at least over several decametres into the rock matrix. Experimentally derived average pore diffusion coefficients for Cl^- are: Ävro granite = 5.8×10^{-11} m^2/s ± 2.7×10^{-11} m^2/s, quartz monzodiorite = 8.4×10^{-11} m^2/s ± 5.5×10^{-11} m^2/s, diorite = 3.8×10^{-11} m^2/s ± 4.1×10^{-12} m^2/s (n = 2) at a temperature of 25°C.
- Depending on the distance to the nearest water-conducting fracture and the depth of the rock sample, the porewater preserves signatures of exchange with fracture groundwaters during Holocene and Pleistocene times.
- For the Holocene period, porewater compositions indicate exchange with fracture groundwater of present-day type, Holocene thermal maximum type, and glacial or glacio-lacustrine type meteoric waters. Exchange with Baltic Sea water seems limited in boreholes KLX03, KLX08 and KLX17A and is probably not present at all with Yoldia and Littorina Sea water.
- For the Pleistocene period, porewater compositions indicate exchange with fracture groundwaters of meteoric water of warm climate (possibly Eemian interglacial) and cold climate periods (early Weichselian or older).

- In addition, old signatures of exchange with pre-Last Glacial Maximum permafrost-related fracture groundwater during Pleistocene times exist.
- A different hydrogeological evolution for boreholes KLX03 and KLX17A compared to borehole KLX08 is observed, with deeper, young meteoric recharge measured in KLX08.
- Down to depths of about 400 m, porewater is of a dilute to brackish Na-HCO_3 type and present-day meteoric influence dominates in porewaters in boreholes KLX03 and KLX17A.
- In all three boreholes, warmer climate meteoric influences from temperature maximums during the Pleistocene prior to the last glaciation (possibly during Eemian interglacial) have occurred. In boreholes KLX08 and, at shallow levels, KLX17A, warmer climate meteoric influences from the thermal maximum during the Holocene (7,000–4,000 years BP) occur, which cannot be further resolved in the fracture groundwaters.
- Cold climate influence from the last glaciation occurs in the still dilute Na-HCO_3 type porewaters between about 135–350 m depth in boreholes KLX03 and KLX17A, and down to about 500 m depth in borehole KLX08. At a few locations, pre Last Glacial Maximum cold climate influence is present in boreholes KLX08 and KLX03.
- A distinct change in chemical and isotopic composition to a highly mineralised Na-Ca-SO_4 and Ca-Na-SO_4 general type porewater is observed between about 430–550 m depth in boreholes KLX03 and KLX17A, and between about 620–750 m depth in borehole KLX08. One possibility is that these signatures may have evolved from fracture groundwaters influenced by permafrost related freeze-out processes a long time ago, certainly before the Last Glacial Maximum, and most probably at shallower depth.
- Modelling of a porewater profile extending from a conducting fracture into the intact rock matrix indicated that changes in fracture groundwater composition during Holocene time left their (superimposed) signatures a few metres into the rock matrix. Further into the rock matrix, older (i.e. prior to the last glaciation), warm-climate signatures are still preserved, lending additional support to the hydrogeochemical conceptual model.

10 References

Antonsson K, Brooks S J, Seppä H, Telford R J, Birks H J B, 2006. Quantitative palaeotemperature records inferred from fossil pollen and chironomid assemblages from Lake Gilltjarnen, northern central Sweden. Journal of Quaternary Science 21(8): 831–841.

Antonsson K, Seppä H, 2007. Holocene temperatures in Bohuslan, southwest Sweden: a quantitative reconstruction from fossil pollen data. Boreas 36(4): 400–410.

Crank J, 1975. The mathematics of diffusion. 2nd addition. Oxford University Press.

Dahlin P, Ehrenborg J, 2006. Oskarshamn site investigation. Boremap mapping of core drilled borehole KLX08. SKB P-06-42, Svensk Kärnbränslehantering AB.

Desaulniers D E, Kaufmann R S, Cherry J A, Bentley H W, 1986. ^{37}Cl-^{35}Cl variations in a diffusion-controlled groundwater system. Geochim. Cosmochim. Acta 50, 1757–1764.

Drake H, Sandström B, Tullborg E-L, 2006. Mineralogy and geochemistry of rocks and fracture fillings from Forsmark and Oskarshamn: Compilation of data for SR-Can. SKB R-06-109, Svensk Kärnbränslehantering AB.

Drake H, Tullborg E-L, 2009a. Fracture mineralogy of the Laxemar site. Final Report. SKB R-08-99, Svensk Kärnbränslehantering AB.

Drake H, Tullborg E-L, 2009b. Paleohydrogeological events recorded by stable isotopes, fluid inclusions and trace elements in fracture minerals in crystalline rock, Simpevarp area, SE Sweden. Applied Geochemistry 24, 715–732.

Eggenkamp H G M, Middelbourg J J, Kreulen R, 1994. Preferential diffusion of ^{35}Cl relative to ^{37}Cl in sediments of Kau Bay, Halmahera, Indonesia. Chem. Geol. 116, 317–325.

Ehrenborg J, Dahlin P, 2005. Oskarshamn site investigation. Boremap mapping of core drilled borehole KLX03. SKB P-05-24, Svensk Kärnbränslehantering AB.

Eichinger F, 2009. Matrix porewater – fracture groundwater interaction in crystalline bedrock based on natural tracers: An archive for long-term hydrogeological evolution. PhD Thesis, Institute of Geological Sciences, University of Bern, Bern, Switzerland.

Gimeno M J, Auqué L F, Gómez J, Acero P, 2009. Water-rock interaction modelling and uncertainties of mixing modelling. SDM-Site Laxemar. SKB R-08-110, Svensk Kärnbränslehantering AB.

Gimmi T, Waber H N, 2004. Modelling of tracer profiles in porewater of argillaceous rocks in the Benken borehole: Stable water isotopes, chloride, and chlorine isotopes. Nagra Technical Report NTB 04-05, Wettingen, Switzerland.

Gimmi T, Waber H N, Gautschi A, Rübel A, 2007. Stable water isotopes in porewater of Jurassic argillaceous rocks as tracers for solute transport over large spatial and temporal scales. Water Resour. Res. 43, W04410, doi:10.1029/2005WR004774.

Gitterman K E, 1937. Thermal analysis of seawater. CRREL TL 287, USA Cold Region Research and Engineering Laboratory, Hanover, NH, USA.

Gustafsson J, Gustafsson C, 2007. Oskarshamn site investigations. RAMAC, BIPS and deviation logging in borehole KLX17A and HLX43. SKB P-07-12, Svensk Kärnbränslehantering AB.

Heikkilä M, Seppä H, 2003. A 11,000 yr palaeotemperature reconstruction from the southern boreal zone in Finland. Quaternary Science Reviews 22(5-7): 541–554.

Jäckli H, 1970. Klassifikation von Grundwasservorkommen. Eclogae Geol. Helv. 63, 389–434.

Karlén W, Bodin A, Kuylenstierna J, Näslund J-O, 1995. Climate of Northern Sweden during the Holocene. Journal of Coastal Research, Special Issue 17, 49–54.

Kjellström E, Strandberg G, Brandefelt J, Näslund J-O Smith B, Wohlfarth B, 2009. Climate conditions in Sweden in a 100,000-year time perspective. SKB TR-09-04, Svensk Kärnbränslehantering AB.

Laaksoharju M, Smellie J, Tullborg E-L, Wallin B, Drake H, Gascoyne M, Gimeno M, Gurban I, Hallbeck L, Molinero J, Nilsson A-C, Waber H N, 2009. Bedrock hydrogeochemistry Laxemar, Site descriptive model, SDM-Site Laxemar. SKB R-08-93, Svensk Kärnbränslehantering AB.

Lichtner P C, 2004. Flotran User's Manual: Two phase, non-isothermal coupled thermal-hydrologic-chemical (THC) reactive flow and transport code. LANL Report LA-UR-01-2349, Los Alamos National Laboratory, Los Alamos, NM, USA.

Lin Li C, 2001. Long Term Diffusion Experiment. Microscopic Observation of Disturbance in Drillcore Samples from KA3065A02 and KA3065A03. SKB IPR-01-03, Svensk Kärnbränslehantering AB.

Lundqvist J, 1992. Glacial stratigraphy in Sweden. Geological Survey of Finland Special Paper 15. 43–59.

Lundqvist J, Wohlfarth B, 2001. Timing and east-west correlation of south Swedish ice marginal lines during the Late Weichselian. Quaternary Science Reviews 20, 1127–1148.

Marion G M, Farren R E, Komrowski A J, 1999. Alternative pathways for seawater freezing. Cold Region Science and Technology 29, 259–266.

Mattsson K-J, Dahlin P, 2007. Oskarshamn site investigation. Boremap mapping of telescopic drilled borehole KLX17A. SKB P-07-158, Svensk Kärnbränslehantering AB.

Mazurek M, Alt-Epping P, Bath A, Gimmi T, Waber H N, 2009. Natural Tracer Profiles Across Argillaceous Formations: The CLAYTRAC Project. Nuclear Energy Agency – Radioactive Waste Management, NEA No.6253, OECD Paris, France.

Michard G, Pearson F J, Gautschi A, 1996. Chemical evolution of waters during long term interaction with granitic rocks in northern Switzerland. Appl. Geochem. 11, 757–774.

Neretnieks I, 1980. Diffusion in the rock matrix: an important factor for radionuclide retardation? J. Geophys. Res. 85, 4379–4397.

Nordstrom D K, Ball, J W Donahoe, R J, Whittemore D, 1989. Ground water chemistry and water-rock interactions at Stripa. Geochim. Cosmochim. Acta 53, 1727–1740.

Norton D, Knapp R, 1977. The nature of porosity. Am. J. Sci., 277, 913–936.

Ohlsson Y, 2000. Studies of Ionic Diffusion in Crystalline Rock. PhD thesis, Royal Institute of Technology KTH, Stockholm, Sweden. ISBN 91-7283-025-5.

Ota K, Möri A, Alexander W R, Frieg B, Schild M, 2003. Influence of the mode of matrix porosity determination on matrix diffusion calculations. J. Cont. Hydrol., 61, 131–145.

Parkhurst D L, Appelo C A J, 1999. User's Guide to PHREEQC (Version 2) – A Computer Program for Speciation, Batch-Reaction, One-Dimensional Transport, and Inverse Geochemical Calculations: Denver, CO, U. S. Geological Survey, Water-Resources Investigations Report 99-4259; v. W2-13, 2006.

Pearson F J, 1999. What is the porosity of a mudrock? In: A C Aplin, A J Fleet, J H S Macquaker (Eds.), Muds and Mudstones: Physical and Fluid Flow Properties. London, Geol. Soc. Spec. Publ. 158, 9–21.

Pöllänen J, Kristiansson S, 2007. Oskarshamn site investigation. Difference flow logging of borehole KLX17A. Oskarshamn site investigation. SKB P-07-34, Svensk Kärnbränslehantering AB.

Rhén I, Forsmark T, Hartley L, Gylling B, Marsic N, 2008. Bedrock Hydrogeolology: model testing and synthesis, Site descriptive modelling, SDM-Site Laxemar, SKB R-08-91, Svensk Kärnbränslehantering AB.

Rhén I, Forsmark T, Hartley L, Jackson C P, Joyce S, Roberts D, Swift B, Marsic N, Gylling B, 2009. Bedrock Hydrogeolology: model testing and synthesis, Site descriptive modelling. SDM-Site Laxemar. SKB R-08-91, Svensk Kärnbränslehantering AB.

Rogge T, 1997. Eine molekular-diffusive Methode zur Bestimmung des Porenwassergehaltes und der Zusammensetzung von stabilen Isotopen im Porenwasser von Gestein. Unpubl. Diploma Thesis, Institut für Umweltphysik, University of Heidelberg (in German).

Rouhiainen P, Pöllänen J, Sokolnicki M, 2005. Oskarshamn site investigation. Difference flow logging of borehole KLX03. Oskarshamn site investigation. SKB P-05-67, Svensk Kärnbränslehantering AB.

Rübel A P, 2000. Stofftransport in undurchlässigen Gesteinsschichten – Isotopenuntersuchungen im Grund- und Porenwasser. PhD Thesis, Institut für Umweltphysik, Unversity of Heidelberg, Der Andere Verlag, Osnabrück, Germany (in German).

Skagius K, Neretnieks I, 1986. Porosities and diffusivities of some nonsorbing species in crystalline rocks. Water resources research. Vol. 22, pp 289–298.

Smellie J A T, Waber H N, Frape, S K (eds), 2003. Matrix fluid chemistry experiment. Final Report. SKB TR-03-18, Svensk Kärnbränslehantering AB, p 377.

Sokolnicki M, Pöllänen J, 2005. Oskarshamn site investigation. Difference flow logging of borehole KLX08. Oskarshamn site investigation. SKB P-05-267, Svensk Kärnbränslehantering AB.

Söderbäck B (ed), 2008. Geological evolution, palaeoclimate and historical development of the Forsmark and Laxemar-Simpevarp area. SKB R-08-19, Svensk Kärnbränslehantering AB.

Waber H N, Smellie J A T, 2005. Forsmark site investigation. Borehole KFM06A: Characterisation of porewater. Part I: Diffusion experiments. SKB P-05-196, Svensk Kärnbränslehantering AB.

Waber H N, Smellie J A T, 2006a. Oskarshamn site investigation. Borehole KLX03: Characterisation of porewater. Part 1: Methodology and analytical data. SKB P-06-12, Svensk Kärnbränslehantering AB.

Waber H N, Smellie J A T, 2006b. Oskarshamn site investigation. Borehole KLX03: Characterisation of porewater. Part 2: Rock properties and diffusion experiments. SKB P-06-77, Svensk Kärnbränslehantering AB.

Waber H N, Smellie J A T, 2006c. Oskarshamn site investigation. Borehole KLX08: Characterisation of porewater. Part 1: Methodology and analytical data. SKB P-06-163, Svensk Kärnbränslehantering AB.

Waber H N, Smellie J A T, 2008a. Characterisation of porewater in crystalline rocks. Appl. Geochem. 23, 1834–1861.

Waber H N, Smellie J A T, 2008b. Oskarshamn site investigation. Borehole KLX17A: Characterisation of porewater. Part 1: Methodology and analytical data. SKB P-08-43, Svensk Kärnbränslehantering AB.

Waber H N, Gimmi, T, Smellie J A T, 2009. Porewater in the Rock Matrix, Site descriptive modelling, SDM-Site Forsmark. SKB R-08-105, Svensk Kärnbränslehantering AB.

Wahlgren C-H, Curtis P, Hermanson J, Forssberg O, Öhman J, Drake H, Fox A, Triumf C-A, Mattsson H, Thunehed H, 2008. Geology Laxemar, Site descriptive modelling, SDM-Site Laxemar. SKB R-08-54, Svensk Kärnbränslehantering AB.

Westman P, Wastegård S, Schoning K, Gustafsson B, 1999. Salinity change in the Baltic Sea during the last 8,500 years: evidence causes and models. SKB TR-99-38, Svensk Kärnbränslehantering AB.

Wohlfarth B, 2009. Ice-free conditions in Fennoscandia during Marine Oxygen Isotope Stage 3? SKB TR-09-12, Svensk Kärnbränslehantering AB.

Appendix

Data tables

Table A-1. Geological information and water content derived by different techniques of rock samples used for porewater investigations from boreholes KLX03, KLX08 and KLX17A.

SKB sample no	UniBern sample no	Average borehole length	Average elevation [1]	Lithology	Fracture intensity [2]	Distance to nearest water-cond. fracture [3]	Number of samples	Water content by drying at 105°C (average) [4]		Water content by diffusive isotope exchange [5]	
		m	m			m		wt.%	1 σ wt.%	wt.%	error
SKB 07250	KLX03-1	159.22	–135.33	Ävrö Granite	moderate	5	3	0.217	0.014	0.180	0.027
SKB 07251	KLX03-2	202.66	–177.31	Ävrö Granite	moderate	1	3	0.214	0.004	0.213	0.028
SKB 07252	KLX03-3	253.72	–226.74	Ävrö Granite	moderate	4	3	0.242	0.019	0.250	0.026
SKB 07423	KLX03-4	304.10	–275.53	Ävrö Granite	moderate	10	3	0.369	0.040	–	–
SKB 07424	KLX03-5	355.66	–325.54	Ävrö Granite	moderate	27	3	0.212	0.016	0.221	0.026
SKB 07425	KLX03-6	411.72	–379.92	Ävrö Granite	moderate	3	3	0.173	0.005	0.196	0.009
SKB 07426	KLX03-7	462.76	–429.47	Ävrö Granite	moderate	3	3	0.276	0.051	0.213	0.027
SKB 07427	KLX03-8	524.63	–489.64	Ävrö Granite	weak	65	3	0.375	0.073	0.368	0.027
SKB 07428	KLX03-9	590.12	–553.24	Ävrö Granite	weak	32	1	0.190	–	–	–
SKB 07429	KLX03-10	643.13	–604.72	Quartz-Monzodiorite	moderate	16	1	0.068	–	–	–
SKB 07430	KLX03-11	695.95	–656.05	Quartz-Monzodiorite	high	31	3	0.122	0.006	0.149	0.025
SKB 07431	KLX03-12	803.23	–760.35	Quartz-Monzodiorite	very high	7	3	0.258	0.010	0.299	0.028
SKB 07432	KLX03-13	841.18	–797.26	Quartz-Monzodiorite	weak	34	3	0.103	0.012	–	–
SKB 05349	KLX03-14	894.53	–849.17	Quartz-Monzodiorite	weak	75	3	0.083	0.010	0.083	0.025
SKB 05351	KLX03-15	942.47	–895.83	Quartz-Monzodiorite	weak	27	3	0.089	0.023	–	–
SKB 05352	KLX03-16	979.78	–932.12	Quartz-Monzodiorite	weak	10	3	0.094	0.023	0.106	0.025
SKB 09700	KLX08-1	150.22	–105.66	Ävrö Granite	very high	3	4	0.422	0.144	–	–
SKB 09701	KLX08-2	199.45	–148.37	Fine-grained Granite	high	4	3	0.348	0.094	–	–
SKB 09702	KLX08-3	200.26	–149.07	Ävrö Granite	high	3	4	0.289	0.062	0.381	0.007
SKB 09709	KLX08-4	250.19	–192.36	Ävrö Granite	moderate	13	2	0.315	0.049	0.361	0.020
SKB 09710	KLX08-5	302.34	–237.38	Ävrö Granite	very high	2	3	0.195	0.029	0.178	0.005
SKB 09711	KLX08-6	347.10	–275.89	Ävrö Granite	moderate	37	3	0.192	0.059	0.144	0.013
SKB 09712	KLX08-7	395.65	–317.63	Ävrö Granite	high	3	4	0.201	0.050	0.247	0.006
SKB 09713	KLX08-8	451.62	–365.70	Ävrö Granite	high	3		–	–	–	–
SKB 09714	KLX08-9	499.78	–406.97	Ävrö Granite	high	16	2	0.414	0.044	–	–
SKB 09715	KLX08-10	550.23	–450.17	Ävrö Granite	moderate	66	1	0.292	–	0.262	0.022
SKB 09716	KLX08-11	601.68	–494.21	Diorite	moderate	12	3	0.218	0.077	0.143	0.018
SKB 09717	KLX08-12	660.03	–544.12	Diorite	moderate	4	2	0.175	0.013	0.454	0.013
SKB 09718	KLX08-13	702.05	–580.04	Diorite	high	23	3	0.151	0.043	0.192	0.014
SKB 09719	KLX08-14	750.80	–621.67	Ävrö Granite	low	72	3	0.246	0.062	0.189	0.006
SKB 09720	KLX08-15	802.22	–665.50	Ävrö Granite	low	52	3	0.248	0.078	0.157	0.014
SKB 09721	KLX08-16	857.98	–712.88	Ävrö Granite	low	4	3	0.331	0.160	0.720	0.008

Table A-1. continued.

SKB sample no	UniBern sample no	Average borehole length	Average elevation [1]	Lithology	Fracture intensity [2]	Distance to nearest water-cond. fracture [3]	Number of samples	Water content by drying at 105°C (average) [4]		Water content by diffusive isotope exchange [5]	
		m	m			m		wt.%	stdev	wt.%	error
SKB 09722	KLX08-17	903.28	–751.17	Ävrö Granite	low	49	3	0.263	0.107	0.180	0.015
SKB 09723	KLX08-18	945.75	–787.01	Quartz-Monzodiorite	moderate	92	3	0.183	0.080	0.353	0.007
SKB 09724	KLX08-19	983.18	–818.37	Quartz-Monzodiorite	low	>100	3	0.238	0.085	0.226	0.014
SKB 09748	KLX17A-1	112.09	–70.42	Ävrö Granite	very high	1	5	0.575	0.068	0.485	0.008
SKB 09749	KLX17A-2	112.47	–70.76	Ävrö Granite	very high	1	5	0.581	0.090	0.612	0.007
SKB 09750	KLX17A-3	113.26	–71.44	Ävrö Granite	very high	1	5	0.820	0.165	0.508	0.007
SKB 09751	KLX17A-4	113.89	–71.99	Ävrö Granite	very high	1	5	0.625	0.306	0.447	0.006
SKB 09752	KLX17A-5	114.30	–72.35	Ävrö Granite	very high	1	5	0.385	0.191	0.210	0.005
SKB 09753	KLX17A-6	114.67	–72.67	Ävrö Granite	very high	1	4	0.353	0.104	0.537	0.007
SKB 09754	KLX17A-7	114.97	–72.94	Ävrö Granite	very high	2	4	0.300	0.094	0.243	0.007
SKB 09755	KLX17A-8	115.37	–73.28	Ävrö Granite	high	2	6	0.301	0.067	0.401	0.005
SKB 09756	KLX17A-9	115.81	–73.67	Ävrö Granite	high	2	3	0.250	0.049	0.218	0.005
SKB 09757	KLX17A-10	116.17	–73.98	Ävrö Granite	moderate	3	6	0.308	0.064	0.242	0.005
SKB 09758	KLX17A-11	116.47	–74.24	Ävrö Granite	moderate	3	5	0.355	0.097	0.349	0.006
SKB 09759	KLX17A-12	116.84	–74.57	Ävrö Granite	moderate	3	5	0.349	0.067	0.307	0.005
SKB 09760	KLX17A-13	117.18	–74.86	Ävrö Granite	moderate	4	3	0.321	0.022	0.245	0.005
SKB 09761	KLX17A-14	117.70	–75.32	Ävrö Granite	low	4	5	0.303	0.036	0.289	0.005
SKB 09762	KLX17A-15	118.21	–75.77	Ävrö Granite	low	5	5	0.268	0.030	0.244	0.005
SKB 09763	KLX17A-16	118.73	–76.21	Ävrö Granite	low	5	6	0.246	0.024	0.253	0.005
SKB 09768	KLX17A-17	120.87	–78.08	Ävrö Granite	low	7	5	0.232	0.045	0.187	0.004
SKB 09775	KLX17A-18	123.62	–80.48	Ävrö Granite	low	10	5	0.219	0.029	0.373	0.005
SKB 09790	KLX17A-19	128.78	–84.99	Ävrö Granite	low	15	4	0.254	0.020	0.240	0.004
SKB 09802	KLX17A-20	133.76	–89.33	Ävrö Granite	moderate	20	5	0.102	0.013	0.107	0.003
SKB 09803	KLX17A-21	239.20	–181.09	Ävrö Granite	moderate	22	4	0.249	0.007	0.229	0.004
SKB 09804	KLX17A-22	332.18	–261.36	Ävrö Granite	moderate	3	4	0.239	0.007	0.254	0.004
SKB 09805	KLX17A-23	435.72	–349.97	Ävrö Granite	high	4	4	0.167	0.008	–	–
SKB 09806	KLX17A-24	540.38	–438.65	Ävrö Granite	low	>100	5	0.148	0.005	0.159	0.004
SKB 09807	KLX17A-25	635.69	–518.17	Ävrö Granite	low	>100	5	0.140	0.005	0.222	0.020

[1] Reference elevation relative to sea level and corrected for altitude (KLX03 = 18.5 m, KLX08 = 24.3 m, KLX17A = 27.6 m) and borehole inclination (KLX03 = 74.9°, KLX08 = 60.3° , KLX17A = 61.3°).

[2] Fracture intensity above and below sample (from WellCAD images by /Ehrenborg and Dahlin 2005, Dahlin and Ehrenborg 2006, Mattson and Dahlin 2007/).

[3] Approximate distance from the porewater sample to nearest water-conducting fracture in the borehole according to the borehole differential flow log (PFL data from /Rouhiainen et al. 2005, Sokolnicki and Pöllänen 2005, Pöllänen and Kristiansson 2007/).

[4] Error is standard deviation of multiple samples and assumed to be ± 10% in case of a single sample.

[5] Error calculated using Gauss' error propagation (see text).

Table A-2. Water-loss porosity and pore diffusion coefficients for chloride of rock samples used for porewater investigations from boreholes KLX03, KLX08 and KLX17A.

UniBern sample no	Average borehole length	Average elevation	Lithology	Distance to nearest water-cond. fracture [1]	Mass of core in out-diff. exp.	Bulk density (wet) [2]	Number of samples	Water-loss porosity (average) [3]		D_p chloride (25°C)	D_p uncertainty range [4]	
	m	m		m	g	g/cm^3		vol.%	stdev		+ error	– error
KLX03-1	159.22	–135.33	Ävrö Granite	5	1,015.640	2.72	3	0.59	0.04	2.6×10^{-11}	1.1×10^{-11}	7.6×10^{-12}
KLX03-2	202.66	–177.31	Ävrö Granite	1	1,028.960	2.72	3	0.58	0.01			
KLX03-3	253.72	–226.74	Ävrö Granite	4	1,020.191	2.71	3	0.65	0.05	–		
KLX03-4	304.10	–275.53	Ävrö Granite	10	1,031.454	2.72	3	1.00	0.11	–		
KLX03-5	355.66	–325.54	Ävrö Granite	27	1,028.396	2.75	3	0.58	0.04	–		
KLX03-6	411.72	–379.92	Ävrö Granite	3	1,007.473	2.74	3	0.47	0.01	–		
KLX03-7	462.76	–429.47	Ävrö Granite	3	1,027.610	2.76	3	0.76	0.14	6.9×10^{-11}	1.2×10^{-11}	1.1×10^{-11}
KLX03-8	524.63	–489.64	Ävrö Granite	65	1,015.631	2.74	3	1.02	0.20	–		
KLX03-9	590.12	–553.24	Ävrö Granite	32	1,002.790	2.73	1	0.52	0.05	–		
KLX03-10	643.13	–604.72	Quartz-Monzodiorite	16	982.509	2.73	1	0.19	0.02	–		
KLX03-11	695.95	–656.05	Quartz-Monzodiorite	31	1,036.704	2.79	3	0.34	0.02	–		
KLX03-12	803.23	–760.35	Quartz-Monzodiorite	7	1,050.850	2.78	3	0.72	0.03	3.8×10^{-11}	1.6×10^{-11}	1.1×10^{-11}
KLX03-13	841.18	–797.26	Quartz-Monzodiorite	34	1,053.568	2.79	3	0.29	0.03	–		
KLX03-14	894.53	–849.17	Quartz-Monzodiorite	75	1,044.860	2.80	3	0.23	0.03	–		
KLX03-15	942.47	–895.83	Quartz-Monzodiorite	27	1,041.053	2.81	3	0.25	0.06	–		
KLX03-16	979.78	–932.12	Quartz-Monzodiorite	10	1,047.565	2.80	3	0.26	0.06	6.9×10^{-11}	2.9×10^{-11}	2.0×10^{-11}
KLX08-1	150.22	–105.66	Ävrö Granite	3	972.646	2.67	4	1.12	0.38	–		
KLX08-2	199.45	–148.37	Fine-grained Granite	4	991.830	2.67	3	0.92	0.25	–		
KLX08-3	200.26	–149.07	Ävrö Granite	3	986.680	2.68	4	0.77	0.16	7.5×10^{-11}	3.1×10^{-11}	2.2×10^{-11}
KLX08-4	250.19	–192.36	Ävrö Granite	13	999.319	2.68	2	0.84	0.13	–		
KLX08-5	302.34	–237.38	Ävrö Granite	2	996.973	2.66	3	0.52	0.08	–		
KLX08-6	347.10	–275.89	Ävrö Granite	37	985.143	2.68	3	0.51	0.16	6.1×10^{-11}	1.0×10^{-11}	1.8×10^{-11}
KLX08-7	395.65	–317.63	Ävrö Granite	3	994.440	2.69	4	0.54	0.13	3.8×10^{-11}	1.6×10^{-11}	1.1×10^{-11}
KLX08-8	451.62	–365.70	Ävrö Granite	3	1,023.237	2.65	–	–	–	–		
KLX08-9	499.78	–406.97	Ävrö Granite	16	1,001.100	2.69	2	1.10	0.12	–		
KLX08-10	550.23	–450.17	Ävrö Granite	66	974.470	2.65	1	0.77	0.08	5.5×10^{-11}	2.3×10^{-11}	1.6×10^{-11}
KLX08-11	601.68	–494.21	Diorite	12	1,049.620	2.92	3	0.63	0.22	–		
KLX08-12	660.03	–544.12	Diorite	4	1,037.105	2.84	2	0.49	0.04	4.1×10^{-11}	1.7×10^{-11}	1.9×10^{-11}
KLX08-13	702.05	–580.04	Diorite	23	1,062.495	2.85	3	0.43	0.12	3.5×10^{-11}	1.4×10^{-11}	1.0×10^{-11}
KLX08-14	750.80	–621.67	Ävrö Granite	72	974.722	2.67	3	0.65	0.16	9.3×10^{-11}	3.8×10^{-11}	2.7×10^{-11}
KLX08-15	802.22	–665.50	Ävrö Granite	52	972.254	2.66	3	0.66	0.21	–		
KLX08-16	857.98	–712.88	Ävrö Granite	4	1,017.109	2.74	3	0.90	0.43	–		

Table A-2. continued.

UniBern sample no	Average borehole length	Average elevation	Lithology	Distance to nearest water-cond. fracture [1]	Mass of core in out-diff. exp.	Bulk density (wet) [2]	Number of samples	Water-loss porosity (average) [3]		D_p chloride (25°C)	D_p uncertainty range [4]	
	m	m		m	g	g/cm^3		vol.%	stdev		+ error	– error
KLX08-17	903.28	–751.17	Ävrö Granite	49	990.374	2.69	3	0.70	0.29	1.2×10^{-10}	4.8×10^{-11}	3.4×10^{-11}
KLX08-18	945.75	–787.01	Quartz-Monzodiorite	92	1,037.604	2.81	3	0.51	0.22	–		
KLX08-19	983.18	–818.37	Quartz-Monzodiorite	>100	1,039.380	2.80	3	0.66	0.24	1.4×10^{-10}	6.0×10^{-11}	4.2×10^{-11}
KLX17A-1	112.09	–70.42	Ävrö Granite	1	616.602	2.71	5	1.55	0.18	6.9×10^{-11}	2.8×10^{-11}	2.1×10^{-11}
KLX17A-2	112.47	–70.76	Ävrö Granite	1	578.931	2.69	5	1.55	0.24	–		
KLX17A-3	113.26	–71.44	Ävrö Granite	1	602.385	2.66	5	2.15	1.35	5.8×10^{-11}	2.4×10^{-11}	1.7×10^{-11}
KLX17A-4	113.89	–71.99	Ävrö Granite	1	999.145	2.70	5	1.19	1.08	–		
KLX17A-5	114.30	–72.35	Ävrö Granite	1	625.473	2.71	5	1.04	0.51	–		
KLX17A-6	114.67	–72.67	Ävrö Granite	1	631.580	2.86	4	1.00	0.29	–		
KLX17A-7	114.97	–72.94	Ävrö Granite	2	617.625	2.73	4	0.82	0.26	–		
KLX17A-8	115.37	–73.28	Ävrö Granite	2	630.351	2.73	6	0.61	0.41	–		
KLX17A-9	115.81	–73.67	Ävrö Granite	2	631.588	2.73	3	0.68	0.13	–		
KLX17A-10	116.17	–73.98	Ävrö Granite	3	584.920	2.71	6	0.83	0.17	–		
KLX17A-11	116.47	–74.24	Ävrö Granite	3	645.285	2.73	5	0.97	0.26	–		
KLX17A-12	116.84	–74.57	Ävrö Granite	3	623.745	2.72	5	0.95	0.18	5.2×10^{-11}	2.2×10^{-11}	1.5×10^{-11}
KLX17A-13	117.18	–74.86	Ävrö Granite	4	632.550	2.76	3	0.88	0.06	–		
KLX17A-14	117.70	–75.32	Ävrö Granite	4	629.622	2.74	5	0.83	0.10	–		
KLX17A-15	118.21	–75.77	Ävrö Granite	5	819.550	2.74	5	0.73	0.08	–		
KLX17A-16	118.73	–76.21	Ävrö Granite	5	634.256	2.73	6	0.67	0.07	1.7×10^{-11}	7.2×10^{-12}	5.1×10^{-12}
KLX17A-17	120.87	–78.08	Ävrö Granite	7	1,008.455	2.73	5	0.63	0.12	–		
KLX17A-18	123.62	–80.48	Ävrö Granite	10	1,036.723	2.85	5	0.62	0.08	–		
KLX17A-19	128.78	–84.99	Ävrö Granite	15	1,012.810	2.74	4	0.69	0.05	–		
KLX17A-20	133.76	–89.33	Ävrö Granite	20	1,110.550	3.04	5	0.25	0.13	–		
KLX17A-21	239.20	–181.09	Ävrö Granite	22	1,016.925	2.74	4	0.68	0.02	–		
KLX17A-22	332.18	–261.36	Ävrö Granite	3	1,038.257	2.76	4	0.66	0.02	–		
KLX17A-23	435.72	–349.97	Ävrö Granite	4	1,015.640	2.68	4	0.45	0.02	–		
KLX17A-24	540.38	–438.65	Ävrö Granite	>100	1,007.375	2.70	5	0.40	0.01	–		
KLX17A-25	635.69	–518.17	Ävrö Granite	>100	999.034	2.69	5	0.37	0.01	–		

[1] Approximate distance from the porewater sample to nearest water-conducting fracture in the borehole according to the borehole differential flow log (PFL).

[2] Determined from mass and volume of originally saturated (wet) drillcore sample used for out-diffusion experiment.

[3] Determined on small-sized aliquots (~ 100–350 g); error is the standard deviation of multiple samples and assumed to be ± 10% in case of a single sample.

[4] Uncertainty range for the pore diffusion coefficient is $D_p^* \sqrt{2}$ – D_p (+ error) and D_p – $D_p/\sqrt{2}$ (– error) corresponding to a factor of 2 in the diffusion time from the best-fit D_p.

Table A-3. Chloride concentration and $\delta^{18}O$ and $\delta^{2}H$ in porewater of rock samples from boreholes KLX03, KLX08 and KLX17A.

UniBern sample no	Average borehole length	Average elevation	Lithology	Distance to nearest water-cond. fracture [1]	Experiment solution chemical type [2]	Chloride in porewater	+ error [3]	– error [3]	$\delta^{18}O$ [4]	error [4]	$\delta^{2}H$ [4]	error [4]
	m	m		m		mg/kg_{H2O}			‰ V-SMOW		‰ V-SMOW	
KLX03-1	159.22	–135.33	Ävrö Granite	5	Na-HCO3-(Cl)	819	56	49	–12.4	±1.5	–92	±24
KLX03-2	202.66	–177.31	Ävrö Granite	1	Na-HCO3-(Cl)	765	16	15	–11.4	±1.4	–92	±15
KLX03-3	253.72	–226.74	Ävrö Granite	4	Na-HCO3	502	41	35	–11.5	±2.0	–121	±27
KLX03-4	304.10	–275.53	Ävrö Granite	10	Na-HCO3-(Cl)	374	44	35	–		–	
KLX03-5	355.66	–325.54	Ävrö Granite	27	Na-HCO3	619	50	43	–12.9	±1.6	–93	±22
KLX03-6	411.72	–379.92	Ävrö Granite	3	Na-HCO3-(Cl)	730	22	21	–11.6	±2.0	–	
KLX03-7	462.76	–429.47	Ävrö Granite	3	Ca-Na-SO4-(HCO3)	1,375	304	209	–7.6	±2.0	–84	±15
KLX03-8	524.63	–489.64	Ävrö Granite	65	Na-Ca-SO4-Cl-(HCO3)	5,674	1,334	897	–13.3	±2.1	–97	±17
KLX03-9	590.12	–553.24	Ävrö Granite	32	Na-Ca-Cl-HCO3-SO4	7,601	831	680	–		–	
KLX03-10	643.13	–604.72	Quartz-Monzodiorite	16	Na-Ca-HCO3-Cl	2,260	249	204	–		–	
KLX03-11	695.95	–656.05	Quartz-Monzodiorite	31	Na-Ca-HCO3	511	28	25	–9.1	±3.0	*–23*	*±33*
KLX03-12	803.23	–760.35	Quartz-Monzodiorite	7	Na-(Ca)-HCO3-Cl	4,896	185	172	–11.0	±1.5	–59	±14
KLX03-13	841.18	–797.26	Quartz-Monzodiorite	34	Na-Ca-HCO3-Cl	4,405	302	645	–		–	
KLX03-14	894.53	–849.17	Quartz-Monzodiorite	75	Na-Ca-HCO3-Cl	4,632	617	486	–4.8	±3.8	–	
KLX03-15	942.47	–895.83	Quartz-Monzodiorite	27	Ca-Na-HCO3-Cl	6,484	599	1,025	–		–	
KLX03-16	979.78	–932.12	Quartz-Monzodiorite	10	Na-Ca-HCO3-Cl	5,123	1,619	989	–6.5	±3.5	–28	±38
KLX08-1	150.22	–105.66	Ävrö Granite	3	Na-Ca-HCO3	99	49	24	–		–	
KLX08-2	199.45	–148.37	Fine-grained Granite	4	Na-Ca-HCO3	138	50	29	–		–	
KLX08-3	200.26	–149.07	Ävrö Granite	3	Na-Ca-HCO3	127	34	22	–9.6	±0.9	–83	±9
KLX08-4	250.19	–192.36	Ävrö Granite	13	Na-Ca-HCO3	117	21	15	–8.4	±1.2	–82	±10
KLX08-5	302.34	–237.38	Ävrö Granite	2	Na-Ca-HCO3-Cl	705	122	90	–7.3	±1.8	–77	±14
KLX08-6	347.10	–275.89	Ävrö Granite	37	Na-Ca-HCO3	772	340	179	–8.5	±2.2	–97	±16
KLX08-7	395.65	–317.63	Ävrö Granite	3	Na-HCO3-Cl	364	118	71	–12.8	±1.2	–108	±1
KLX08-8	451.62	–365.70	Ävrö Granite	3	Na-Ca-HCO3	–			–		–	
KLX08-9	499.78	–406.97	Ävrö Granite	16	Na-Ca-HCO3-Cl	613	69	56	–		–	
KLX08-10	550.23	–450.17	Ävrö Granite	66	Na-Ca-HCO3-Cl	997	99	99	–14.3	±1.8	–104	±16
KLX08-11	601.68	–494.21	Diorite	12	Na-Ca-HCO3	240	129	61	–12.4	±3.3	–99	±28
KLX08-12	660.03	–544.12	Diorite	4	Na-Ca-HCO3	388	31	27	–8.4	±1.7	–90	±17
KLX08-13	702.05	–580.04	Diorite	23	Na-Ca-HCO3	687	270	150	–7.7	±1.8	–84	±15
KLX08-14	750.80	–621.67	Ävrö Granite	72	Na-Ca-HCO3-SO4	1,532	505	302	–4.9	±2.0	–71	±15
KLX08-15	802.22	–665.50	Ävrö Granite	52	Ca-Na-SO4	2,721	1,220	636	–1.9	±2.3	–54	±17
KLX08-16	857.98	–712.88	Ävrö Granite	4	Ca-Na-SO4	2,761	669	446	–9.7	±0.5	–72	±4

Table A-3. continued.

UniBern sample no	Average borehole length	Average elevation	Lithology	Distance to nearest water-cond. fracture [1]	Experiment solution chemical type [2]	Chloride in porewater	+ error [3]	– error [3]	$\delta^{18}O$ [4]	error [4]	$\delta^{2}H$ [4]	error [4]
	m	m		m		mg/kg_{H2O}			‰ V-SMOW		‰ V-SMOW	
KLX08-17	903.28	–751.17	Ävrö Granite	49	Ca-Na-SO4	6,054	1,478	985	–2.7	±2.0	–51	±15
KLX08-18	945.75	–787.01	Quartz-Monzodiorite	92	Na-Ca-HCO3-Cl	3,038	746	498	–6.6	±1.0	–58	±9
KLX08-19	983.18	–818.37	Quartz-Monzodiorite	>100	Na-Ca-Cl-HCO3	8,215	2,008	1,339	–2.6	±1.5	–41	±11
KLX17A-1	112.09	–70.42	Ävrö Granite	1	Na-Ca-HCO3	91	10	8	–9.5	±0.6	–74	±5
KLX17A-2	112.47	–70.76	Ävrö Granite	1	Na-Ca-HCO3	81	9	7	–10.5	±0.4	–80	±3
KLX17A-3	113.26	–71.44	Ävrö Granite	1	Na-Ca-HCO3	70	7	6	–10.5	±0.5	–80	±4
KLX17A-4	113.89	–71.99	Ävrö Granite	1	Na-(Ca)-HCO3	77	8	7	–10.1	±0.4	–79	±4
KLX17A-5	114.30	–72.35	Ävrö Granite	1	Na-(Ca)-HCO3	106	11	9	–9.9	±1.0	–75	±9
KLX17A-6	114.67	–72.67	Ävrö Granite	1	Na-(Ca)-HCO3	143	15	13	–9.7	±0.5	–75	±4
KLX17A-7	114.97	–72.94	Ävrö Granite	2	Na-(Ca)-HCO3	161	18	14	–9.8	±1.0	–75	±10
KLX17A-8	115.37	–73.28	Ävrö Granite	2	Na-(Ca)-HCO3	249	27	22	–9.6	±0.9	–77	±7
KLX17A-9	115.81	–73.67	Ävrö Granite	2	Na-(Ca)-HCO3	209	23	19	–10.0	±1.0	–81	±9
KLX17A-10	116.17	–73.98	Ävrö Granite	3	Na-HCO3	170	18	15	–10.0	±0.9	–82	±8
KLX17A-11	116.47	–74.24	Ävrö Granite	3	Na-(Ca)-HCO3	183	20	16	–10.9	±0.7	–83	±5
KLX17A-12	116.84	–74.57	Ävrö Granite	3	Na-HCO3	160	17	14	–11.4	±0.7	–87	±6
KLX17A-13	117.18	–74.86	Ävrö Granite	4	Na-HCO3	151	16	13	–11.7	±0.9	–92	±7
KLX17A-14	117.70	–75.32	Ävrö Granite	4	Na-(Ca)-HCO3	200	22	18	–11.2	±0.7	–86	±6
KLX17A-15	118.21	–75.77	Ävrö Granite	5	Na-(Ca)-HCO3	279	30	25	–10.6	±0.9	–83	±8
KLX17A-16	118.73	–76.21	Ävrö Granite	5	Na-(Ca)-HCO3	275	30	25	–10.7	±1.0	–82	±7
KLX17A-17	120.87	–78.08	Ävrö Granite	7	Na-(Ca)-HCO3	287	31	25	–10.6	±0.9	–81	±8
KLX17A-18	123.62	–80.48	Ävrö Granite	10	Na-(Ca)-HCO3	200	22	18	–10.4	±0.5	–83	±4
KLX17A-19	128.78	–84.99	Ävrö Granite	15	Na-(Ca)-HCO3	310	34	28	–7.9	±0.9	–82	±7
KLX17A-20	133.76	–89.33	Ävrö Granite	20	Na-(Ca)-HCO3	213	23	19	–7.6	±1.8	–84	±12
KLX17A-21	239.20	–181.09	Ävrö Granite	22	Na-HCO3	279	30	25	–11.0	±0.8	–97	±7
KLX17A-22	332.18	–261.36	Ävrö Granite	3	Na-(Ca)-HCO3	629	68	56	–12.8	±0.7	–98	±6
KLX17A-23	435.72	–349.97	Ävrö Granite	4	Na-(Ca)-HCO3	709	78	64	–		–	
KLX17A-24	540.38	–438.65	Ävrö Granite	>100	Na-Ca-HCO3-SO4-Cl	6,823	748	612	–5.1	±1.3	–35	±10
KLX17A-25	635.69	–518.17	Ävrö Granite	>100	Ca-Na-SO4-Cl	4,960	544	445	–4.8	±1.5	–38	±16

[1] Approximate distance from the porewater sample to nearest water-conducting fracture in the borehole according to the borehole differential flow log (PFL).

[2] Chemical type corresponds to that of porewater except for HCO_3, which might not be a major anion in porewater with Cl^- > 1,500 mg/kgH_2O (see text).

[3] Uncertainty band calculated form standard deviation of water content measurements.

[4] Numbers in *italic font* are not reliable; error calculated according to Gauss' law of error propagation.

Table A-4. Bromide concentration and chlorine and strontium isotope compositions of out-diffusion experimental solutions.

UniBern sample no	Average borehole length	Average elevation	Lithology	Distance to nearest water-cond. fracture [1]	Experiment solution chemical type [2]	Cl^- in exp. solution	$\delta^{37}Cl$ in exp. solution [3]	Br^- in exp. solution [4]	Sr^{2+} in exp. solution [4]	$^{87}Sr/^{86}Sr$	2σ error
	m	m		m		mg/L	‰ SMOC	mg/L	ppm		
KLX03-1	159.22	–135.33	Ävrö Granite	5	Na-HCO3-(Cl)	16.0	–	–	0.024	0.715469	0.000029
KLX03-2	202.66	–177.31	Ävrö Granite	1	Na-HCO3-(Cl)	16.2	2.47	0.091	0.034	0.714463	0.00002
KLX03-3	253.72	–226.74	Ävrö Granite	4	Na-HCO3	14.3	–	–	0.034	0.714416	0.000024
KLX03-4	304.10	–275.53	Ävrö Granite	10	Na-HCO3-(Cl)	13.8	–	0.082	–		
KLX03-5	355.66	–325.54	Ävrö Granite	27	Na-HCO3	12.9	–	–	0.068	0.714817	0.000032
KLX03-6	411.72	–379.92	Ävrö Granite	3	Na-HCO3-(Cl)	15.5	1.89	–	0.088	0.714955	0.000021
KLX03-7	462.76	–429.47	Ävrö Granite	3	Ca-Na-SO4-(HCO3)	35.8	–	0.254	–		
KLX03-8	524.63	–489.64	Ävrö Granite	65	Na-Ca-SO4-Cl-(HCO3)	198.0	1.47	–	1.851	0.708281	0.00002
KLX03-9	590.12	–553.24	Ävrö Granite	32	Na-Ca-Cl-HCO3-SO4	125.5	2.13	–	0.74	0.709984	0.000027
KLX03-10	643.13	–604.72	Quartz-Monzodiorite	16	Na-Ca-HCO3-Cl	15.9	–	0.104	–		
KLX03-11	695.95	–656.05	Quartz-Monzodiorite	31	Na-Ca-HCO3	6.8	–	–	0.139	0.71908	0.000027
KLX03-12	803.23	–760.35	Quartz-Monzodiorite	7	Na-(Ca)-HCO3-Cl	120.0	0.64	–	0.272	0.717795	0.000037
KLX03-13	841.18	–797.26	Quartz-Monzodiorite	34	Na-Ca-HCO3-Cl	43.5	–	0.231	–		
KLX03-14	894.53	–849.17	Quartz-Monzodiorite	75	Na-Ca-HCO3-Cl	30.3	1.53	–	0.203	0.721149	0.000023
KLX03-15	942.47	–895.83	Quartz-Monzodiorite	27	Ca-Na-HCO3-Cl	56.4	–	0.306	–		
KLX03-16	979.78	–932.12	Quartz-Monzodiorite	10	Na-Ca-HCO3-Cl	41.4	0.61	–	0.166	0.717054	0.000034
KLX08-1	150.22	–105.66	Ävrö Granite	3	Na-Ca-HCO3	3.4	–	–	–		
KLX08-2	199.45	–148.37	Fine-grained Granite	4	Na-Ca-HCO3	4.5	–	–	–		
KLX08-3	200.26	–149.07	Ävrö Granite	3	Na-Ca-HCO3	3.3	–	0.016	–		
KLX08-4	250.19	–192.36	Ävrö Granite	13	Na-Ca-HCO3	3.4	–	–	0.185	0.715976	0.000013
KLX08-5	302.34	–237.38	Ävrö Granite	2	Na-Ca-HCO3-Cl	12.5	–	–	–		
KLX08-6	347.10	–275.89	Ävrö Granite	37	Na-Ca-HCO3	13.5	–	0.054	0.278	0.716791	0.000010
KLX08-7	395.65	–317.63	Ävrö Granite	3	Na-HCO3-Cl	6.7	–	–	–		
KLX08-8	451.62	–365.70	Ävrö Granite	3	Na-Ca-HCO3	6.4	–	–	–		
KLX08-9	499.78	–406.97	Ävrö Granite	16	Na-Ca-HCO3-Cl	24.2	0.40	–	0.19	0.717947	0.000032
KLX08-10	550.23	–450.17	Ävrö Granite	66	Na-Ca-HCO3-Cl	27.1	0.44	0.168	0.185	0.717305	0.000013
KLX08-11	601.68	–494.21	Diorite	12	Na-Ca-HCO3	5.4	–	–	0.144	0.722642	0.000013
KLX08-12	660.03	–544.12	Diorite	4	Na-Ca-HCO3	6.0	–	–	–		
KLX08-13	702.05	–580.04	Diorite	23	Na-Ca-HCO3	10.5	–	–	0.184	0.720575	0.000015
KLX08-14	750.80	–621.67	Ävrö Granite	72	Na-Ca-HCO3-SO4	42.5	3.43	0.180	0.492	0.715582	0.000011
KLX08-15	802.22	–665.50	Ävrö Granite	52	Ca-Na-SO4	61.8	1.22	0.297	1.32	0.714670	0.000010
KLX08-16	857.98	–712.88	Ävrö Granite	4	Ca-Na-SO4	84.4	–	0.533	–		

Table A-4. continued.

UniBern sample no	Average borehole length	Average elevation	Lithology	Distance to nearest water-cond. fracture [1]	Experiment solution chemical type [2]	Cl^- in exp. solution	$\delta^{37}Cl$ in exp. solution [3]	Br^- in exp. solution [4]	Sr^{2+} in exp. solution [4]	$^{87}Sr/^{86}Sr$	2σ error
	m	m		m		mg/L	‰ SMOC	mg/L	ppm		
KLX08-17	903.28	–751.17	Ävrö Granite	49	Ca-Na-SO4	128.0	1.26	0.767	2.042	0.713231	0.000019
KLX08-18	945.75	–787.01	Quartz-Monzodiorite	92	Na-Ca-HCO3-Cl	53.4	–	0.300	–		
KLX08-19	983.18	–818.37	Quartz-Monzodiorite	>100	Na-Ca-Cl-HCO3	183.1	0.66	1.162	0.856	0.715639	0.000016
KLX17A-1	112.09	–70.42	Ävrö Granite	1	Na-Ca-HCO3	4.3	–	–	–		
KLX17A-2	112.47	–70.76	Ävrö Granite	1	Na-Ca-HCO3	3.2	–	–	–		
KLX17A-3	113.26	–71.44	Ävrö Granite	1	Na-Ca-HCO3	5.4	–	–	–		
KLX17A-4	113.89	–71.99	Ävrö Granite	1	Na-(Ca)-HCO3	4	–	–	–		
KLX17A-5	114.30	–72.35	Ävrö Granite	1	Na-(Ca)-HCO3	3.4	–	–	–		
KLX17A-6	114.67	–72.67	Ävrö Granite	1	Na-(Ca)-HCO3	3.8	–	–	–		
KLX17A-7	114.97	–72.94	Ävrö Granite	2	Na-(Ca)-HCO3	2.9	–	–	–		
KLX17A-8	115.37	–73.28	Ävrö Granite	2	Na-(Ca)-HCO3	4.9	–	–	–		
KLX17A-9	115.81	–73.67	Ävrö Granite	2	Na-(Ca)-HCO3	4	–	–	–		
KLX17A-10	116.17	–73.98	Ävrö Granite	3	Na-HCO3	3.9	–	–	–		
KLX17A-11	116.47	–74.24	Ävrö Granite	3	Na-(Ca)-HCO3	3.6	–	0.025	–		
KLX17A-12	116.84	–74.57	Ävrö Granite	3	Na-HCO3	4.2	–	–	–		
KLX17A-13	117.18	–74.86	Ävrö Granite	4	Na-HCO3	3.1	–	0.019	–		
KLX17A-14	117.70	–75.32	Ävrö Granite	4	Na-(Ca)-HCO3	4.6	–	–	–		
KLX17A-15	118.21	–75.77	Ävrö Granite	5	Na-(Ca)-HCO3	6.8	–	–	–		
KLX17A-16	118.73	–76.21	Ävrö Granite	5	Na-(Ca)-HCO3	5.1	–	–	–		
KLX17A-17	120.87	–78.08	Ävrö Granite	7	Na-(Ca)-HCO3	6.3	–	–	–		
KLX17A-18	123.62	–80.48	Ävrö Granite	10	Na-(Ca)-HCO3	5.5	–	0.051	–		
KLX17A-19	128.78	–84.99	Ävrö Granite	15	Na-(Ca)-HCO3	6.5	–	–	–		
KLX17A-20	133.76	–89.33	Ävrö Granite	20	Na-(Ca)-HCO3	2.2	–	–	–		
KLX17A-21	239.20	–181.09	Ävrö Granite	22	Na-HCO3	7.9	–	–	–		
KLX17A-22	332.18	–261.36	Ävrö Granite	3	Na-(Ca)-HCO3	14.4	–	–	–		
KLX17A-23	435.72	–349.97	Ävrö Granite	4	Na-(Ca)-HCO3	10.6	–	0.070	–		
KLX17A-24	540.38	–438.65	Ävrö Granite	>100	Na-Ca-HCO3-SO4-Cl	91.5	–	0.527	–		
KLX17A-25	635.69	–518.17	Ävrö Granite	>100	Ca-Na-SO4-Cl	62.2	–	0.331	–		

[1] Approximate distance from the porewater sample to nearest water-conducting fracture in the borehole according to the borehole differential flow log (PFL).

[2] Chemical type corresponds to that of porewater except for HCO_3, which might not be a major anion in porewater with $Cl^- > 1{,}500$ mg/kgH_2O (see text).

[3] Analytical error = 0.15‰ SMOC (2σ).

[4] Bromide measurements by ICP-MS, strontium measurements by MS.

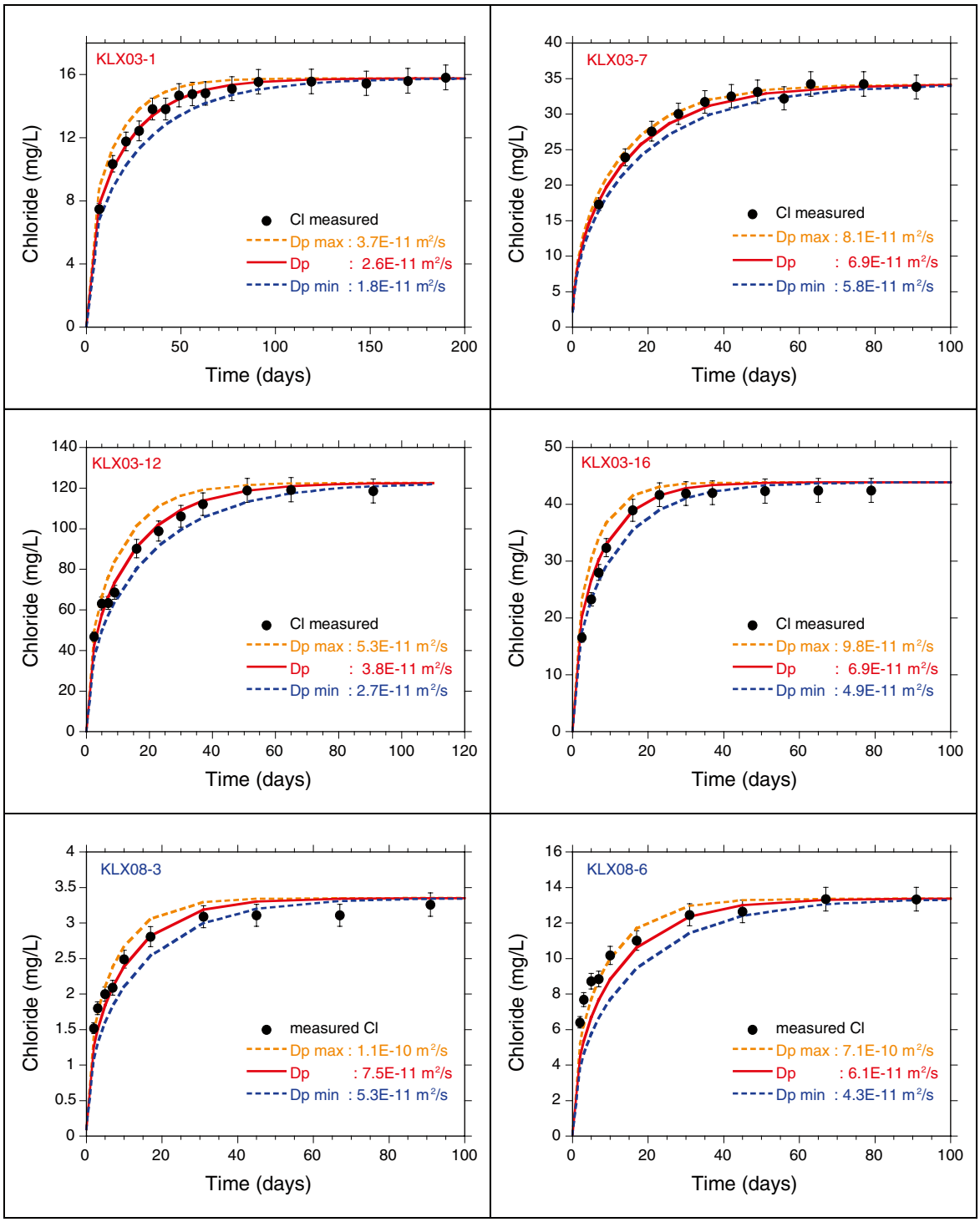

Figure A-1. *Model fits to the measured chloride time-series data of the out-diffusion experiments performed on large-sized (approx 1 kg) drillcore samples from boreholes KLX03, KLX08 and KLX17A. The best fit curve delivering the pore diffusion coefficient, D_p, for chloride at 25°C is shown in red. The uncertainty range (D_p min and D_p max) is given by values that are larger/smaller by a factor 1.41 (square root of 2) corresponding to a factor of 2 in the diffusion time (orange and blue curves).*

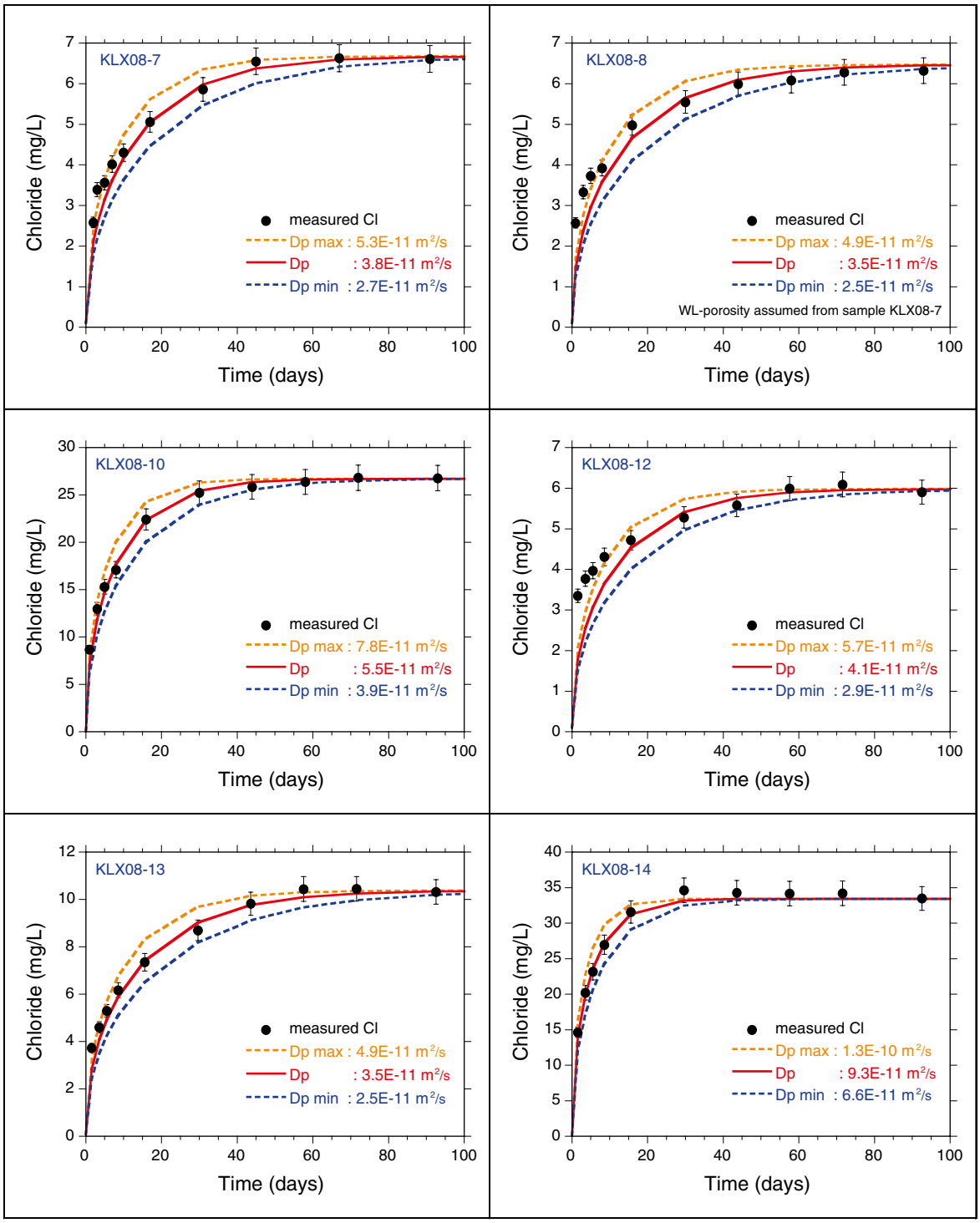

Figure A-1. *continued.*

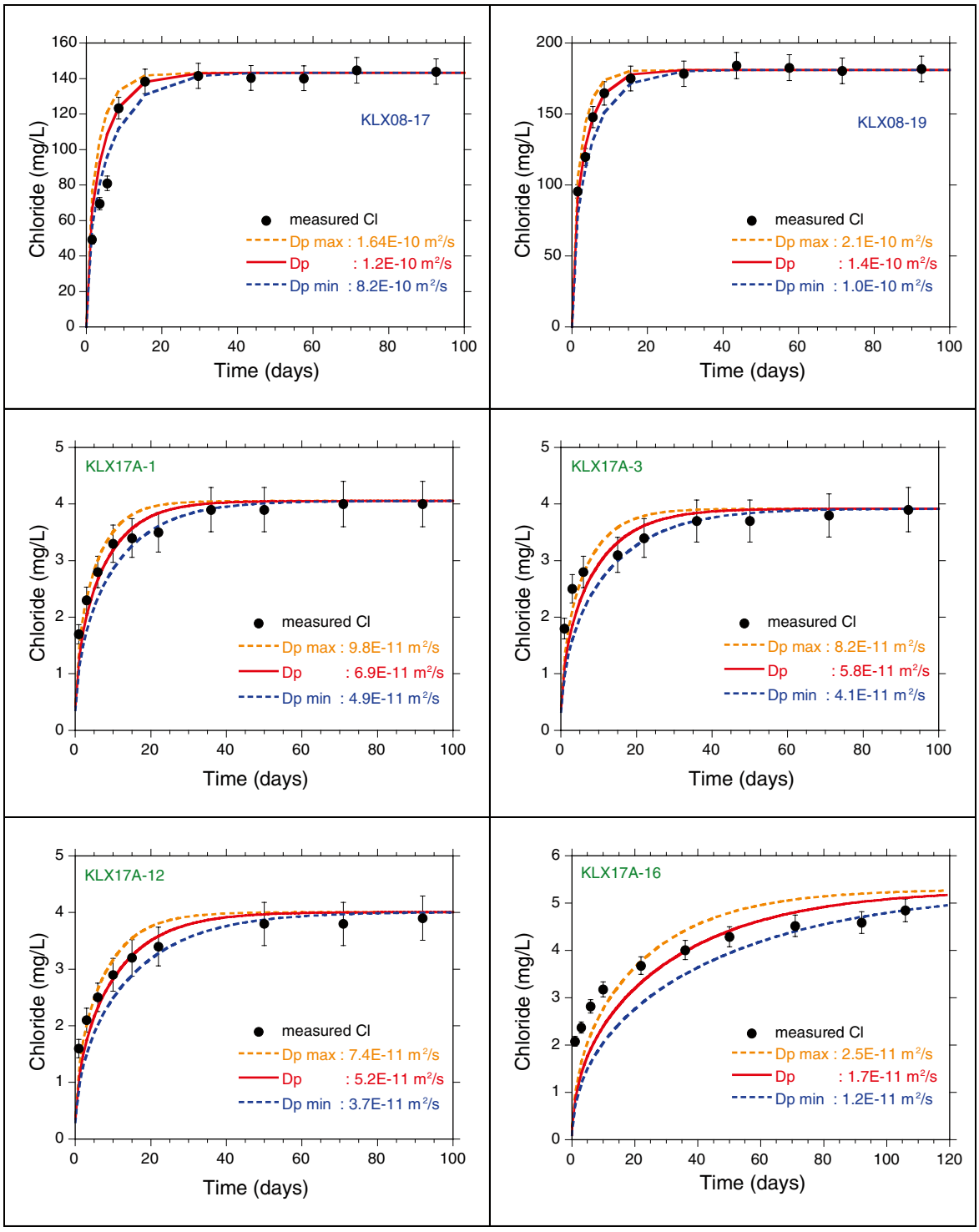

Figure A-1. *continued.*